Using Fisher information approach in nonlinear dynamical systems

A thesis presented

by

Avan Safar Elias Al-Saffar

to

School of Mathematics and Statistics

in partial fulfillment of the requirements for the degree of

Doctor of Philosophy

University of Sheffield, UK

June, 2018

Supervisor: Dr. Eun-jin Kim

Abstract

Simple nonlinear systems do not necessarily have simple dynamical properties

The aim of this thesis is to investigate nonlinear dynamical systems that exist in various fields such as engineering and science. Nonlinear dynamical systems permit the understanding and development of models of simple and complex phenomena. Specifically, this thesis includes an investigation of the following systems; the logistic model, the Gompertz model, predator-prey model, and three species model. In addition, we perform a comparison between the two most popular growth models; logistic and Gompertz models from the viewpoint of variability. The main focus is on the use of Fisher information as a measure of variability/sustainability which depends on the gradient of Probability Density Function (PDF).

In this work, we present two case studies for each dynamical system. The first case study describes the analysis of these systems in their deterministic conditions whereas the second one presents the investigation of these systems in their indeterministic conditions (perturbed conditions), where the model parameters involve perturbations, elucidating the effects of these perturbations on the behaviour of the system. The variation in the model parameter values is considered in order to observe the behaviour of the different dynamical systems and detect dynamical changes in the behaviour of each species.

Since Fisher information is considered as a measure of an intrinsic accuracy of the dynamical systems, therefore, we obtain Fisher information for different values of parameters in order to select the optimal parameter value where a peak of Fisher information is observed, which indicates to less variability in the behaviour of the system. Thus, the existence of Fisher information peak which linked to the narrowest PDF is investigated in the frame of time trace analysis.

In summary, the main contribution of this work to the field is to assess the significance of Fisher information index for nonlinear dynamical systems including perturbations in the model parameters. Applying this measure to more complicated systems and comparing the results to other widely used measures would be of interest for future work.

Dedication

This thesis is gratefully dedicated to my country

IRAQ

And my great town

ALQOSH

Acknowledgement

I remember writing the acknowledgement of my master's thesis. I thought I knew a lot about science. The truth is, I knew nothing. Now, I have finished my PhD. I know a little more than when I started. Undertaking a PhD has been a life-changing experience for me, and I take this opportunity to express my sincere appreciation to everyone who has supported and guided me during this amazing journey.

The first three years of this PhD study scholarship was fully sponsored by the human capacity development program (HCDP), Ministry of Higher Education and Scientific research, Kurdistan Regional Government of Iraq. During these long four years of this research study, the author would like to show his gratitude to the following people for their support, contributions and encouragement.

- The supervisor, Dr. Eun-jin Kim for her time and support. It was my pleasure to gain experience from her in understanding the physical meaning of research and for teaching me how to never be satisfied with my work.

- A special thank you goes to my son *Sharbel*, for refreshing my day, after long hours at the university, with his smile, hug and kisses when he was waiting for me at the door and my husband Bashar Cholagh as well for his time that he spent taking care of our boy Sharbel and for the nice and tasty food.

- I should not forget to thank my parents for the values that they taught me and their trust about my ability to accomplish what I am doing. My brothers and sisters for their help and supports. Also, I would like to thank my grandmothers, uncles and aunts, relatives and friends who always supported me and asked about the progress of my study.

Lastly, I offer my regards and blessings to all of those who supported me in any respect during the completion of the project within the University of Sheffield and outside it.

Contents

1 Introduction **1**

1.1 Background and motivation 1

1.2 Overview of the thesis 14

2 The logistic model **17**

2.1 Introduction 17

2.2 The model 19

2.3 The logistic model with oscillatory parameters 21

2.4 Case-1 : The same perturbation in the positive and negative feedback 22

2.4.1 Results for fixed ω and varying N_0 24

2.4.2 Results for fixed N_0 and varying ω 27

2.4.3 Probability Density Function 31

2.4.4 Fisher information 35

2.4.5 Role of Fisher information as a measure of sustainability . . . 41

2.4.6 Fisher information dependence on x_0 46

2.4.7 The logistic model with extra modification 48

2.5 Comments on different modulations 49

2.5.1 Case-2: Perturbation in the positive feedback 50

2.5.2 Case-3: Perturbation in the negative feedback 52

2.6 Conclusions 55

3 The Gompertz model **57**

3.1 Introduction 57

3.2 The model and motivation 59

3.3 The Gompertz equation with oscillation 60

3.4 Case-1: The same fluctuation in the growth and death rates 61

3.4.1 Results for fixed ω and varying D_0 in the oscillatory term . . 62

3.4.2 The cross-over behaviour between $x = x_0$ and $x = x_1^*$ 63

3.4.3 Probability Density Function 66

3.4.4 Fisher information 68

3.5 The Gompertz equation with different modulations 71

3.5.1 Case-2: Perturbation in the positive feedback 71

3.5.2 Case-3: Perturbation in the negative feedback 75

3.6 Conclusions 77

4 A dynamical system with two-components **79**

4.1 Introduction 79

4.2 The predator-prey model 81

4.2.1 Estimating parameters in predator-prey model 82

4.2.2 The dynamics and variability of predator-prey model 83

4.2.3 Effects of changing the prey mortality rate 85

4.2.4 Fisher information for the predator-prey model 87

4.3 Modifications to the predator-prey model 91

4.3.1 Prey density dependence 91

4.3.2 The predator-prey model with a periodic function in the immune population 95

4.3.3 Fisher information in the modified predator-prey model 104

4.4 Conclusions 107

5 A dynamical system with three-components **109**

5.1 Introduction 109

5.2 Mathematical definition of the three species model 110

5.2.1 Local stability analysis and equilibria 112

5.3 Modifications to the three species model 118

5.3.1 Dynamic properties of the model 118

5.3.2 Effects of varying the amplitude ϵ 120

5.3.3 Effects of varying Ω 122

5.4 Conclusions 124

6 Conclusions and future work **125**

6.1 Summary of the results 125

6.2 Future work 128

A A dimensionless form for the predator-prey model **131**

B A dimensionless form for the three species model **134**

C Fisher information construction for the logistic model **136**

D Fisher information construction for the predator-prey model **138**

E Fisher information construction for the three species model **140**

Bibliography **142**

List of Figures

2.1 Different colours represent different initial conditions, the population shows a transient growth followed by exponential growth, then approaches the equilibrium point at $x = K = 10$ where convergence to K happens from any initial state. 21

2.2 $3D$ plot of the maximum values of x, $Max(x)$, in $z - axis$, N_0 in $x - axis$ and ω in $y - axis$. $Max(x)$ values are monotonically decreasing as ω increases for $K = 10$, $B = 0$, and $x_0 = 0.1$. 23

2.3 Maximum values of x for varying N_0 and different values of ω, $x_0 = 0.1$, $B = 0$. The difference between the above curves is the time that the population spend before showing a steady state at the carrying capacity $K = 10$. 25

2.4 The linear relationship between N_0 and ω with fixed values of $K = 10$, $B = 0$ and $x_0 = 0.1$. 27

2.5 Time trace of x for different values of $x_0 = 0.1, 5$ and $\omega = 1, 10$. For a small value of ω, x tends to reach the carrying capacity $K = 10$ while for large ω, x maintains its initial conditions. 28

2.6 Maximum and minimum values of x against ω for $N_0 = 5$ and $K = 10$ with $x_0 = 0.1$ in panels (a), (c) and (e) and $x_0 = 5$ in panels (b), (d) and (f). (c), (d), (e) and (f) are shown in log-log scale. 30

2.7 PDF of x for $N_0 = 5$, $B = 0$, $K = 10$ and $x_0 = 0.1$. Different values of ω are used in panels (a)-(f). A bimodal PDF is observed for all the cases. 32

2.8 PDF of x for $N_0 = 5$, $B = 0$, $K = 10$ and $x_0 = 5$ by using different values of ω in panels (a)-(f). A bimodal PDF with different distance between the two peaks is observed for all the cases. 34

2.9 (a) A uniform PDF with zero Fisher information, (b) A PDF of x with medium Fisher information and (c) A steeply sloped PDF of x with large Fisher information (high gradient). 35

2.10 F_T against the total time T for $N_0 = 5$, $x_0 = 0.1$, $K = 10$, $B = 0$ and different values of ω. We observe a larger value of F_T at $\omega = 1$. . . . 38

2.11 Asymptotic values of F_T against ω for $x_0 = 0.1$, $N_0 = 5$, $B = 0$ and $K = 10$. 39

2.12 F_T against T for $N_0 = 5$, $K = 10$, $B = 0$ and $x_0 = 5$. Panels (a)-(f) are for different values of ω. 40

2.13 Asymptotic values of F_T against ω for $x_0 = 5$, $N_0 = 5$, $B = 0$ and $K = 10$. F_T increases monotonically as ω increases. 40

2.14 PDF of x for $x_0 = 0.1$, $K = 10$, $B = 0$ and $N_0 = 5$, with a periodic stimulus. Left panels are for the optimal case ($\omega = 1$) while the right panels are for non-optimal case ($\omega = 10$). The PDFs with optimal value $N_0 = 5\omega$ in left panels are more resilient to the a periodic stimulus than the PDFs for $\omega = 10$. 42

2.15 PDF of x for $B = 0$, $x_0 = 5$, $K = 10$ and $N_0 = 5$, with periodic stimulus. We use the smallest ω in the left panel and the largest ω in the right panel in regards to Figs. 2.12 and 2.13. 45

2.16 F_T against x_0 for $N_0 = 5$, $B = 0$, $K = 10$ and $\omega = 0.5$ (ω is an arbitrary value). The important feature of the above figure is a distinct peak of F_T at $x_0 \simeq 10$. Panel (b) is in log-scale. 46

2.17 PDF of x for $N_0 = 5$, $B = 0$, $K = 10$ and $\omega = 0.5$ with different values of x_0. A bimodal PDF is observed for all the initial conditions with different distance between the two peaks. 47

2.18 Mean values of cancer population at different values of c and fixed $K = 10$, $N_0 = 5$, $\omega = 1$, $B = 0$. Similar behaviour is observed for all the values of c with a difference in the time where cancer cells start to eradicate. 49

2.19 PDF of x for different N_0 and ω. $x_0 = 0.1$, $B = 0$, $K = 10$ and $C = 1$. We observe a notable unimodal PDF for all the cases. 51

2.20 $Max(x)$ as a function of ω for $N_0 = C = 5$, $x_0 = 0.1$ and $B = 0$. $Max(x)$ values are monotonically decreasing as ω increases and finally show a static state at x_0. 52

2.21 PDF of x for two different N_0; $N_0 = 0.5$ in the upper panels and $N_0 = 1$ in the lower panels. We fix $x_0 = 0.1$, $B = 1$, $K = 10$ and $C = 1$. A bimodal PDF is observed. 53

2.22 The time evolution of x for different values of N_0 and ω and fixed $x_0 = 0.1$, $K = 10$, $B = 1$ and $C = 1$. The population grows boundlessly for small ω and larger N_0 as in panel (c). 54

3.1 Maximum values of x for fixed $\omega = 1, 2, 5, 10$ and varying D_0 with $x_0 = 0.1$, and $B = 0$. The difference between the above curves is the time that the population spend before approaches its maximum values at e. 63

3.2 The time evolution of x for different values of $x_0 = 0.1, 2$ and $\omega = 1, 10$. For a small value of ω, $x(t)$ tends to reach the carrying capacity e while for large ω, $x(t)$ maintains its initial condition. 64

3.3 Maximum and minimum values of x against ω for $D_0 = 7$ and $x_0 = 0.1$ in panels (a), (c) and (e) and $x_0 = 2$ in panels (b), (d) and (f). (c), (d), (e) and (f) are explained in log-log scale. 65

3.4 PDF of x for $D_0 = 7$ and $\omega = 0.5$ with different values of x_0. A bimodal PDF is observed for all x_0 with different distance between the two peaks. 67

3.5 PDF of x for $D_0 = 7$ and $\omega = 2$ with different values of x_0. We notice a bimodal PDF for all x_0 with different distance between the two peaks. 68

3.6 Asymptotic values of Fisher information averaged over time, F_T, against x_0 for $\omega = 0.5$, $D_0 = 7$ and $B = 0$. 70

3.7 Time trace of x for different values of $D_0 = b = 1, 2, 7$ with $x_0 = 0.1$ and $\omega = 1, 10, 50$. For sufficiently small ω, the amplitude of the fluctuation is larger than the amplitude for larger values of ω. 72

3.8 PDF of x for different D_0 and ω with $x_0 = 0.1$, $B = 0$ and $b = D_0$. The distance between the two peaks is getting smaller as ω increases. 73

3.9 $Max(x)$ as a function of ω for $D_0 = b = 7, x_0 = 0.1$ and $B = 0$. $Max(x)$ values are monotonically decreasing as ω increases and finally show a static state at $x \simeq 1$. 74

3.10 Time evolution of x in the left panels and PDFs of x in the right panels for different values of $x_0 = 0.1, 5, 10$, and fixed $D_0 = b = 7$ and $\omega = 1$. 75

3.11 PDF of x for two different amplitude to be $D_0 = 0.5$ and 1 in the upper and lower panels, respectively. We fix the other parameter values to be $x_0 = 0.1$, $B = 1$, and $c = 1$. 76

3.12 Time trace of x for two different D_0; $D_0 = 1$ and $D_0 = 10$ in the upper and lower panels, respectively and different ω. For all cases, we fix $x_0 = 0.1$, $B = 1$, and $c = 1$. 77

4.1 Time evolution in the upper panels and phase portrait in panel (c) for different initial conditions. A sensitivity to initial values (x_0, y_0) is observed for predator-prey model. Same parameter values are used for both curves but differ by the initial conditions. 84

4.2 The evolution of predator-prey model for different prey mortality rate ($b = 1, 3, 6, 10$). This figure gives representation of different possible behaviour corresponding to various b. A blue line represents prey population and the green line stands for predator population. 86

4.3 The evolution of predator equilibrium points for different prey mortality rate. Other parameters are $c = 5$, $d = 0.5$, $a = 15$ and $[x_0, y_0] = [12, 5]$. The equilibrium points are monotonically decreasing as b increases. 87

4.4 F_T against prey mortality rate b. We fix $[x_0, y_0] = [12, 5]$, $a = 15, c = 5, e = 0.5$ and varying b, A local maximum for F_T is noticed at $b = 3$. 89

4.5 PDF of predator and prey population in the upper panels and phase portrait for different prey mortality rate ($b = 1, 3, 6$) in the lower panel. Other parameter values are taken as $[x_0, y_0] = [12, 5]$, $a = 15, c = 5, e = 0.5$. A very tight cycle is noticed for $b = 3$. 90

4.6 Time evolution for different parameter values with a logistic equation in the prey density. Same parameter values are used in the upper panels, but with different $[x_0, y_0]$, similar case for the lower panels. A blue line for cancer cells and green for immune cells. 92

4.7 Time trace and phase portrait for different initial values and fixed parameter values $\alpha = \beta = \gamma = 1$. The left panels represent the time trace and right panels stand for the phase portrait. 94

4.8 Time evolution in the left panels and phase portrait in the right panels for $\alpha = 1$, $\beta = 1.291$, $\gamma = 1$, $\delta = 1$, $\Omega = 1$ and $F = 0.1$ with different initial conditions. We observe a fixed point $(u_2^*, v_2^*) = (0.8032, 0.1968)$ which is stable and attracts all the solutions. 97

4.9 Time evolution in the left panels and phase portrait in the right panels for $\alpha = 1$, $\beta = 1.291$, $\gamma = 1$, $\delta = 1$, $\Omega = 1$ and $F = 3$ with different initial conditions. We observe a stable node $(u_1^*, v_1^*) = (0, 1.1619)$ for all initial conditions. 98

4.10 Maximum values of population against Ω for different amplitude with $\alpha = 1$, $\beta = 1.291$, $\gamma = 1$ and $\delta = 1$. $Max(x)$ values are monotonically decreasing as Ω increases for both amplitude values. The difference between panels (a) and (b) is that for larger values of amplitude, we observe the eradication of the cancer cells. 100

4.11 Maximum values of cancer population (prey) on the $z-axis$, F on the $x-axis$ and Ω in the $y-axis$ in a $3D$ plot. A monotonic decrease is noticed in the prey population for a sufficiently large Ω. We fixed $[u_0, v_0] = [1, 1]$, $\alpha = 1$, $\beta = 1.291$, $\gamma = 1$ and $\delta = 1$. 101

4.12 Maximum values of cancer population (prey species) when it is equal and less than 0.0e-05 for $[u_0, v_0] = [1, 1]$, $\alpha = 1$, $\beta = 1.291$, $\gamma = 1$ and $\delta = 1$. 102

4.13 Time trace of population for different values of F with and without fluctuation for $[u_0, v_0] = [1, 1]$, $\alpha = 1$, $\beta = 1.291$, $\gamma = 1$, $\delta = 1$ and $\Omega = 1$. Blue line represents prey while the green line stands for predator. 103

4.14 Fisher information against F for $[u_0, v_0] = [1, 1]$, $\alpha = 1$, $\beta = 1.291$, $\gamma = 1$, $\delta = 1$ and $\Omega = 1$. A peak for F_T is observed at $F = 2.62$ which leads to state with less variability. 105

4.15 Time evolution of x, PDFs and phase portrait for different values of F and fix other parameter values as $[u_0, v_0] = [1, 1]$, $\alpha = 1.291$, $\beta = 1$ and $\Omega = 1$. 106

5.1 Time evolution and phase portrait of Eqs. (5.2) for different a_{23}, the other parameters are shown in Table (5.1) and $[u_0, v_0, r_0] = [1, 1, 1]$. A blue line represents cancer, green for immune and red for healthy cells. The right panels are a phase portrait for each a_{23} after removing the initial transient. 114

5.2 The average of x as a function of the periodic amplitude, fixing all the parameter values as shown in Table (5.1), $[u_0, v_0, r_0] = [1, 1, 1]$ and changing the value of a_{23}. 115

5.3 Time evolution of x for different values of a_{23}, $[u_0, v_0, r_0] = [1, 1, 1]$ and the other parameters are shown in Table (5.1). 116

5.4 F_T as a function of amplitude for $[u_0, v_0, r_0] = [1, 1, 1]$ and fixed other parameter values. A peak is noticed at $a_{23} = 1.5$ which is the same value where the cancer cells begin to vanish in Figs. 5.2. and 5.3. . . . 117

5.5 Average values of each population against the amplitude a_{23} for $[u_0, v_0, r_0] = [1, 1, 1]$, different ϵ and fixed the other parameter values. A blue line for cancer cells, green for immune cells and red for healthy cells. . . . 119

5.6 F_T against the amplitude a_{23} for $\Omega = \Omega_1 = 1$, $\epsilon = 0.1$ and $[u_0, v_0, r_0] = [1, 1, 1]$. A peak is observed at $a_{23} = 1.5$ which is the same value where the cancer cells start vanishing in Fig. 5.5. 120

5.7 We use different values of ϵ to plot the dynamics of the model for fixed parameter values such as $a_{23} = 1.5$, $\Omega = \Omega_1 = 1$ and $[u_0, v_0, r_0] = [1, 1, 1]$. Blue line for cancer cells, green for immune cells and red for healthy cells. 121

5.8 We display the average of each species in different colours as a function of ϵ with fixed values for the other parameters. No changes are noticed in the average values which means that our model is independent of ϵ. 122

5.9 The average values of each species against Ω for two different values of ϵ with fixed $\Omega_1 = 1$, $[u_0, v_0, r_0] = [1, 1, 1]$ and $a_{23} = 1.5$. No changes are observed in the average values as Ω increases. 123

List of Tables

2.1 Different values of ω and N_0 26

2.2 Mean values for $x_0 = 0.1$, $K = 10$ and $B = 0$ without periodic stimulus. 43

2.3 % Change in mean values for $x_0 = 0.1$, $K = 10$ and $B = 0$ with periodic stimulus. 43

2.4 Mean values for $x_0 = 5$, $K = 10$ and $B = 0$ without periodic stimulus. 46

2.5 % Change in mean values for $x_0 = 5$, $K = 10$ and $B = 0$ with periodic stimulus. 46

5.1 Parameter values for numerical simulation 112

Chapter 1

Introduction

1.1 Background and motivation

The concept of dynamics refers to change, forces capable of action, whereas the static state means fixed or stationary. It is necessary to understand and even to change the rules governing our world and how they influence us; in order to achieve this, the concept of *"dynamics"* has been employed. We need dynamical systems to explain the environment we live in and even to make changes to the environment that surrounds us in order to shape it and develop a full understanding.

The origin of dynamical systems theory derives from the mechanisms of Newton, which have been developed and used to analyse systems of moving particles under the influence of outer intensity [16]. Dynamical systems are groups of variables whose values vary over time and may display an interaction. In this respect, we can divide dynamical systems into two sets: deterministic which have no randomness involved in their mechanism (the state of a system for all the coming stages can be determined by obtaining full knowledge of the state for a system at certain point of time), or stochastic dynamical systems include randomness. Depending on the systems' variables, the state of a system can be determined over time. The state of a system is described by a

vector (a state variable of the dynamical system is defined as $x_1, x_2, ..., x_n$) and a trajectory in the state space can be determined through the evolution of a dynamical system which can be displayed in a geometrical figure, constructing an attractor. An investigation must be conducted to specify the effects of change in the individual system variables, which are considered as functions of time, on the evolution of a dynamical system [16, 51, 71, 79].

On the other hand, dynamical systems can be divided into two large groups: discrete-time or continuous-time systems. Discrete-time systems can be represented by difference equations whereas continuous-time systems can be described by differential equations. In our work, we will only consider systems described by differential equations, which means in their continuous conditions which develop in continuous time. In the following, we display the dynamical systems in the form of first-order differential equations [68] as:

$$\begin{aligned} \frac{dx_1}{dt} &= f_1(t, x_1, x_2, \ldots, x_n), \\ \frac{dx_2}{dt} &= f_2(t, x_1, x_2, \ldots, x_n), \\ \vdots \quad &= \qquad \vdots \\ \frac{dx_n}{dt} &= f_n(t, x_1, x_2, \ldots, x_n), \end{aligned} \tag{1.1}$$

which can be displayed in a vector style as:

$$\dot{x} = \frac{dx}{dt} = f(t, x)\,, \tag{1.2}$$

here, t represents time and x is the system state. $\dot{x}$ indicates the differentiation of x with respect to t. $f(t, x)$ represents a density dependence according to biologists whereas for mathematicians it stands for nonlinearity. From the above equation, we can conclude the dynamical characteristics and valuable details of the corresponding system. For example, for the logistic equation, $f(t, x)$ has its maximum population size K (carrying capacity of the system) where $f(t, x)$ increases monotonically as x

increases, $f(t, x)$ decreases monotonically as x exceeds its maximum size K, and $f(t, x) = 0$ when $x = 0$ [4, 61]. Investigating these properties starts with the equilibrium points [1] from the following quantity:

$$\frac{dx}{dt} = 0 \,,$$

where the rate of change of the state variable x is zero over the time taken for the system to attain equilibrium. As a result, it is possible to investigate the stability of the system as it achieves its equilibrium. That is, including a small disturbance in the system to determine whether the equilibrium is a stable point that attracts all the solutions or an unstable point. For steady states, the characteristics of stability and dependence on initial conditions and other parameter values are very important in different dynamical systems [16, 61]. The importance of perturbations in the model parameters in different forms has become a significant subject of debate in several fields of study such as biology, medicine and ecology [11, 38, 44]. In this thesis, as a robust method to understand the biological system's response to the parameter changes and its basic dynamics, we emphasise the significance of computational study on biological processes, specifically, by employing several population growth models with different interactions and perturbations such as logistic and Gompertz models with one species (see Chapters 2 & 3), predator-prey model with two species (see Chapter 4), and finally, a three species model (see Chapter 5).

The main difference between the linear and nonlinear dynamical systems is represented by their ability to produce an analytical solution. Linear systems can be divided into parts that are then regrouped to obtain the exact solution, with nonlinear dynamical systems it is difficult to find the solution; instead, numerical calculations can be obtained. As a result, an obvious explanation of the parameters' role and their physical or biological significance can be concluded from a simple model regardless of its dynamics. In this regard, the example cited by Strogatz [92] provides a good analogy for

[1] equilibrium points for the mean value of the perturbation in the non-autonomous systems.

the linear and nonlinear systems, "*if you listen to your two favorite songs at the same time, you won't get double the pleasure* ".

When the growth of yeast cell population depends only on the biological environment, the use of growth models can be justified but this is not the case with human populations, where other factors such as war, emigration and unemployment play an important role in the growth process [97]; as a result, this motivated us to manipulate the parameters in several dynamical systems. Also, a growth model is proposed to represent two consumers with a single resource where the consumer's body size displays a significant role in their interaction. The results of this study show that the consumer with larger size obtains greater benefits in contrast to the consumer with smaller size in the facilitation area [77]. The models in this thesis are based on models studied earlier by many researchers to investigate their dynamics and stability using different approaches and mechanisms (see [3, 17, 32, 40, 42, 94, 96, 101, 107]). In our study, we modify those models by including a periodic modulation in the model parameters and study the influence of this perturbation on the behaviour of the system.

Significant efforts have been made to analyse dynamical systems through allocation of human and economic resources, resulting in effective findings as well as failures. Several researchers have applied intrinsic and extrinsic modifications to different dynamical systems with different approaches to track these systems' behaviour and capture some of their basic characteristics.

A dynamical system of first-order differential equation is used in many fields such as economic, biological, social sciences, genetic and engineering as a popular mathematical model. An astonishing set of dynamic behaviours can arise from this simple and deterministic equation. One of these models is the *logistic model* which is widely used and investigated [24, 38, 56, 88]. Investigating the functionality of this model leads to information about its equilibrium solutions and its stability from stable point, stable limit cycle to chaotic (though absolutely deterministic), also, can be studied by including a small perturbation in the model parameters. Even the simple logistic model, which has been investigated in different area using different techniques, still has much

to offer. In the same behaviour as the logistic model, the so called *Gompertz model* has earned special consideration. Both models are used to describe growth processes. The usual growth style for any population is a lag phase or transient growth followed by exponential growth, to then approach the maximum population size (carrying capacity of the population) (see Fig 2.1). Although the logistic equation has been more studied, the Gompertz growth equation may better meet the features of some growth processes [17, 32, 40, 61, 67, 73, 97]. One common property between the two models is that they share as a characteristic an *S-shaped* growth process that manifests as a slow early phase, followed by rapid growth, then finally, a static steady solution (static state remains the same) [66, 97]. On the other hand, a comparison study has been conducted to compare these two models in their stochastic conditions, investigating the response of the two models after including different types of stochastic noises and comparing their time-dependent PDF. Also, an information length index is used to measure the change that occurs within the process of growth for the two models and compare the results [94]. On the other hand, another study by Nobile et al. [67] has been found which concentrates on comparison between the logistic and Gompertz equations in the context of the dynamics of population described by first order difference equation.
The logistic and Gompertz models are the most common models which have been used for tumour cell population (see [10, 46] and the references there in). For more insight into the general behaviour of these models, it is recommended to investigate their dynamics after including both internal and external perturbations. In spite of the simplicity of the logistic and Gompertz models, they cover a wide range of dynamic behaviours.

such models but with more species as the predator-prey model. The Lotka-Volterra predator-prey model consists of two simple differential equations (coupled logistic equations) and has the ability to understand the interaction between species. For each initial value, the model shows a limit cycle solution where the phase plane is a sim-

ple closed curve, implying that the solution is a simple periodic solution. Abrams et a1. [1, 2] made changes to the predator-prey model in order to study the effects of enhancing population size on species; as a result, it was observed that increasing the population size of the predator may have a negative impact on the prey population size, whereas increasing the prey population size may have a positive impact on the population size of the predator. Additionally, the effects of this interaction on each species' growth rate and the functional response which represents the rate of prey consumption by the predator population density has been studied. The functional response of a predator such as a spider, hunting dangerous prey (it has a unique set of defences) such as ants has been investigated using a new proposed model of the type 4 functional response (predator-prey model) [53]. Another example of dangerous prey is the zebra, due to its ability to defend itself from the attack of a predator by biting and kicking [36]. We further cite another example of employing a system of two differential equations for two associated species, where the first species will grow and multiply depending on the food available in its environment, and the second species will die because of lack of food if live alone; otherwise, the two species could both survive in the case of the second species feeding on the first type [98]. Further investigation on the predator-prey model has been done by such as by Costa et al. [90] who studied the predator-prey model by including new terms for the influence of cytokines on cancer, the aggressiveness of cancer and the spread of lymphocytes. On the other hand, the authors of [31] presented and investigated a predator-prey model with the possibility of infection of both prey and predator, based on examining the stability of the model equilibrium points and studying the effects of the infection rate numerically. In regard to the above examples of predator-prey model, it must be mentioned that these models have been studied and developed to understand the dynamic evolution of populations by many researchers using different techniques (see [7, 18, 69, 70, 105, 106]).

Since 1975, cancer has been amongst the most commonly diagnosed disease around the world as a cause of death. Approximately 32.5 million people diagnosed with cancer within the five years previously were alive at the end of 2012. However, be-

cause surgery and/or radio- and chemotherapies are unable to destroy the cancer in all patients, more efforts are required in eradicating cancer cells. Current efforts are focused on destroying cancer populations by developing different dynamical population systems. Many publications have demonstrated great progress by putting forward mathematical models for the cancer population which are supported by experimental results of population dynamics ([22, 43] and the references there in).

It must be remarked that there are many different kinds of anticancer therapies, including Hormonal therapy, Chemotherapy, Immunotherapy, etc., and the kind of therapy given may be critical in determining whether the cancer population will be eliminated or not ([22] and the references there in). Immunotherapy involves the use of cytokines, usually along with adoptive cellular immunotherapy (ACI). Cytokines are a group of proteins secreted by cells of the immune system in both natural and artificial immune responses, whereas ACI refers to the injection of cultured immune cells that contain anti-tumour reactivity into a tumour bearing host ([43, 80] and the references there in). d'Onofrio et al. [22] show in their investigation of "aggressive" and "non-aggressive" cancer models that the system is sensitive to the initial values whereas it does not depend on the amplitude of the perturbations included in the system. This finding can be compared to our conclusions drawn in Chapters 4 & 5 where the behaviour of our models of two and three species, is found to depend on the amplitude of the periodic perturbations and not on the initial conditions. Furthermore, they noticed that addition of new features to a set of equations to investigate their dynamics instead of employing another specific model is an interesting phenomenon in human biology. The numerical simulations of many immunotherapy models show that while immunotherapy will not completely destroy the cancer cells, the rest may be eradicated by the immune system, or may continue in the case of dormant cancer. Cancer dormancy means that the tumour stays in an inanimate state in the host body for months or maybe for years before it begins to be visible, due to its cell population not increasing during this period (see [22, 47] and the references there in).

In 2005, Sarkar and Banerjee [82] conducted a stability analysis of the stochastic tu-

mour system, both analytically and numerically, based on the possibility that the observation obtained could help to control the growth of tumour cells. Introducing a small periodic perturbation in the system parameters was found useful through giving a significant opportunity to control the functionality of the system. Later, in 2007, when Perez et al. [80] studied the effects of including a cytokine-based periodic immunotherapy treatment in the tumour growth model with a delay, it was observed that while the immunotherapy applied was not able to eradicate the cancer cells, it did at least keep them under control, suggesting that different therapeutic process may be applicable. In the presence of a periodic perturbation, cancer cells show lower functionality and become a target for immune cells, thereby affecting the cancer growth rate. Hence, many studies to investigate the effects of different noises applied for tumour growth system have been found such as that of Bose and Trimper [10] who used a stochastic model for tumour growth with immunisation. They determined the death rate in the logistic model as an immunisation, whereas they included a multiplicative internal noise in the birth growth rate. In addition to adding noise to the logistic model in order to reduce the effects of the environment of tumour, a specific dose was found useful to eliminate tumour growth. Also, Pillis et al. [20, 21] conducted several studies on tumour growth with an immune response and chemotherapy from the viewpoint of phase-space analysis by varying the model parameters. The results show the importance of using optimal control therapy which is able to push the model into a desirable basin of attraction, in contrast to the classical periodic chemotherapy. By driving the model to the healthy stable state (disease-free state), the treatment can be stopped. More examples of using mathematical models to optimize chemotherapy treatment have been discovered by many researchers (e.g. [9, 93]), because the response of the immune system is not adequate on its own to defeat the tumour cells' growth where the tumour is immunogenic. The model studied by Pillis et al. [21] consisted of tumour cells, immune cells and normal or healthy cells where the competition between these cells varied depending on the cells themselves, the competition between the normal and tumour cells relying on the resources available, whereas the tumour and immune

cells compete in a predator-prey style.

Among all previous examples of different dynamical systems in different areas, researchers have investigated and drawn observations from the system behaviour analytically and numerically using different approaches while the dynamics of such systems has hardly been investigated from the perspective of information theory. We will now present a brief summary of the origin of information theory as an approach to examine the variability/sustainability of dynamical systems, supported by some examples.

In 1925, R. A. Fisher [26] was the first researcher to introduce the concept of information from a technical point of view during his work on estimation theory and to provide a definition of information for statisticians. In mathematics, information theory has developed as a relatively modern discipline for investigating systems such as decision making, estimating parameters, etc. Later, in 1948, Shannon and Wiener published their works describing the logarithmic procedure of information to be used in communication theory. Information theory can be applied in a wide range of fields due to its importance as a branch of the mathematical theory of probability and mathematical statistics [23, 26, 45, 84]. Fisher information is expressed as a measure to estimate a parameter or as a measure of collecting information, more than likely about the state of a system or as a measure of disorder of a system. Fisher, Shannon and Wiener were the people most responsible for developing and stimulating the basic mathematical and statistical characters of the theory of information. Later, Frieden [30] published a book that presented a measurement theory involving a new measure of information (not dependent on Shannon or Boltzmann Measures for entropy) which was relatively unknown to physicists by "Fisher information". Therein he demonstrated how Fisher information flows from a physical source impact to a data space and describes measurement scenarios not only in terms of physics but also science in general.

To that effect, information theory mathematically plays a significant role in the concept of entropy in thermodynamics and statistical mechanics. Comprehensive literature can be found regarding investigation of the relation between information theory and entropy (see [13, 27, 85]). It is recognized that Fisher information, regardless of the time

difference between the two (nearly twenty years), is a more robust tool when explored in relation to the concept of Shannon entropy and this is demonstrated by many different examples. To demonstrate this more logically, we now display the mathematical definition of Shannon entropy by the following formula:

$$H = S(p) = -\int p(x) \ln p(x)\, dx, \tag{1.3}$$

where $p(x)$ is a probability density in its continuous state. Whereas Fisher information index is defined as:

$$I = \int \frac{1}{p(x)} \left(\frac{\partial p(x)}{\partial x} \right)^2 dx. \tag{1.4}$$

x is vector-valued and $p(x)$ is the probability density function of x. From the two definitions above, we can conclude that both distinguish the contents of information from the probability density. On the other hand, there is a significant difference between them, namely that Shannon entropy is a global quantity while Fisher information is a local measure which strongly relies on the gradient of the Probability Density Function (PDF), Fisher information is a function of $p(x)$ and measures the degree of disorder (variability) of the system [74].

Since many researches have proved that the concept of Shannon entropy has an insufficient role in investigating quantum problems we do not have a "principle of entropy conservation" as such. Therefore, the evolution of a new concept of information is useful which goes beyond Shannon entropy ([58] and the references there in). The first information measure was applied by Fisher in 1925 [26] in mathematical statistics in order to measure information about an unknown parameter using the data provided. Then it became of interest for engineers, biologists, physicists and others. Generally, we require information whenever we start working on designing an experiment or conducting a statistical investigation. Based on the publication of a growing body of research to investigate deterministic and stochastic systems and their variabil-

ity/sustainability, the usage of Fisher information index has been widely explored. For example, Zwietering et al. [109] studied the similarities and differences among dynamical models in the view of sustainability. The models are rewritten in such a way that they contain perturbations in the model parameters.

The study of the variability/sustainability of dynamical systems is assessed in terms of Fisher information analysis. Based on its function as an index of the system's disorder, Cabezas et al. [14] used Fisher information as a statistical measure of change in order to investigate the sustainability of the model of five functional groups in addition to perturbation scenarios, seasonal forcing function. The regime of the model is determined by a set of values in which the state of the model fluctuates; in the case of absence of changes in the model variables, the model will continue to fluctuate in a stable state. On the other hand, it is more desirable to have changes in the model regimes because of their importance from the viewpoint of sustainability. Also, Nagy [65] showed that Fisher information can define the intrinsic accuracy where used to measure the narrowness of a distribution.

The simulation outcomes show that plausible steps such as improving the efficiency of immune cells and reducing cancer cells lead to a better ordered, more functional, and possibly more sustainable behaviour. On the other hand, simulation may display opposite results, leading to a less ordered, less functional and less sustainable behaviour. Therefore, due to its sensitivity, Fisher information is used to investigate the changes in dynamic regimes. Systems in the steady state do not lose or gain Fisher information over time. If a system has larger Fisher information this indicates that its variability has decreased (increasing its order), although these results may not be desirable. On the other hand, in the case of low Fisher information, this means that the system's variability has increased (loss of order) [13, 14, 29, 72].

The use of Fisher information has been suggested by many researchers who have conducted studies on the dynamical behaviour in prey as well as predators in different models that include oscillatory terms from the perspective of sustainability. For example, Rico-ramirez et al. [78] used Fisher information to choose the optimal parameter

values in three different dynamical systems for performing an assessment of the behaviour of Fisher information against the model parameters to measure which would lead to reduction of the variability in these systems. As a result, even Fisher information was not found very useful as a measure of sustainability in some dynamical systems but it was observed to have importance for detecting the variability in the dynamical systems presented in [78].

The above verbal description can be seen from a simple analysis of simple dynamical systems such as logistic model, Gomertz model and predator-prey model. The study's objective is inspired by the observed effects of modifications applied to these models. Specifically, for the predator-prey model (coupled logistic equations), we observe that a nonzero immunisation rate has an important effect on the functionality of the system. The fundamental difference between the previous works with dynamical systems and our work is that we are employing Fisher information as a measure of variability/sustainability.

A family of models have been investigated analytically as well as numerically to demonstrate different cases such as perturbed and non-perturbed models. In this thesis, we focus on the importance of parameters in the dynamical systems because changing parameter values allows the same model to show different behaviours. Therefore, the objective of this work is to evaluate and apply measures based on different dynamical models in order to detect these changes in their behaviour. A statistical tool was needed in order to deduce the statistical value of the simulation results. Instead of assuming the birth and death rates to be constant, we are interested in exploring some models in which the parameters fluctuate over time and both birth and death rates are density-dependent, otherwise the population will grow exponentially and there will be no crowding effects on the birth and death rates. In order to study the behaviour of dynamical systems using Fisher information, it is necessary to measure probability density function as a derivative of the Fisher information index.

Modifications on the model parameters have been applied by including a periodic modulation in order to track the behaviour of the system, such as to distinguish between

a non-oscillatory behaviour where the solution tends directly to the steady state, and an oscillatory behaviour where the solution fluctuates around the steady state. In other words, we extend the deterministic systems to make them stochastic by including a random perturbation in the systems' parameters in different positions. How do these modifications in the model parameters affect the functionality of those models?

Several dynamical systems were compared to describe a bacterial/tumour growth curve (or to describe the systems' sustainability/functionality) with and without a periodic perturbation from the viewpoint of the systems' sustainability and robustness. They were compared statistically by using Fisher information index as a measure of variability. Moreover, the models were compared with respect to their ease of use. Experimental scientists may find those results helpful to implement clinical trials. Specifically, we believe that special attention is required to control the growth of the cancer population as cancer is the most terrifying killer in the modern world.

A system of three dynamical equations is performed for three species (a group of cells) that coexist and fight for survival, to detect the relation of changes in Fisher information with this system' sustainability, regime change and performance. Fisher information has been used as a variability/sustainability index by looking for a nonsustainable case which exists when one of the species (cancer population) becomes extinct. Different treatment doses are estimated in order to obtain the most desirable case (optimal dose) for eradication of the cancer cells [78].

This thesis specifically focuses on the dynamics and variability/sustainability for different dynamical systems and aims to improve Fisher information efficiency in the case of including a periodic fluctuation in the system parameters. One way to achieve this goal is to track the behaviour of the models presented in this thesis by changing the parameter values. In order to do so, we extend the deterministic models to include a periodic modulation in the model parameters, then we use Fisher information index as a measure of variability/sustainability, followed by a sequence of tests with the aim of drawing a general conclusion. The results from other researchers, in addition to our extensions, are assumed to be very valuable and significant.

1.2 Overview of the thesis

In this work, for the convenience of the reader, we briefly review several models with one, two and three components (one or more species) in their deterministic conditions, then, we modify them by including perturbations in the model parameters, and investigate these models analytically as well as numerically from the point of view of variability/sustainability using Fisher information approach. The structure of this thesis is organized as follows:

Chapter Two begins with a brief introduction about the logistic model and Fisher information. First we describe the deterministic logistic model by giving a short summary of its dynamic and stability. Then, we explain the modification made to the logistic model in three different cases, with focus on the first case where a periodic modulation is added to the positive and negative feedback, and the behaviour of the model monitored for different parameter values. For each case from the above, the analytical study and numerical simulations are described. We present the calculations of Probability Density Function (PDF) formula to characterise the detailed dynamics of the logistic model at different values of ω and x_0. We also explain the construction of the mathematical definition of Fisher information in order to investigate the variability/sustainability of the logistic model at different values of ω and x_0 with particular attention to the description of the significant characteristics of the perturbed logistic model. The other two cases of the logistic model with perturbations in the positive or negative feedback are presented in addition to the PDF at different values of ω. The conclusions are also included in this chapter. (This work is already published in the Mathematical Bioscience Journal [5]).

In Chapter Three, we explain calculation of the Fisher information index for the perturbed Gompertz model and compare the results with those for the logistic model presented in Chapter Two. This chapter begins with a brief summary regarding the work done for the Gompertz model, and then we present the investigation of the de-

terministic and perturbed Gompertz model analytically and numerically. Our goal is to observe the different behaviours of the Gompertz model by monitoring the model parameter values which regulate its behaviour. Modifications are applied to the Gompertz equation and we concentrate on the case where a periodic modulation appears in both positive and negative feedback for different parameter values. Then, we find PDF and Fisher information values at different initial conditions. In section 3.8, we display the other cases of Gompertz equation when a periodic perturbation is considered in the positive or negative term. Finally, conclusions are included in the last section. (The observations above are organised in a draft and ready for submission).

In Chapter Four, we provide an overview of the predator-prey model which represents the tumour-immune system in the first section. The analysis of local stability is conducted about the equilibrium points, and the corresponding biological effects are noted for the deterministic coupled logistic equations in addition to Fisher information plot as a function of prey mortality rate connected to the PDF. We also modify the two-components system to include a logistic expression in the prey growth rate (cancer cells population) and a periodic modulation (immunotherapy treatment) is included in the second equation which stands for immune cells population to mimic the cancer population and enhance the growth of the immune cells. Again, Fisher information index is employed in this section. This chapter ends with brief conclusions. A dimensionless formula for the predator-prey model is provided in separated appendix.

The first section in Chapter Five provides an introduction to the three-components system. Then, we introduce a mathematical model of three interacting cell populations, its dynamics and equilibria. It is hard to obtain the analytical solution as the model contains complex mathematical expressions. Valuable modifications to the model parameters are introduced in order to deduce their effects on the behaviour of the cancer cells population and to conclude the most important properties of the three species system. The analysis of the impact of the model with a periodic perturbation is performed. Moreover, the importance of the choice of amplitude value is demonstrated along with the Fisher information. In this chapter, Fisher information index is successfully em-

ployed in order to detect the significant parameter values in which the cancer cells are eradicated. Finally, a summary of findings is included in the last section.

The final chapter concludes the thesis by discussing the key observations and possible refinements of the proposed Fisher information index. We also offer a future perspective of potential topics which may be worthy of study by future researchers. It is hoped that the results and explanation for the three different models will help clarify the purpose of using Fisher information and provide simple solutions to deal with such problems.

Chapter 2

The logistic model

2.1 Introduction

The nonlinear dynamical systems have been applied to complex phenomena as simple models, e.g. in astrophysical and geophysical, environmental and biological systems. Specifically, in the last few years, it has been observed that these models can make a useful contribution in understanding biological systems as ever-improved experimental data has become available. In 1838, Verhults was the first scientist to suggest the use of a logistic model (which is sometimes called the Verhulst model) to describe population growth (see [56, 88]). In particular, the logistic model is widely used to model the growth of biological systems such as tumour cells, bacteria, etc. (see e.g. [39, 108] and the references there in). As an average field equation, the comprehensive impact of micro-scale (small-scale) variables is found by control parameters for both positive and negative feedback, while the time evolution of macroscopic (large-scale) variables has been described by the logistic model.

The logistic equation is often used in its continuous state and is expressed by a differential equation rather than being a discrete variable expressed by a difference equation (see [35, 67]). An equilibrium point (the so-called carrying capacity) results from the

balance between the positive and negative feedback where the system reaches its equilibrium point over a long period of time regardless of the initial condition of the system. Therefore, we observe a single value of a carrying capacity with the loss of the memory of the initial point (The system does not remember its initial condition). The simplicity of the complementary effects of the positive feedback which represents the growth of the population in the logistic equation and the negative feedback (which regulates its growth) provided the motivation to investigate the logistic model in detail, thus we employ the simplest model for a self-regulated system where the growth is organized within a system.

The dynamic and sustainability of complex nonlinear dynamical systems have been investigated using information theory. They have been especially studied using Fisher information as a valuable measure of variability/sustainability of dynamical systems including self-organising systems. This is mainly achieved by investigating the logistic model's variability/sustainability for different perturbations in positive and/or negative feedback using Fisher information.

The logistic model with perturbations in the model parameters by periodic or random modulation (e.g. [3,39,50,52,57,76,101,102,104]) or to couple the evolution of other systems (e.g. [15]) has been investigated by many researchers to study its response and behaviour, such as, a bimodal probability density function was found in the case of a correlation between a multiplicative noise in the positive feedback and an additive noise. Our motivation is to investigate the logistic model's variability/sustainability for different perturbations. Here we calculate Probability Density Function (PDF) for different modulations in the model parameters and clarify the basic mechanisms that determine the form of PDF. We will see the case where the system maintains a long-term memory of initial values leading to a broad bimodal distribution. This is mainly achieved when the perturbation time scale is much shorter than the system's response time. We compute Fisher information averaged over the total time (F_T) to study the variability/sustainability of a system in different cases. We illustrate that a purely oscillatory growth rate can lead to a finite amplitude solution, while self-organisation

of these systems can grow exponentially as the negative feedback includes a periodic fluctuation. Also, a periodic stimulus is added to the logistic model to examine the most sustainable state derived from F_T analysis.

It should also be noted that the growth of cell populations driven by fluctuating environments has been investigated (see e.g. [95]); furthermore, the effect of different oscillatory modulations in the system's parameters has been studied in other dynamical systems (e.g. [25, 62, 63, 75, 87, 89]), whereas the functionality of these systems from the information theory perspective is not obvious.

The remainder of Chapter Two is organized as follows. We introduce our model in Section 2.2 and the logistic model with perturbations in different cases in Section 2.3. In Section 2.4 we describe the characteristic properties of the logistic model when the model parameters for both positive and negative feedback have the same periodic perturbation, the computation of PDF, and Fisher information analysis. Additionally, we describe testing the stability of our system by adding periodic stimulus. In Section 2.5, we summarise the results for different types of modulation of the model parameters. Conclusions are provided in Section 2.6.

2.2 The model

We can represent the dynamics of a population x (> 0) with a logistic equation as follows:

$$\frac{dx}{dt} = Nx\left(1 - \frac{x}{K}\right). \tag{2.1}$$

Here, N (> 0) is the net growth rate, and K (> 0) is the carrying capacity of the system representing the maximum population size that can be supported by the system, in other words, the carrying capacity is specified through the system resources in which the population will be embedded. The system in Eq. (2.1) has two possible steady

states $x_1^* = 0$ and $x_2^* = K$. While x can represent the population of any species of interest such as tumour, rabbit, bacteria, etc., it must be remarked that x in this study is assumed to be the population of bacteria to be specific unless stated otherwise. The linear term Nx with $N > 0$ represents the net effect of bacteria growth (e.g. by eating food) and its death (e.g. by nature death, or antibiotics) which affords a positive feedback, whereas the nonlinear term Nx^2/K represents a negative feedback due to the crowding effect as their growth is inhibited by limited resources. For a constant $N > 0$, x reaches the carrying capacity K as $t \to \infty$ regardless of the initial value of $x(t = 0) = x_0$ (see Fig. 2.1). The numerical and analytical solution is easily found for Eq. (2.1).

If the population x is smaller than K, the growth of the population will increase exponentially with a high percentage whereas for small value of x, the parenthesis is small in which the population grows very slowly. Finally, if the population x exceed the certain carrying capacity (K), then the growth of the population will grow negatively where *"The death rate is higher than the growth rate"* [60, 91, 92]. Fig. 2.1 shows the behaviour of the population for different initial conditions $x(t = 0) = x_0$.

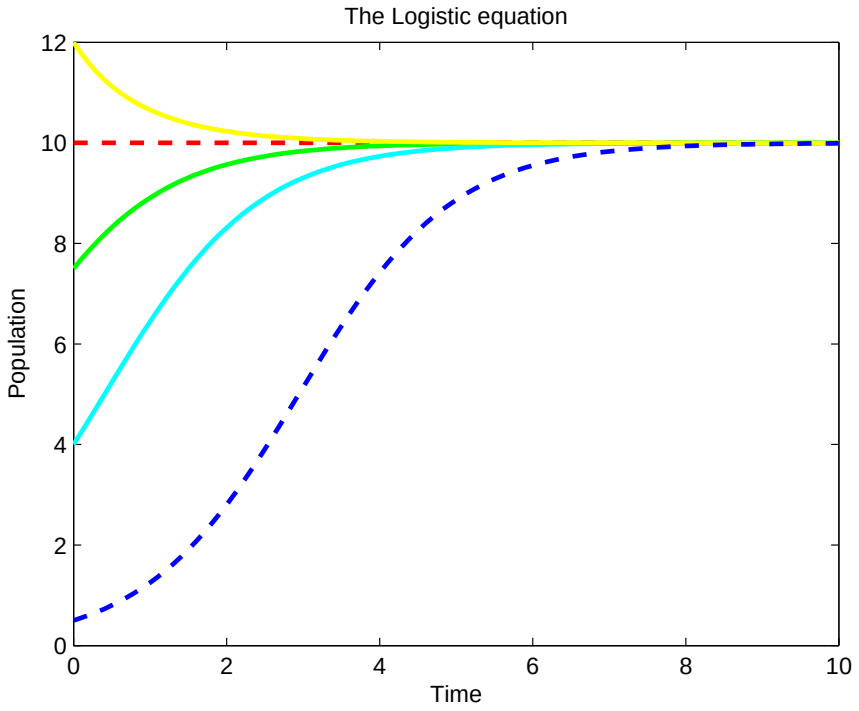

Figure 2.1: Different colours represent different initial conditions, the population shows a transient growth followed by exponential growth, then approaches the equilibrium point at $x = K = 10$ where convergence to K happens from any initial state.

2.3 The logistic model with oscillatory parameters

For the constant net growth rate N in Eq. (2.1), the logistic model has widely been investigated. This is in contrast to the case when the negative feedback contains a periodic perturbation such as the results presented in [50, 104], where a decrease in self-regulation is noticed. We show some characteristics of the cases where the model parameters for only positive or negative feedback contain a periodic perturbation (cyclic variations) while our main concern is the case where the a periodic perturbation in positive and negative feedback is strongly correlated. This is mainly achieved by replacing the constant growth rate N by the following periodic modulation:

$$N = B + N_0 \sin(\omega t), \tag{2.2}$$

where B is a constant growth, while N_0 and ω are the amplitude and frequency of the periodic modulation.

We use numerical and analytical methods to analyse the logistic system (after adding a combined term of constant and purely oscillatory part) in three different cases. It must be pointed out that for the first two cases, the oscillatory control parameter effects vanish for the large values of ω, while the results are different for the third case of the logistic system. For this reason, we examine the behaviour of the system for $B = N_0$ where we observe that the solution grows boundlessly for smaller values of ω.

The three different cases of the logistic equation are governed by the following nonlinear ordinary differential equations:

Case-1:The same perturbation in the positive and negative feedback

$$\frac{dx}{dt} = [B + N_0 \sin(\omega t)]\ x\ (1 - \frac{x}{K}).$$

Case-2: Perturbation in the positive feedback

$$\frac{dx}{dt} = [B + N_0 \sin(\omega t)]\ x - \frac{Cx^2}{K}.$$

Case-3: Perturbation in the negative feedback

$$\frac{dx}{dt} = Cx - \frac{[B + N_0 \sin(\omega t)]\ x^2}{K}.$$

We will go through each case separately as in the following sections:

2.4 Case-1 : The same perturbation in the positive and negative feedback

$$\frac{dx}{dt} = [B + N_0 \sin(\omega t)]\ x\ (1 - \frac{x}{K}). \tag{2.3}$$

The analytical solution to Eq. (2.3) is found as in the following expression:

$$x(t) = \frac{-Kx_0 \exp\left(Bt + \frac{N_0}{\omega}(1 - cos(\omega t))\right)}{(x_0 - K) - x_0 \exp\left(Bt + \frac{N_0}{\omega}(1 - cos(\omega t))\right)}, \tag{2.4}$$

where x_0 is the initial value of x at $t = 0$ and $K = 10$. For comprehensive understanding of the system, for $B = 0$, we present results for different values of N_0 and ω in $3D$ plot, with $x - axis$ represents the values of N_0, $y - axis$ stands for the values of ω and $z - axis$ shows maximum values of x in Eq. (2.3) as follows:

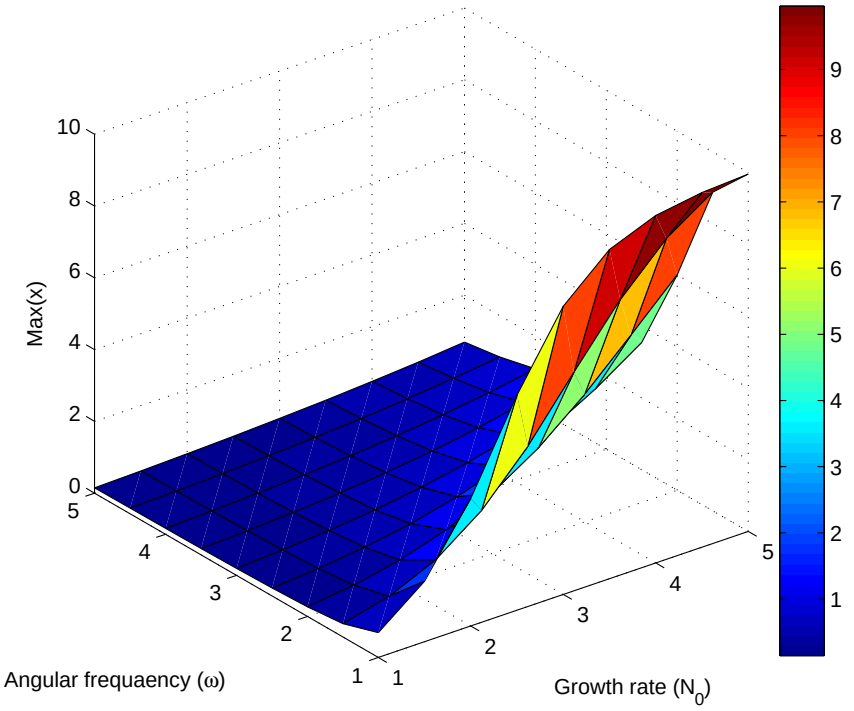

Figure 2.2: $3D$ plot of the maximum values of x, $Max(x)$, in $z - axis$, N_0 in $x - axis$ and ω in $y - axis$. $Max(x)$ values are monotonically decreasing as ω increases for $K = 10$, $B = 0$, and $x_0 = 0.1$.

Fig. 2.2 shows maximum values of x as a function of N_0 and ω. We observe that the

maximum values tend to monotonically increase with the modulation amplitude for small values of ω and decrease as ω increases. This leads to conclude that x does not deviate far from its initial values, effectively leading to the maintenance of the memory of its initial values for large values of ω.

2.4.1 Results for fixed ω and varying N_0

In this section, we consider the effect of varying N_0 on the behaviour of the system in Eq. (2.3) for different values of $\omega = 1, 5$, and 10 (these particular values of ω are chosen arbitrarily).

Fig. 2.3 shows that for $\omega = 1$ (red dashed-line), the solution grows exponentially as N_0 increases, then a stable equilibrium point at the carrying capacity $K = 10$ is observed, and convergence to K occurs when $N_0 \geqslant 5$. That is, the effect of the periodic perturbation disappears for a sufficiently large N_0, such as $N_0 \geqslant 5$. Similar behaviour is noticed for $\omega = 5$ and 10 (blue and green dashed-lines), but the difference is the value of N_0 where the solution approaches its asymptotic value as shown in Fig. 2.3.

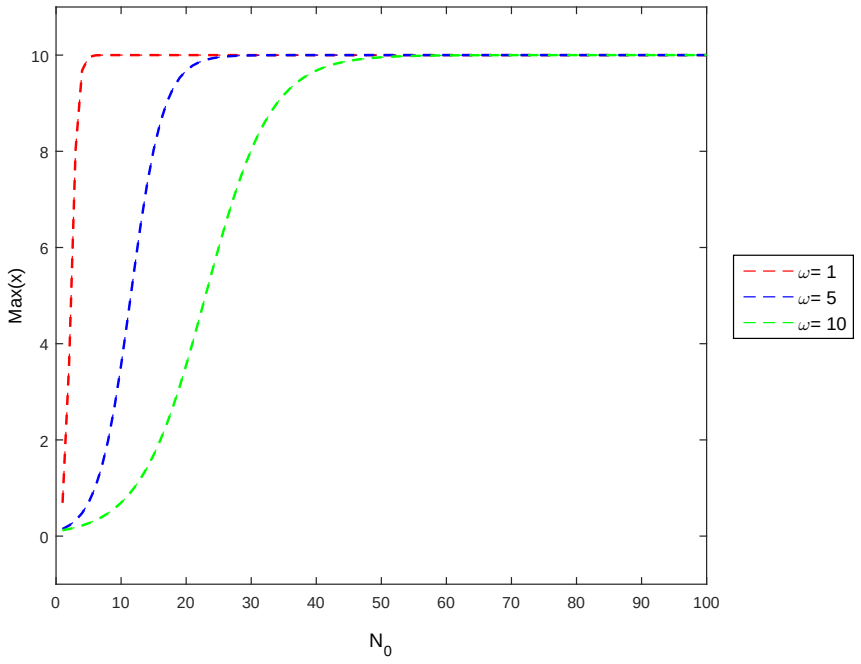

Figure 2.3: Maximum values of x for varying N_0 and different values of ω, $x_0 = 0.1$, $B = 0$. The difference between the above curves is the time that the population spend before showing a steady state at the carrying capacity $K = 10$.

In consideration of the above figure, there has been much interest in finding the relationship between N_0 and ω, where the other parameter values are fixed, such as $x_0 = 0.1$, $B = 0$ and $K = 10$. We vary N_0 and ω in order to observe the dynamics of the system. The system is linearly increasing as N_0 and ω increase, this leads to a linear relationship as we can see in table (2.1) and Fig. 2.4, which means that as ω increases, then N_0 increases.

Table 2.1: Different values of ω and N_0

ω	N_0	**mean**		ω	N_0	**mean**	
1	5	5.2809		42	210	5.2808	
1.5	7.5	5.2804		56	280	5.2808	
2	10	5.2806		62.7	313.5	5.2808	
4.4	22	5.2809		75	375	5.2808	
6	30	5.2807		78	390	5.2808	
10.1	50.5	5.2808		80	400	5.2808	
15	75	5.2807		90	450	5.2808	
18	90	5.2808		105.9	529.5	5.2808	
24.5	122.5	5.2808		120	600	5.2808	
30	150	5.2808		150	750	5.2808	

For example, when $\omega = 1$, we plot $Max(x)$ on the $y-axis$ and N_0 on the $x-axis$, we observe that the solution reaches carrying capacity $K = 10$ when $N_0 = 5$, by choosing different values of ω, we obtain the above table (Table 2.1), and we present the results from the above table in the following figure:

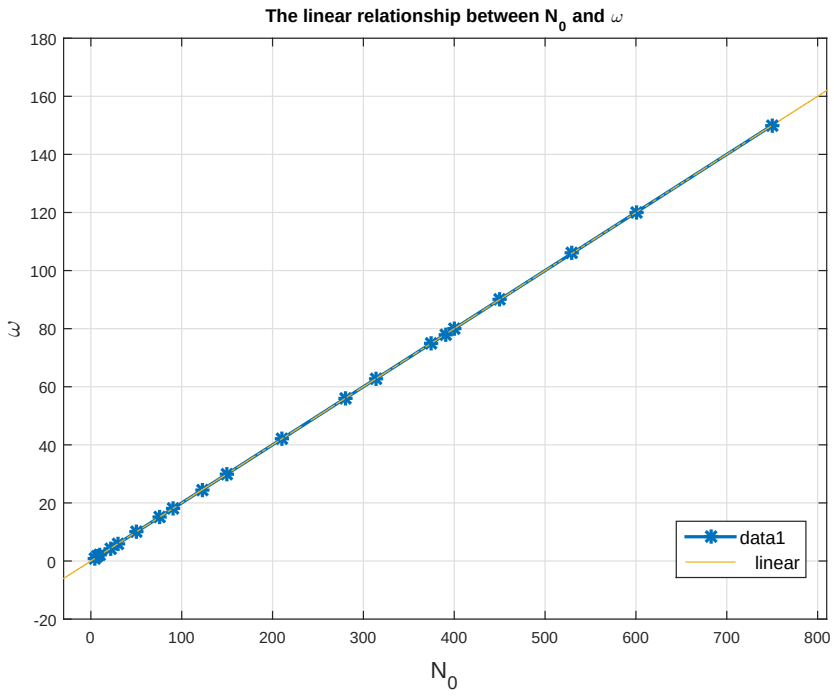

Figure 2.4: The linear relationship between N_0 and ω with fixed values of $K = 10$, $B = 0$ and $x_0 = 0.1$.

The most common characteristic in Fig. 2.4 is that ω shows a linearly increasing function of N_0. The stars in the above figure represent the intersection values of N_0 and ω where we find a basic fitting for our data as $y = 0.2x + 1.3077e - 14$, with $1.3077e - 14$ as a norm of residuals and this fitting curve can be seen as a yellow line in Fig. 2.4.

2.4.2 Results for fixed N_0 and varying ω

In this section, for $B = 0$, we fix N_0 and K to be $N_0 = 5$ and $K = 10$ in order to investigate the influence of varying ω (the angular frequency in the periodic modulation) on the logistic model response as t and x can always be re-scaled by N_0 and K, respectively. From the analytical solution in Eq. (2.4), our interesting observation is the cross-over behaviour of x between x_0 and K in the limit of increasing t. For instance, when $B = 0$, the fluctuates between $|N_0|$ and $-|N_0|$ in time with zero average. More

specifically, at times when $\omega = 0$, $\cos(\omega t) = 1$, x takes its minimum value $x_{min} = x_0$ while at times when $\cos(\omega t) = -1$, x reaches its maximum value as in the following expression:

$$x_{max} = \frac{K x_0}{x_0 + (K - x_0)\exp\left(-\frac{2N_0}{\omega}\right)}. \tag{2.5}$$

One interesting feature of the case $B = 0$ is where the killing impact from natural death or antibiotics is quite strong. In population genetics, this case would correspond to the random sampling of gametes with no selective advantage (see §6-7 in [42]) if the periodic modulation is replaced by a short-correlated noise. In the following, we show one of the results of the same periodic perturbation in positive and negative feedback which is the maintenance of an initial condition and bimodal distribution.

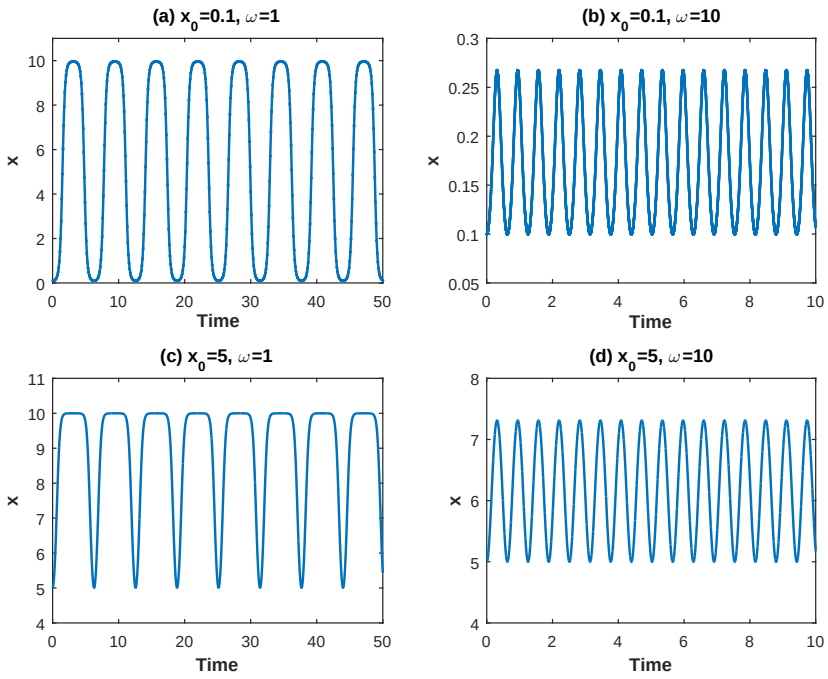

Figure 2.5: Time trace of x for different values of $x_0 = 0.1, 5$ and $\omega = 1, 10$. For a small value of ω, x tends to reach the carrying capacity $K = 10$ while for large ω, x maintains its initial conditions.

In Fig. 2.5, we investigate the dynamics of the logistic model for different values of ω and x_0. The first interesting observation of this model is that the minimum values

of x are equal to x_0, as analytically predicted above. On the other hand, maximum values of x according to Eq. (2.5) are the same maximum values in Fig. 2.5(a)-(d). For example, $x_{max} = 0.2672$ in Fig. 2.5(b) and this is mainly obtained by Eq. (2.5) where $K = 10$, $x_0 = 0.1$, $N_0 = 5$ and $\omega = 10$. One more interesting characteristic is that the system maintains its initial conditions for sufficiently large ω in which the time-scale of the perturbation is much shorter than the system's response time. This is because as the population x starts with a small initial value, can never reach the carrying capacity of the system $x = 10$ due to frequent periodic change in the constant growth rate N, staying close to $x = x_0$ as the bacteria do not have enough time to undergo a fundamental exponential growth before they dissolve. That is, the time interval when $N > 0$ is too short for large ω. As a result, the population of bacteria fluctuates only near $x = x_0$, never reaching the carrying capacity K. In comparison, for a sufficiently small ω, the time-scale of the perturbation becomes much larger than the growth rate (i.e. the mean square root value of the growth rate), and in this case, x will be able to reach the carrying capacity regardless of x_0. That is, as there is enough time for the bacteria to grow when $N > 0$ before decaying when $N < 0$, allowing the bacteria to increase. Mathematically, this is because a fast exponential growth during the time with $N > 0$ wins over the decay during the time with $N < 0$.

In consideration of the above figure, there have been two cases of the population, and much interest on the case where a cross-over between $x \to K$ and $x \to x_0$ is observed. We illustrate these cases of x in Fig. 2.6(a)-(d), where we plot the maximum and minimum values of x (in time) on the $y - axis$ in blue solid line and red dashed-line, respectively, against ω on the $x - axis$. In detail, we use two different initial values for x to be $x_0 = 0.1$ and $x_0 = 5$ in Panels (a) and (b), respectively while we show Panels (a) and (b) in log-log scale in Panels (c) and (d) in order to have a close look for small ω. As a result, we present how the maximum values of x are monotonically decreasing as ω increases.

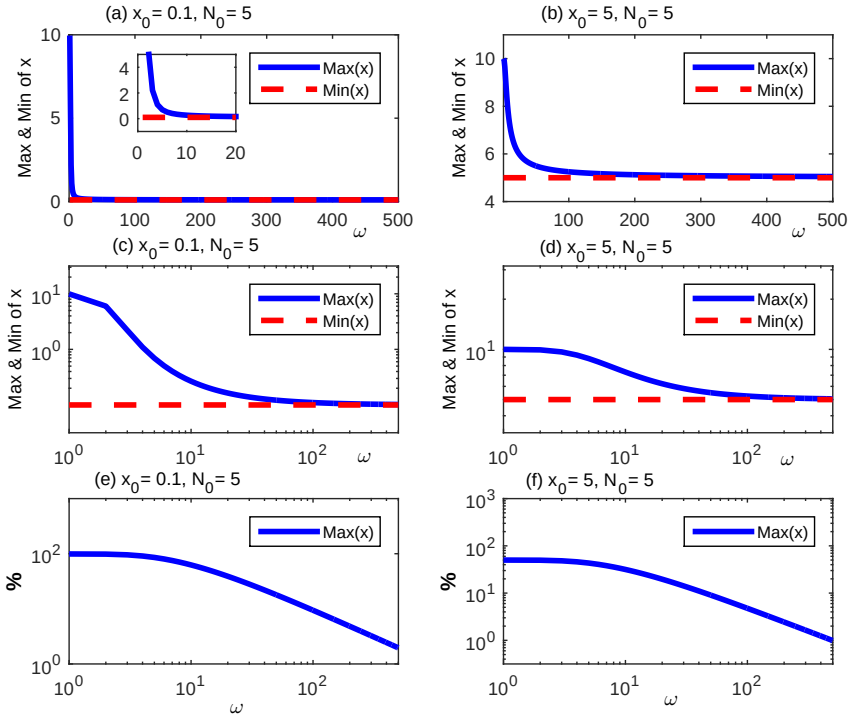

Figure 2.6: Maximum and minimum values of x against ω for $N_0 = 5$ and $K = 10$ with $x_0 = 0.1$ in panels (a), (c) and (e) and $x_0 = 5$ in panels (b), (d) and (f). (c), (d), (e) and (f) are shown in log-log scale.

There is also an evidence from the analytical solution in regards to the minimum of x which is approximately equals to x_0 as we can see in panels (a), (b), (c), and (d). On the other hand, for the maximum values of x and for the two cases of different initial points $x_0 = 0.1$ and $x_0 = 5$, there is an essential difference which is a much steeper decrease in the maximum curve for $x_0 = 0.1$ than for $x_0 = 5$. As the maximum values of x are obtained by the approach to the carrying capacity, the steep drop in the maximum represents the inability of the system to grow and reach this carrying capacity when the control parameter changes too rapidly in time for larger values of ω, as noted previously. In this light, x does not deviate far from its initial values, effectively leading to the maintenance of the memory of its initial values. This is consistent with the results shown in Fig. 2.5. In the following expression we compute the ratio of the change in the maximum of x to determine the maintenance of initial

conditions.

$$\left(\frac{\textbf{Initial value} - \textbf{Maximum of } x}{\textbf{Maximum of } x}\right) \times 100\ \%. \tag{2.6}$$

For sufficiently large $\omega \gg 1$, we observe nearly straight lines in Fig. 2.6(e)-(f) which indicates that the percentage change decreases with ω as a power-law in both cases where Panels (e) and (f) are presented in log-log scale.

2.4.3 Probability Density Function

In this section, we present our efforts to show the influence of ω and x_0 on the Probability Density Function (PDF). According to the method proposed by Cabezas et al. [13, 25] and Rico-ramirez et al. [78], we calculate the PDF of x by relating the probability of observing the system at a particular value of x to the amount of time the system state spends at x through conservation of the probability:

$$p[x]\, dx = p[t]\, dt. \tag{2.7}$$

Since t is a continuous variable with a uniform probability density:

$$p[t] = constant = A, \tag{2.8}$$

we obtain PDF of x from Eqs. (2.7)-(2.8) as:

$$p[x] = p[t] \left|\frac{dt}{dx}\right| = A \left|\frac{dt}{dx}\right| = \frac{A}{u}, \tag{2.9}$$

where

$$u = \frac{dx}{dt}. \tag{2.10}$$

Since u is simply given by Eqs. (2.1)-(2.2), then, we can express $p[x]$ in Eq. (2.9) as:

$$p[x] = \frac{A}{(B + N_0 \sin(\omega t))\; x\; \left(1 - \frac{x}{K}\right)}. \tag{2.11}$$

Here, we need to consider Eq. (2.4) and replace it by a function which only depends on x, as Eq. (2.11) contains the time-dependent function $(\sin \omega t)$. As a result, we present $(\cos \omega t)$ as follows:

$$\cos(\omega t) = 1 + \frac{\omega}{N_0} \ln\left[\frac{x_0\,(x - K)}{x\,(x_0 - K)}\right], \tag{2.12}$$

and by using the expression $\left(\sin(\omega t) = \sqrt{1 - \cos^2(\omega t)}\right)$, we obtain $(\sin(\omega t))$ in Eq. (2.11) from Eq. (2.12). By using Eqs. (2.11) and (2.12), we present the PDFs of x for different values of ω in Fig. 2.7.

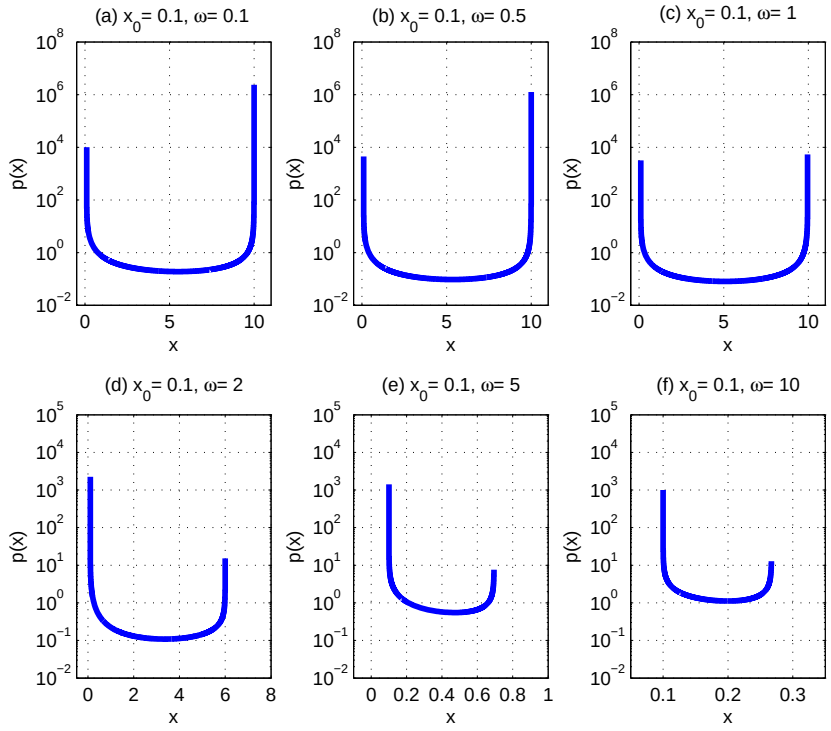

Figure 2.7: PDF of x for $N_0 = 5$, $B = 0$, $K = 10$ and $x_0 = 0.1$. Different values of ω are used in panels (a)-(f). A bimodal PDF is observed for all the cases.

The most interesting feature in Fig. 2.7 is a bimodal PDF for different values of ω with different distance between the two peaks. This bimodal distribution is the outcome of

the maintenance of the initial condition $x_0 = 0.1$ (left peak) against the tendency of x getting closer to a carrying capacity ($10 = K$) (right peak), as mentioned earlier. In particular, we observe that for sufficiently large $\omega \gg N_0/2\pi$ and small initial conditions (far from the carrying capacity), x can never reach $x = 10$ because of frequent periodic change in N, where the time-scale of perturbation is much shorter than the growth rate. Therefore a very tight distribution has found close to the initial values due to the case when the system remember its initial values (population at the start). On the other hand, for small $\omega \ll N_0/2\pi$, x reaches the carrying capacity regardless of x_0 where the time-scale of the perturbation is much larger than the growth time. As a result, it must be noted that the figure above show a PDF with two peaks, the first one at the initial value $x_0 = 0.1$ and the second peak appears at the carrying capacity $x = 10$. In this light, for the parameter $N_0/\omega = 5$, it is observed a bimodal PDF with broadest distance between the two PDF peaks. Therefore, we can conclude that the right peak reduces for large ω in contrast with the left peak at the starting point which is getting higher followed by the narrowing of the PDF.

In consideration of the above observations about the system's PDF and its initial conditions, in Fig. 2.8 we show a PDF for different values of ω when $x_0 = 5$. A bimodal PDF with different distance between the two peaks is noticed for all cases as ω increases. For small ω, x reaches the carrying capacity while for large ω, x starting far from $x = 10$ can never reach $x = 10$ and only fluctuates around $x_0 = 5$. In a comparison between the PDF in Figs. 2.7 and 2.8, the left PDF peak around $x_0 = 5$ has no significant growth for any value of ω before the PDF get tight in Fig. 2.8. In other words, narrowing of the PDF occurs while the right PDF peak is still larger than the left PDF peak. Specifically, in Fig. 2.7(c) just before the narrowing of the PDF, the height of the left peak is about [99.9981]% of the height of the right peak while in Fig. 2.8(b), the height of the left peak is only [49.6632] % of the right peak.

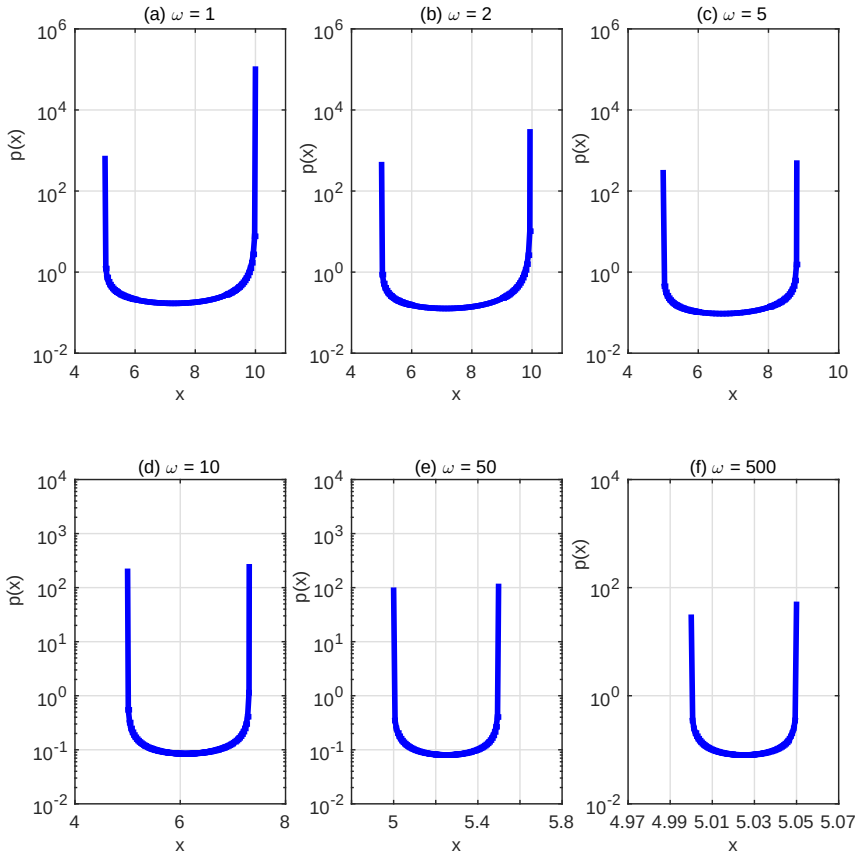

Figure 2.8: PDF of x for $N_0 = 5$, $B = 0$, $K = 10$ and $x_0 = 5$ by using different values of ω in panels (a)-(f). A bimodal PDF with different distance between the two peaks is observed for all the cases.

The fact that the PDFs in Fig. 2.8 show significant peaks at $x = x_0$ and $x = K$ leads to the difference in PDFs with $x_0 = 0.1$ and $x_0 = 5$. In particular, for a constant amplitude N (population growth rate), the logistic equation possess a stable fixed point and unstable point which correspond to the blow-up points of Eq. (2.11) at $x = 0$ and $x = 10$. Thus, the closest x_0 to $x = 0$, the higher the left peak around x_0 as seen in the case of $x_0 = 0.1$. When x_0 is far from $x = 0$ (as in the case of $x_0 = 5$), the PDF does not form such a high peak around x_0.

We illustrate these features using Fisher information as indicated below. For initial conditions $x_0 = 0.1$ (much less than K), there is an optimal value of ω (satisfying $\frac{N_0}{\omega} =$

5), which can maintains the distinct bimodal PDF with the largest distance between the two PDF peaks whereas for the initial condition $x_0 = 5$ (closer to K), such an optimal value of ω does not exist because the peak at $x_0 = 5$ is not significant, as noted above. The implication of the existence of such an optimal value of ω will later related to the utility of Fisher information as a measure of the sustainability.

2.4.4 Fisher information

Previous sections discussed the behaviour of the logistic model when the model parameters contain a periodic fluctuation. We now use Fisher information index to track this behaviour. In Fig. 2.9, we show different levels of Fisher information as a measure of variability of the observations, for example, we observe larger Fisher information where a PDF bias to a certain x values while a system with high disorder leads to small Fisher information (e.g. "unbiased" PDF).

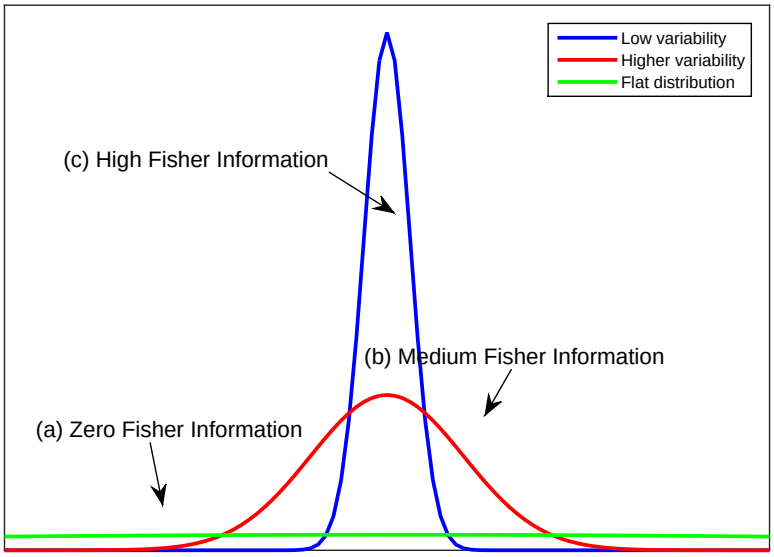

Figure 2.9: (a) A uniform PDF with zero Fisher information, (b) A PDF of x with medium Fisher information and (c) A steeply sloped PDF of x with large Fisher information (high gradient).

Previous work suggested the following sustainability hypothesis: *"sustainable systems do not lose or gain Fisher information over time*" [25, 28, 78].

Fisher information index plays a significant role in the improvement of the sustainability fundamental theory, for example, this has been especially invoked to determine whether a system is sustainable or not in various physical systems (see [34, 78, 81] and the references there in). We recall that Fisher information is a very special uncertainty measure; in contrast to a global measure of uncertainty (e.g., variance, or Shannon's entropy), Fisher information strongly depends on the gradient of the PDF, consequently, it is sensitive to the local oscillatory character of the PDF and relabelling [72, 81, 86, 87].

Cabezac and Fath [25] computed Fisher information for a single variable x from the PDF of x, $p(x,t)$, as follows:

$$I = \int \frac{1}{p[x]} \Big(\frac{dp[x]}{dt} \Big)^2 dt. \tag{2.13}$$

We note that Eq. (2.13) can be extended to n-dimensional system as follows:

$$I = \int \frac{1}{p[x]} \Big[\sum_i^n \Big(\frac{\partial p[x]}{\partial x_i} \frac{dx_i}{dt} \Big) \Big]^2 dt.$$

The time averaged Fisher information (F_T) is calculated by employing Eqs. (2.9), (2.10) along with

$$\frac{dp[x]}{dt} = -\frac{A}{u^2} \frac{du}{dt},$$

in Eq. (2.13) as follows:

$$F_T = \frac{1}{T} \int_0^T \frac{1}{A} \Big(\frac{dp[x]}{dt} \Big)^2 dt = \frac{A}{T} \int_0^T \frac{1}{u^4} \Big(\frac{du}{dt} \Big)^2 dt. \tag{2.14}$$

Here, A is a normalization constant, and F_T is the Fisher information averaged over the total time duration T. In the following figures, we examine the logistic model's

variability/sustainability through calculating F_T for different cases using Fisher information form in Eq. C.4 [1]. We display F_T for different values of ω and for the two initial values of x_0, $x_0 = 0.1$ and 5, and as before we fix values of $N_0 = 5$, $B = 0$ and $K = 10$.

By changing the total time period T for fixed ω and x_0, we calculate F_T, for example, by using $t = [0, 10]$ with $T = 10$, $t = [0, 20]$ with $T = 20$, and so on and show F_T as a function of T. For fixed initial value $x_0 = 0.1$ which is the same as in Fig. 2.7 and for different $\omega = 0.1, 0.5, 1, 2, 5, 10$, we show F_T against T in panels (a)-(f) in Fig. 2.10. For each panel in Fig. 2.10, we employ 1000 data points for $T = 10n$ ($n = 1, 2, 3, ..., 1000$). The common feature for each panel is that F_T is initially subject to transient state then show a static state for a sufficiently large T. In this light, it must be pointed out that the higher asymptotic value of F_T can be seen at $\omega = 1$, whereas the smallest F_T value observed for $\omega = 0.1$.

In consideration of the results in Fig. 2.10, we present F_T with ω in Fig. 2.11 in order to observe how F_T values change as ω increases.

[1] The whole calculation of finding Eq. C.4 is presented in Appendix C

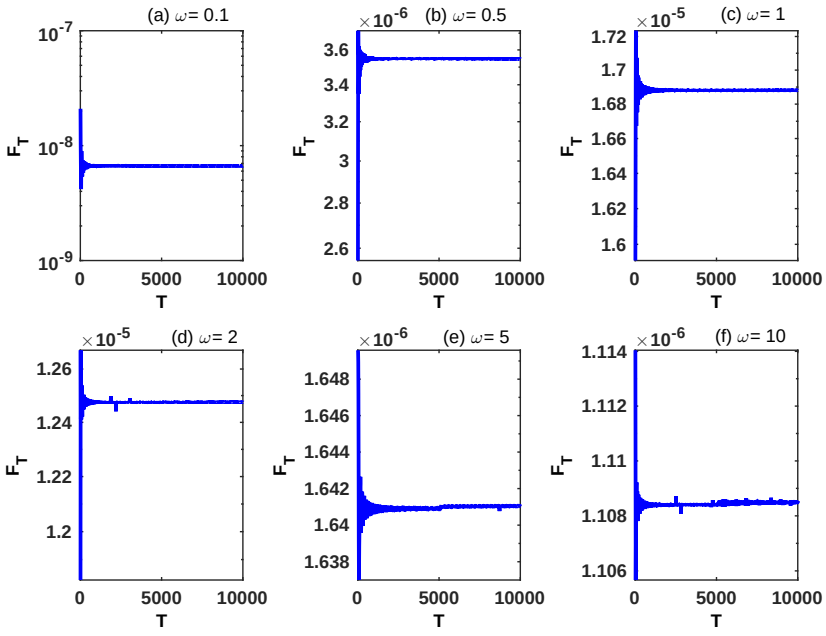

Figure 2.10: F_T against the total time T for $N_0 = 5$, $x_0 = 0.1$, $K = 10$, $B = 0$ and different values of ω. We observe a larger value of F_T at $\omega = 1$.

The interesting feature of the curve in Fig. 2.11 is the existence of a featured maximum F_T around $\omega \simeq 1$ which is associated to the presence of the optimal ω with the maintenance of a bimodal PDF with the two well-separated peaks, discussed with regard to Fig. 2.7.

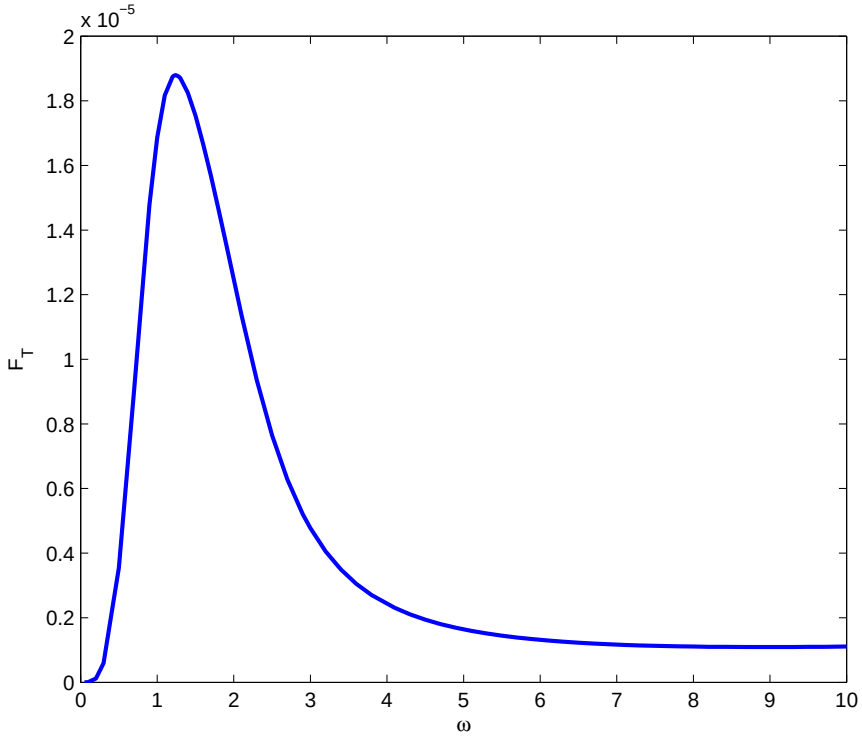

Figure 2.11: Asymptotic values of F_T against ω for $x_0 = 0.1$, $N_0 = 5$, $B = 0$ and $K = 10$.

In consideration of the above results, we show another case with different initial value $x_0 = 5$ with respect to Fig. 2.8. F_T values increase as ω increases without showing any distinct maximum in a comparison of Fig 2.11.

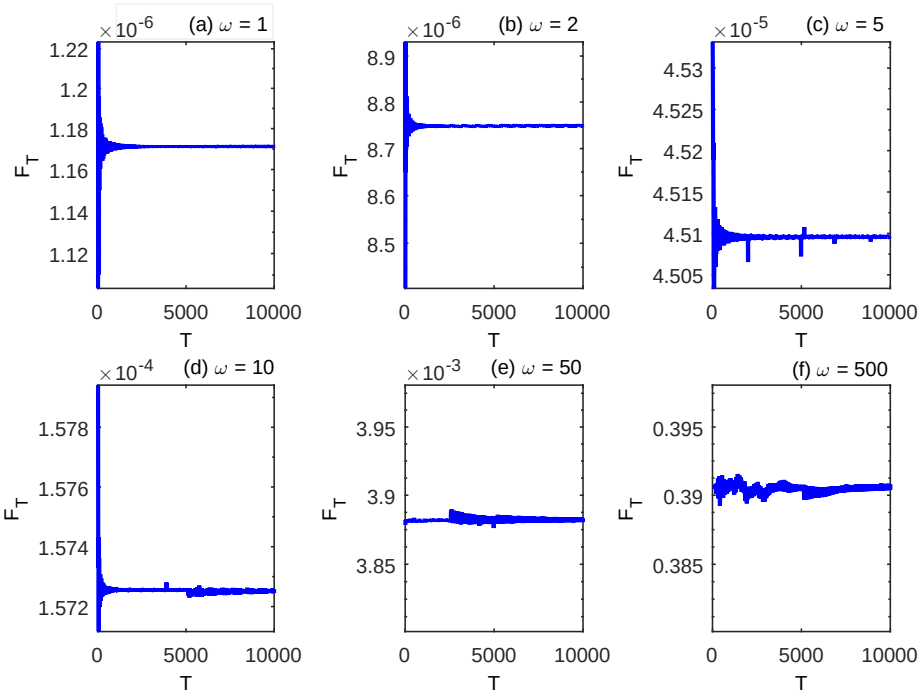

Figure 2.12: F_T against T for $N_0 = 5$, $K = 10$, $B = 0$ and $x_0 = 5$. Panels (a)-(f) are for different values of ω.

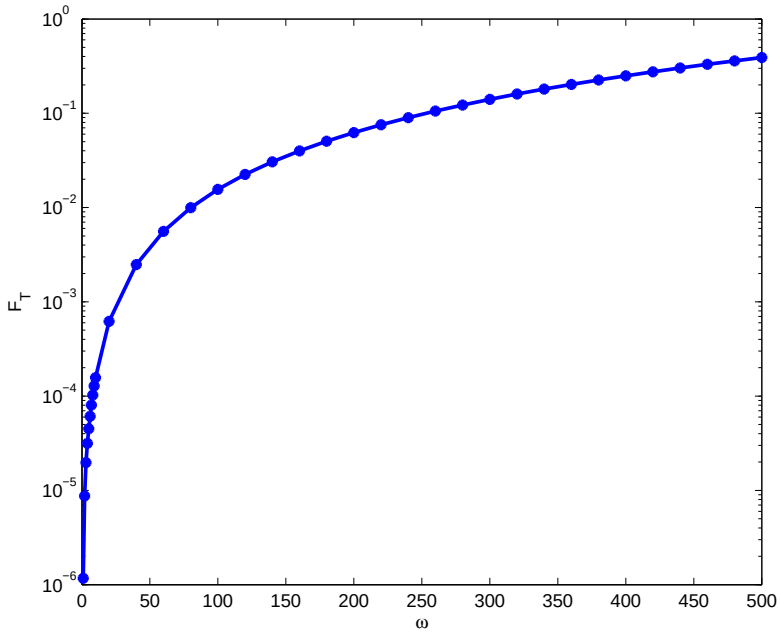

Figure 2.13: Asymptotic values of F_T against ω for $x_0 = 5$, $N_0 = 5$, $B = 0$ and $K = 10$. F_T increases monotonically as ω increases.

In Figs. 2.12 and 2.13, we present F_T against T for different values of ω and the asymptotic values of F_T against ω, respectively, for $x_0 = 5$. F_T values are monotonically increasing in Fig. 2.13, in a precise contrast to Fig. 2.11 and the smaller F_T value has been found at $\omega = 1$ while the higher value of F_T is at $\omega = 500$. In other words, we observe a general tendency of F_T monotonically increasing as ω increases. These observations indicate that the distinct maximum of F_T at optimal ω when $x_0 = 0.1$ does not occur in the case when $x_0 = 5$ as we can relate this finding to the absence of the bimodal PDF with two distinct peaks for $x_0 = 5$ as previously discussed with respect to Fig. 2.8.

2.4.5 Role of Fisher information as a measure of sustainability

Our interesting findings in previous section (2.4.4) show that there is maximum F_T around the optimal value of $\omega \sim N_0/5 = 1$ when $x_0 = 0.1$ and $B = 0$. One can therefore, give a better understanding by investigating the optimal case with maximum F_T. We added a periodic stimulus ($B_1 sin(\omega_1 t)$) to Eq. (2.3) to investigate the variability of this optimal case ($\omega = 1$) as follows:

$$\frac{dx}{dt} = (B + N_0 \sin(\omega t))x\left(1 - \frac{x}{K}\right) + B_1 sin(\omega_1 t), \tag{2.15}$$

then compare the results from the optimal case with non-optimal case's observations. For different values of ω, B_1 and ω_1, we show a PDF for the optimal and non-optimal cases. For example, we investigate the following values $\omega = 1$ (optimal case), $\omega = 10$ (non-optimal case), $B_1 = 1, 10$, $\omega_1 = 1, \sqrt{2}$ and the results are presented in Fig. 2.14.

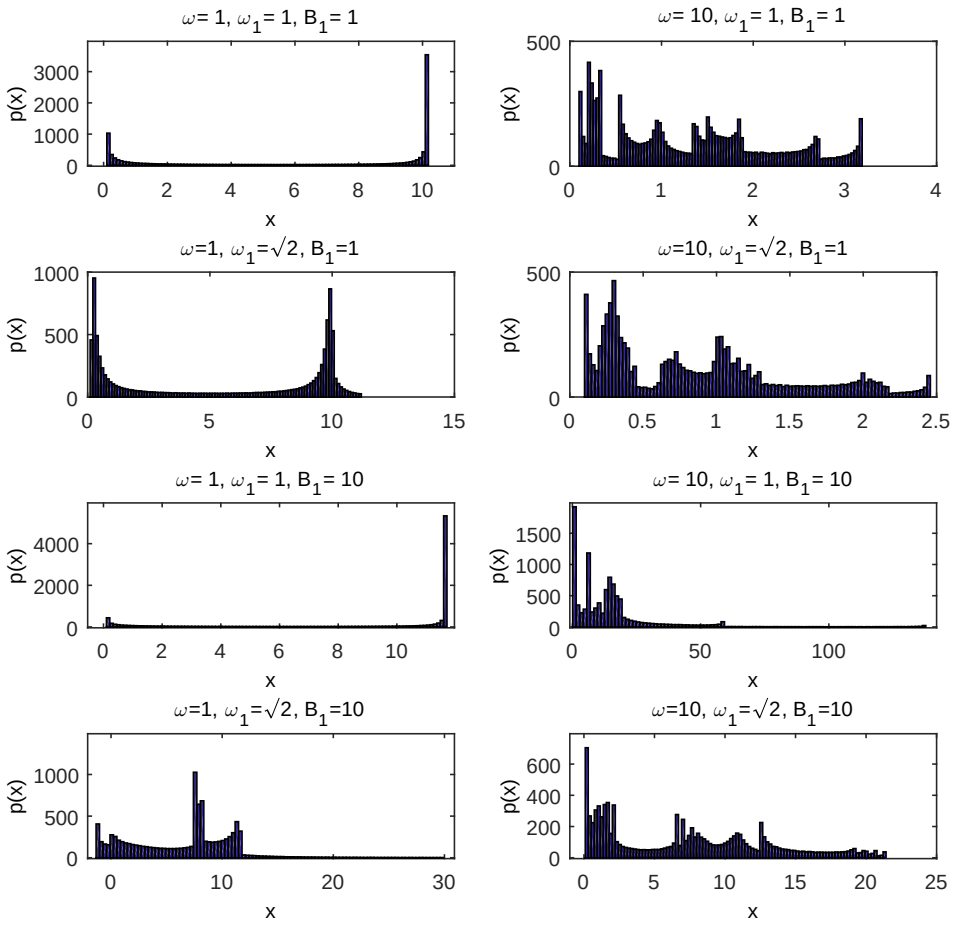

Figure 2.14: PDF of x for $x_0 = 0.1$, $K = 10$, $B = 0$ and $N_0 = 5$, with a periodic stimulus. Left panels are for the optimal case ($\omega = 1$) while the right panels are for non-optimal case ($\omega = 10$). The PDFs with optimal value $N_0 = 5\omega$ in left panels are more resilient to the a periodic stimulus than the PDFs for $\omega = 10$.

In Fig. 2.14, we display how the PDFs are influenced by different periodic stimulus in the left panels when $\omega = 1$ and $\omega = 10$ in the right panels. We notice that the comprehensive change in PDFs for the optimal case $\omega = 1$ in Fig. 2.14 is extremely less than the change in the PDFs in Fig. 2.7(c) and 2.7(f), respectively, indicating that the effectiveness of the periodic stimulus on the optimal case with higher F_T is less than in the non-optimal case. Thus, to strengthen this argument, it is important to employ an-

other index such as the mean value to track the system's behaviour. Specifically, Table (2.2) shows the mean values without periodic stimulus for $\omega = 1$ in the left panel and $\omega = 10$ in the right panel, then presenting the results of computing the ratio of change in the mean values in the case of the periodic stimulus using the following expression in Table (2.3):

$$\frac{\text{Mean without periodic stimulus} - \text{Mean with periodic stimulus}}{\text{Mean value without periodic stimulus}} \times 100\ \% \quad (2.16)$$

In Table (2.3), it must be remarked that for the optimal case $\omega = 1$, the ratio of change in the mean values for different parameter values in the periodic stimulus is much less than that in the non-optimal case ($\omega = 10$). For instance, we observe that the ratio of change in the optimal case is 15.3% while it is 656.1% in the non-optimal case for $B_1 = 1$ and $\omega_1 = 1$ in the periodic stimulus. In other words, the results show that the ratio of change in the non-optimal case is almost 44 times bigger than its equivalent in the optimal case. As a result, we can see that the non-optimal case is more affected by the perturbations in the model parameters compared to the optimal case.

Table 2.2: Mean values for $x_0 = 0.1$, $K = 10$ and $B = 0$ without periodic stimulus.

Mean value in optimal case	Mean value in non-optimal case
5.5433	0.1733

Table 2.3: % Change in mean values for $x_0 = 0.1$, $K = 10$ and $B = 0$ with periodic stimulus.

	Optimal case		Non-optimal case	
	Mean value	% Change	Mean value	% Change
$B_1 = 1, \omega_1 = 1$	6.3927	15.3 %	1.3103	656.1 %
$B_1 = 1, \omega_1 = \sqrt{2}$	5.5515	0.2 %	0.8814	408.6 %
$B_1 = 10, \omega_1 = 1$	8.8326	59.3 %	15.2631	8707.3 %
$B_1 = 10, \omega_1 = \sqrt{2}$	6.5509	18.2 %	7.2068	4058.6 %

It is also important to investigate more values of initial conditions such as $x_0 = 5$ in

order to study the importance of Fisher information for the logistic system's sustainability. We thus perform similar experiment for $x_0 = 5$ by changing the parameter values in the periodic stimulus as we can see in Fig. 2.15 and Tables 2.4, 2.5. Based on the results from Fig. 2.13 as the F_T does not show a maximum value for this initial condition, $x_0 = 5$, as a result, there is not any specific value of ω which is most resilient to perturbations and this indicates the lack of apparent connection between the value of F_T and sustainability. Therefore, one can assume that the F_T is a valuable metric of variability/sustainability if only there is a distinct Maximum of F_T (linked to the presence of PDF with two distinct bimodal peaks).

For a different initial condition such as $x_0 = 5$, we use different values of ω, ranging from $\omega = 1$ with lower value of F_T to $\omega = 500$ which it shows a higher value of F_T to investigate the excitation's effect on the system's dynamics over time with different values of B_1 and ω_1 as we can observe that from the following figure (Fig. 2.15) and Tables 2.4, 2.5.

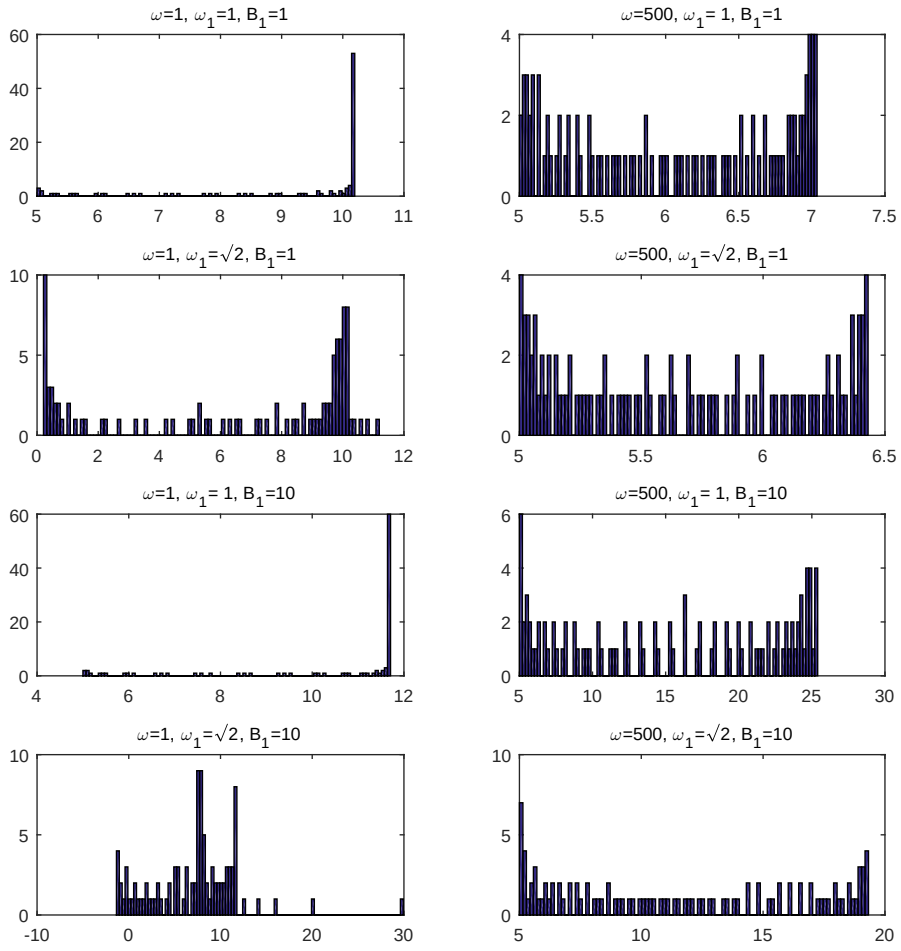

Figure 2.15: PDF of x for $B = 0$, $x_0 = 5$, $K = 10$ and $N_0 = 5$, with periodic stimulus. We use the smallest ω in the left panel and the largest ω in the right panel in regards to Figs. 2.12 and 2.13.

In Figure 2.15, we show how the PDFs behave with a periodic stimulus for fixed $N_0 = 5$, $x_0 = 5$, $K = 10$, $B = 0$ and different ω in comparison with PDFs in Fig. 2.8 with the same values of ω.

Table 2.4: Mean values for $x_0 = 5$, $K = 10$ and $B = 0$ without periodic stimulus.

Mean value for $\omega = 1$	Mean value for $\omega = 500$
8.9308	5.0239

Table 2.5: % Change in mean values for $x_0 = 5$, $K = 10$ and $B = 0$ with periodic stimulus.

	$\omega = 1$		$\omega = 500$	
	Mean value	% Change	Mean value	% Change
$B_1 = 1, \omega_1 = 1$	9.1074	1.98 %	6.0771	20.96 %
$B_1 = 1, \omega_1 = \sqrt{2}$	6.4373	27.9 %	5.6782	13.02 %
$B_1 = 10, \omega_1 = 1$	10.4778	17.3 %	15.571	209.9 %
$B_1 = 10, \omega_1 = \sqrt{2}$	7.0713	20.8 %	11.5765	130.4 %

2.4.6 Fisher information dependence on x_0

In this section, we fix ω and varying x_0 to see how F_T values behave with changing the initial values x_0.

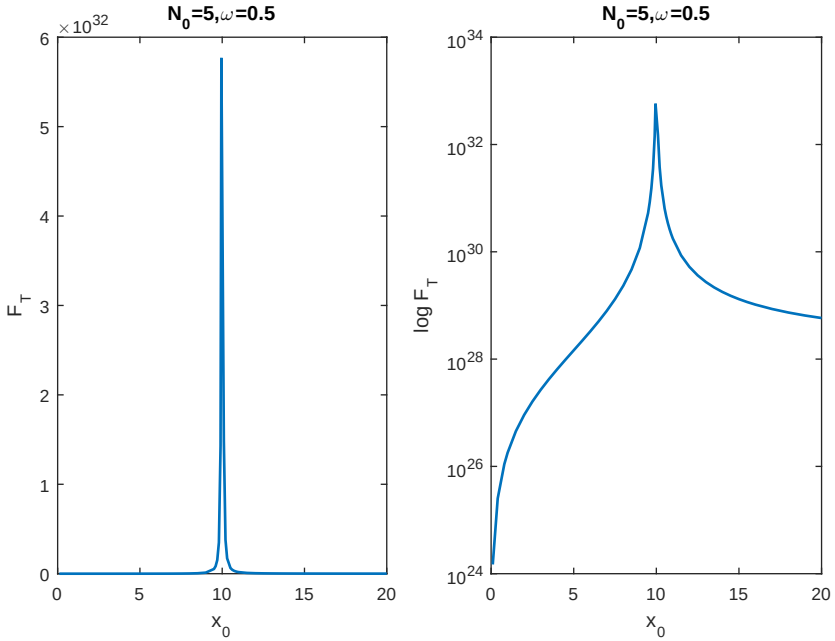

Figure 2.16: F_T against x_0 for $N_0 = 5$, $B = 0$, $K = 10$ and $\omega = 0.5$ (ω is an arbitrary value). The important feature of the above figure is a distinct peak of F_T at $x_0 \simeq 10$. Panel (b) is in log-scale.

In Fig. 2.16, F_T values are monotonically increasing as x_0 increases which means that the variability is decreasing in the system's behaviour as we get closer to the stable point at $x^* = K = 10$. The existence of a maximum in the above curve is the identifying characteristic of F_T which means that we have larger value of F_T at the initial condition closer to the carrying capacity of the population x_0 $(= 9.95) \simeq x^*$ $(K = 10)$ which leads to the state with a less variability (unsustainable state with less dynamics to investigate).

Now, we turn back to the PDF of fixed ω and different x_0 as in the following figure. All the values of initial conditions display a bimodal PDF regardless ω. Also, we can observe that the right peak is higher than the left peak for all initial values less than the carrying capacity $K = 10$. In contrast to the initial conditions larger than the carrying capacity $K = 10$, we can see that the higher peak is moved to the left as the other peak represents the system at x_0 which are larger than the maximum population size.

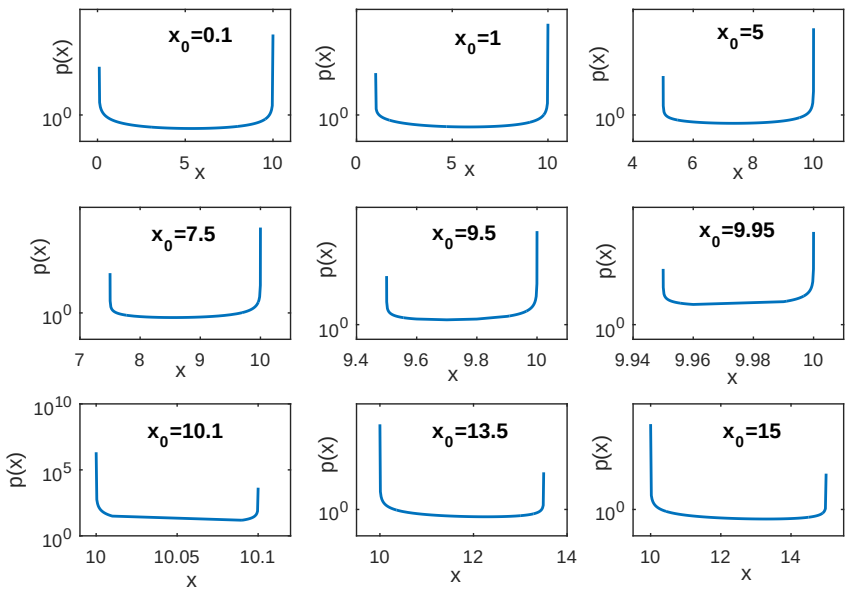

Figure 2.17: PDF of x for $N_0 = 5$, $B = 0$, $K = 10$ and $\omega = 0.5$ with different values of x_0. A bimodal PDF is observed for all the initial conditions with different distance between the two peaks.

The most interesting feature of Figs. 2.16 and 2.17 is the distinct peak of F_T at $x_0 \simeq 10$

which related to the panel $x_0 = 9.95$ in Fig. 2.17 with a PDF bias to a certain x value which is the carrying capacity.

To complete our investigation on the implication of Fisher information for variability/sustainability with different initial conditions, we also perform similar experiments for larger ω such as $\omega = 2$ (figures not shown), similar results were observed with higher Fisher information at the initial conditions which is closest to the carrying capacity $K = 10$.

2.4.7 The logistic model with extra modification

As we are dealing with a population dynamic, let's consider x to be cancer cells population or bacteria population, etc. Specifically, for cancer cells population, our goal is to eliminate the cancer cells in order to reduce their growth and stop their spread to a new area by including a negative term in Eq. 2.3 as a treatment. We investigate its effects on the system's behaviour as in the following equation:

$$\frac{dx}{dt} = (B + N_0 \sin(\omega t))\, x\, (1 - \frac{x}{K}) - cx. \tag{2.17}$$

We investigate different values of c (a dose of treatment) in order to track its functionality in which the cancer population is more response to the treatment (more steeply). In other words, to locate the optimal value of c. For $B = 0$, $N_0 = 5$, $\omega = 1$, and different values of c, we calculate the mean values of the population and slopes in Fig. 2.18 where we display time on the $x - axis$ and the mean values on the $y - axis$ as follows:

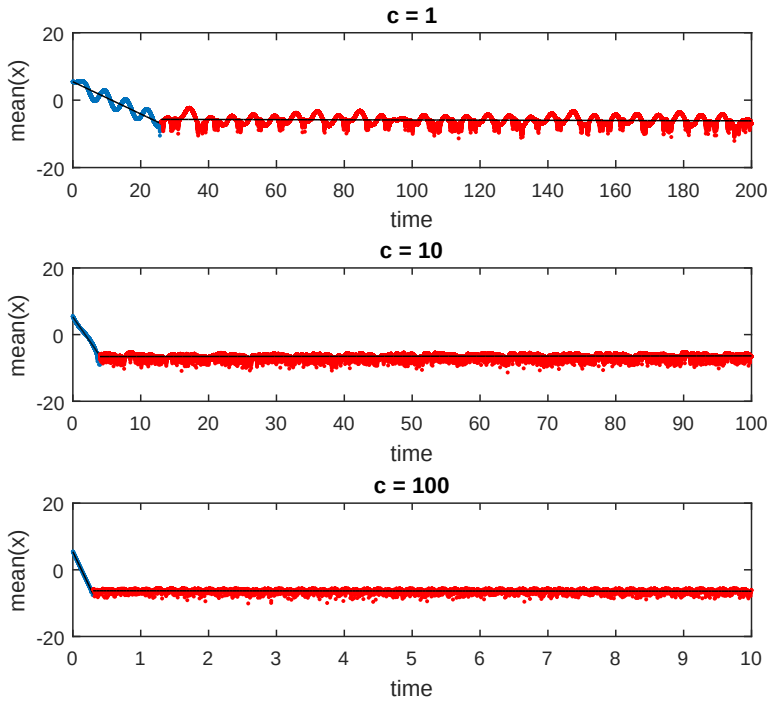

Figure 2.18: Mean values of cancer population at different values of c and fixed $K = 10$, $N_0 = 5$, $\omega = 1$, $B = 0$. Similar behaviour is observed for all the values of c with a difference in the time where cancer cells start to eradicate.

From Fig. 2.18, we observe that the higher value of c shows a more steepest curve which means that the system is more flexible to the larger value of the treatment dose but it will be of interest to detect the optimal value of c where the treatment at this optimal value will eliminate the cancer population. Also, may including perturbations in the constant c in the decaying term $(-cx)$ will be of interest.

2.5 Comments on different modulations

To go beyond the investigation presented in previous sections regarding the case where the same periodic modulation is included in the positive and negative feedback. In the following, we build an investigation to track the behaviour of the logistic equation over

all possible parameter values in two different modulations.

2.5.1 Case-2: Perturbation in the positive feedback

In this section, we present the logistic model (Eq. 2.3) with a constant in the negative feedback (nonlinear term) whereas we vary the parameter N in the positive term (linear term) by including a periodic modulation as in the following equation:

$$\frac{dx}{dt} = (B + N_0 \sin(\omega t))\, x - \frac{Cx^2}{K}, \tag{2.18}$$

here, we consider B, C, and K as constants. The analytical solution for Eq. 2.18 is the solution for the following quantity:

$$x = \frac{e^{(Bt - \frac{N_0}{\omega}\cos(\omega t))}}{\frac{N_0}{K}\int e^{(Bt - \frac{N_0}{\omega}\cos(\omega t))} dt} \tag{2.19}$$

We focus our efforts at changing the values of ω and N_0 in the periodic perturbations and study their effects on PDF of x for $B = 0$, $K = 10$, $C = 1$, and $x_0 = 0.1$, and investigate these effects on the system's behaviour as in Fig. 2.19. Once more, we concentrate on the case where the linear growth rate in Eq. (2.18) has zero average, $B = 0$, and is only driven by a periodic modulation. Although $B = 0$, we realize the existence of the finite amplitude solution. The common feature of this finite amplitude solution is a PDF with one peak appears around the starting value $x_0 = 0.1$ for all the values of N_0 and ω (see Fig. 2.19). This leads to a unimodal PDF for all parameter values in comparison to the bimodal PDF in previous sections due to the influence of a periodic fluctuation in driving a unimodal PDF. We also observe that the PDF becomes shorter as ω increases for different values of N_0 and this is similar to our conclusion in regards the bimodal PDF in previous sections.

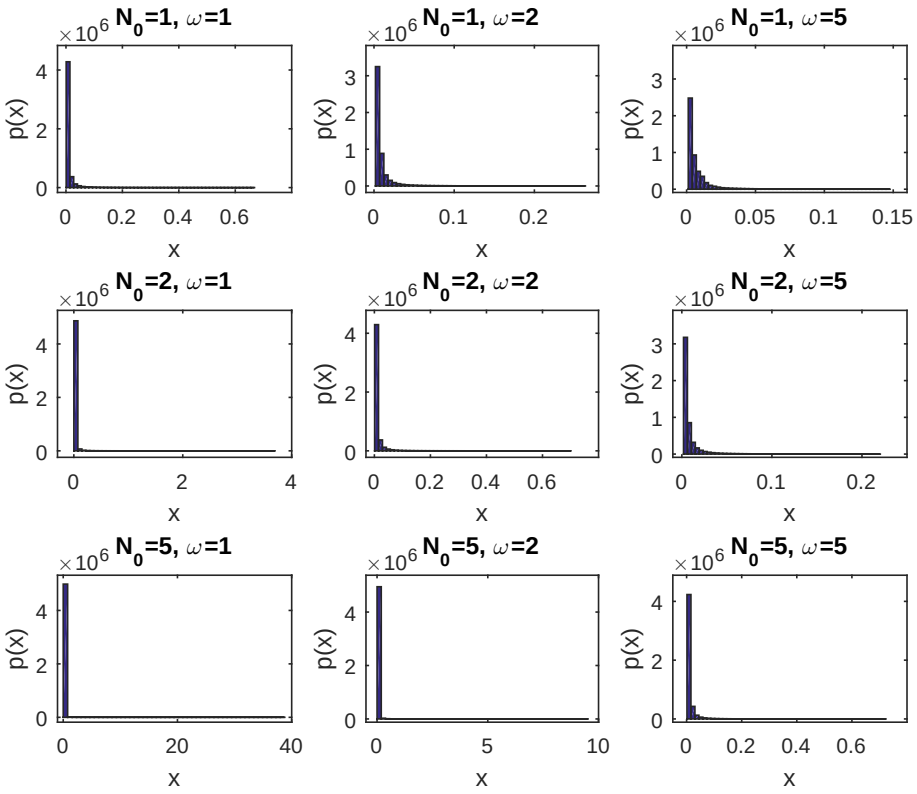

Figure 2.19: PDF of x for different N_0 and ω. $x_0 = 0.1$, $B = 0$, $K = 10$ and $C = 1$. We observe a notable unimodal PDF for all the cases.

In consideration of the above, we present maximum values of x and study the system's behaviour for $N_0 = C = 5$, $x_0 = 0.1$ and vary ω as follows:

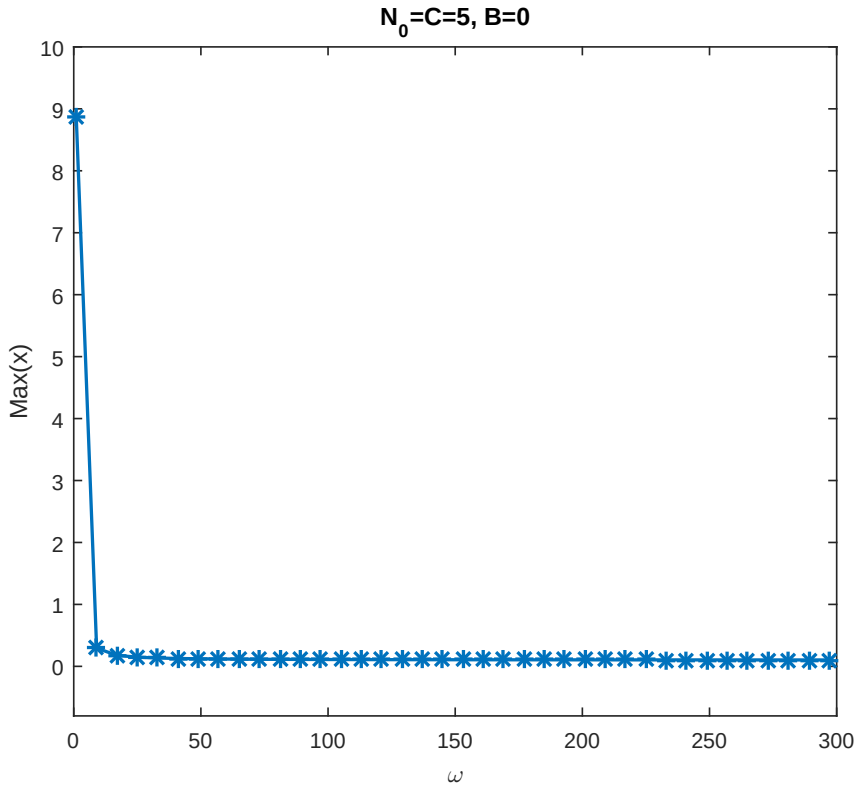

Figure 2.20: $Max(x)$ as a function of ω for $N_0 = C = 5$, $x_0 = 0.1$ and $B = 0$. $Max(x)$ values are monotonically decreasing as ω increases and finally show a static state at x_0.

An interesting behaviour of Fig. 2.20 is observed, the maximum values of x are monotonically decreasing as ω increases and finally approach a static state at the initial condition x_0. We used different initial conditions such as $x_0 = 2$ which show us similar behaviour.

2.5.2 Case-3: Perturbation in the negative feedback

In the absence of a periodic modulation in the positive feedback, we focus in the case where only the negative feedback consists of a periodic modulation whereas the parameter in the positive feedback kept to be a constant C, as in the following equation:

$$\frac{dx}{dt} = Cx - \frac{(B + N_0 \sin(\omega t))\, x^2}{K}. \tag{2.20}$$

The exact solution to Eq. (2.20) is found as in the following expression:

$$x = \frac{K\, a\, b\, C\, x_0}{KCa + N_0\, C\, b\, x_0\, c + N_0\, C\omega\, x_0 + Bx_0\, a\, (b-1)}, \tag{2.21}$$

where

$$a = C^2 + \omega^2,$$

$$b = \exp(Ct),$$

$$c = C\sin(\omega t) - \omega\cos(\omega t).$$

From Eq. (2.20), we expect the solution to grow boundlessly for $B = 0$ as the effect of the nonlinear term is reduced due to the periodic modulation in the model parameters. This means that the population exponentially grows as the amplitude of N_0 relative to B increases and as the nonlinear damping becomes ineffective (e.g. [50, 104]).

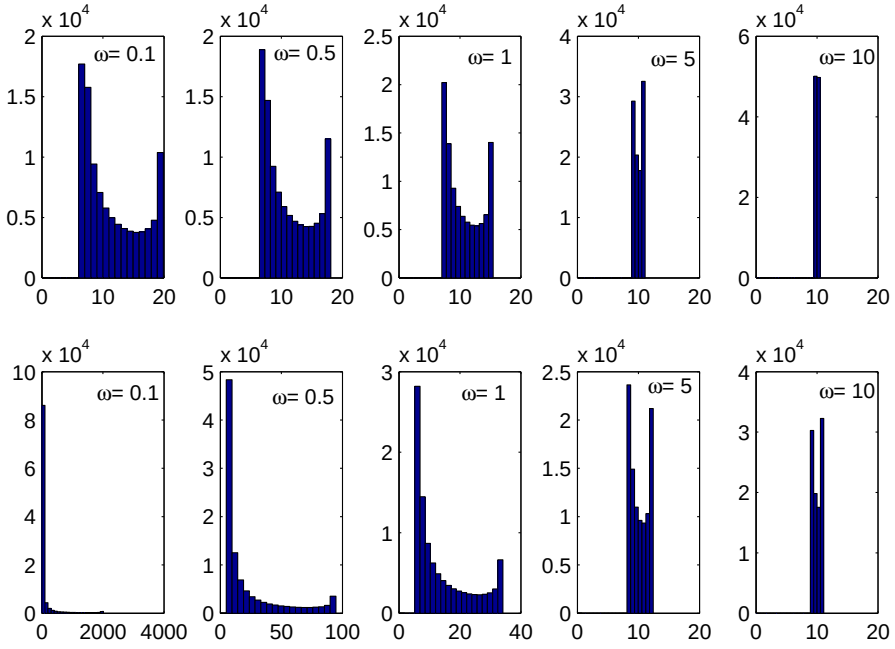

Figure 2.21: PDF of x for two different N_0; $N_0 = 0.5$ in the upper panels and $N_0 = 1$ in the lower panels. We fix $x_0 = 0.1$, $B = 1$, $K = 10$ and $C = 1$. A bimodal PDF is observed.

In Fig. 2.21, we present PDF of x for two different values of the amplitude, $N_0 = 0.5$ in the upper panels and $N_0 = 1$ in the lower panels, respectively, and we fix the other parameter values such as $x_0 = 0.1$, $B = 1$, $K = 10$, and $C = 1$. In the lower panels when $N_0 = 1$, the PDF becomes broader as ω decreases due to the powerful intermittency of x which is reflected from the high-amplitude peaks as ω decreases. In regards the results in Fig. 2.21, we show the time evolution of x for different values of N_0 and ω in the following figure.

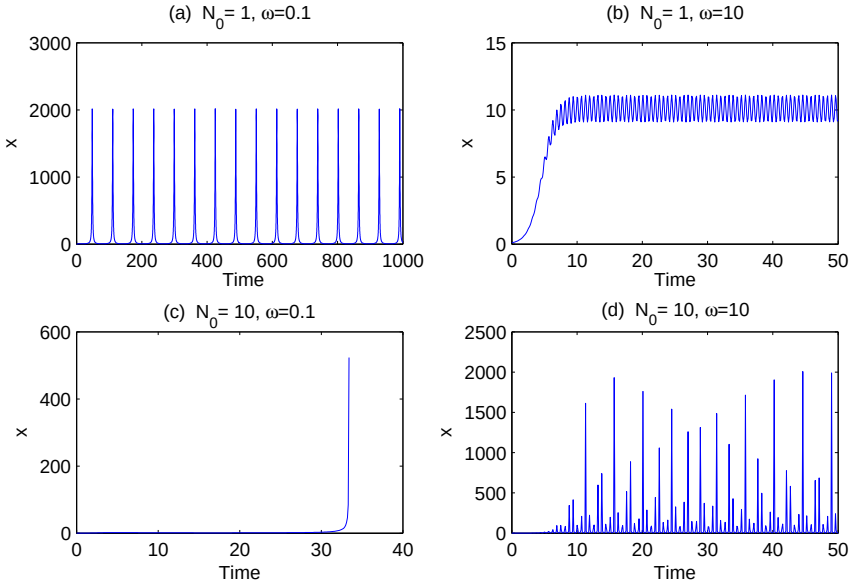

Figure 2.22: The time evolution of x for different values of N_0 and ω and fixed $x_0 = 0.1$, $K = 10$, $B = 1$ and $C = 1$. The population grows boundlessly for small ω and larger N_0 as in panel (c).

For sufficiently large values of N_0 and small ω as in panel (c), it is obvious that the solution grows exponentially whereas for small N_0 and larger value of ω as in panel (b), a static steady state at the carrying capacity $K = 10$ is observed.

2.6 Conclusions

The logistic model with different perturbations in the model parameters for both positive and/or negative feedback has been employed in the view of variability/sustainability; the influence of varying initial values and model parameters has been investigated.

In the case of the same periodic modulation of the model parameters for the positive and negative feedback, one potential feature of our analytical and numerical investigation is that the logistic model shows a bimodal PDF with different distance between the two peaks where it maintains a long-term memory of initial conditions as the system's response time is much longer than the characteristic time scale associated with the disturbance.

From the perspective of information theory, for initial values far from the carrying capacity $K = 10$ such as ($x_0 = 0.1$), we observe a distinct maximum of F_T for an optimal value of parameters $N_0 \sim 5\omega$. On the other hand, the maximum Fisher information does not exist for $x_0 = 5$ where F_T monotonically increases with ω. The analysis of the logistic model under different perturbations in the context of its variability/sustainability yields valuable insight to understand the small population of bacteria or tumour population which do not get killed off by antibiotics (or tumour cells population continued to survive), and the origin of their survival (e.g. [83]), as observed from a PDF peak around this small population x_0. Specifically, a bacteria population of small size (symmetrical to the small starting value x_0 in the logistic model) can stay alive under powerful antibiotics. This leads to maintenance of a bimodal PDF for an optimal condition with the maximum Fisher information. Therefore, the optimal case has the best survival likelihood.

Also, we calculate Fisher information from PDFs for the logistic model at different initial conditions and compare the results with the Gompertz model in the next chapter. This latter investigation leads us to conclude that Fisher information can be used as a measure of sustainability in the case that it has a distinct maximum as a result

of the existence of a bimodal PDF, with two distinct peaks appearing at the initial conditions and at the carrying capacity, respectively. F_T increases with x_0 up to x_0 (= 9.95) $\simeq x^*$ (K = 10) and decreases beyond this initial value. This behaviour results from the high variability in the model parameters beyond x_0 (= 9.95) $\simeq x^*$(= 10).

Chapter 3

The Gompertz model

3.1 Introduction

The Gompertz equation is widely used to describe the growth of plants, birds, fish, bacteria and cancer population, even economic phenomena, while earlier actuaries only showed interest in it [33, 96, 103]. Laird, for example, [48, 49] proposed a family of sigmoidal Gompertzian curves to model the growth of diverse malicious cancers over time. Also, it is important to mention that the changes in the growth rate of the Gompertz equation give a sigmoidal curve (see Fig.1 in [109]) with three stages. The first stage of growth presents an initial transient which does not make it clear what is actually going on, followed by an exponential growth stage, then finally a stationary state. Significant examples of such growth curves are human height and mass, a fish community, and rabbit population (see [99, 109] and the references there in).

The first successful attempt to apply the Gompertz equation to fit cancer growth data was made in the 1960s by Laird [48], where cancer was considered as a cellular population growing in a bounded space with a limited availability of nutrients. Subsequently, many researchers have employed the Gompertz law of growth to fit experimental data on such as tumour cells; in addition, mathematical modifications have been made to the

Gompertz equation by such as Waliszewski [100] who introduced a number of Gompertz model characteristics mathematically. The Gompertz equation (3.2) is found in different fields of applied studies, for example, in medicine for modelling the growth of cancer populations, in actuarial science for determining a mortality law, in biology as a model for characterizing the growth of organisms, in marketing, in ecology, etc. (see [41, 96, 103] and the references there in).

We explore the dynamics of the Gompertz growth model in detail by investigating the behaviour of this model with perturbations in different cases. In particular, we investigate the Gompertz growth model driven by a periodic modulation in different positions from a point of view of variability/sustainability using Fisher information, and make a comparison with the results presented in the previous chapter of the logistic equation. The implicit general findings are that a periodic solution is observed for the perturbed model in addition to a cross-over behaviour between x_0 and $x^* = e$. To estimate the variability/sustainability of the Gompertz equation, we employ the theory and methodology needed for using Fisher information, a large value of Fisher information is observed at x_0 which is closer to $x^* = e$ with shortest PDF.

The remainder of Chapter Three is presented as follows: Section 3.2 sets out our model and motivation. Then, perturbation of the Gompertz equation is explained in Section 3.3. Section 3.4 includes the same periodic modulation in positive and negative feedback, studying its dynamics by computing PDFs and Fisher information analysis. Section 3.5 describes our simple investigation of the Gompertz equation with different types of modulations of the model parameters. Finally, Section 3.6 presents conclusions.

3.2 The model and motivation

For actual purposes, the Gompertz curve is generally written in the following form:

$$x(t) = e^{a(1-e^{-bt})}, \tag{3.1}$$

where a and b are essentially positive quantities ($a > 0, b > 0$) (see [41, 100, 103]). From Eq. (3.1), when t tends towards negative infinity, x approaches zero whereas as t tends towards positive infinity, x approaches the equilibrium point $x^* = e^a$. For our purpose of investigating the variability/sustainability of the Gompertz equation and making a comparison with other dynamical systems, it is more convenient to write the Gompertz equation as a solution of the mathematical model [48] as in the following form:

$$\frac{dx}{dt} = cx - bx\log(x). \tag{3.2}$$

Here, c and b ($c > 0, b > 0$) are experimental coefficients determining the slope of the curve (see [100] and the references there in). c is the net growth rate, and b is the death rate, t stands for scalar time, while x is the population of any species, and x_0 is the population size at the starting observation time. Eq. (3.2) describes a population asymptotically reaching the carrying capacity value $x_1^* = e^{(c/b)}$, x_1^* is the stable equilibrium point whereas the second equilibrium point is $x_2^* = 0$ which is an unstable point. The linear term cx with $c > 0$ represents a positive feedback while the nonlinear term $bx\log(x)$ with $b > 0$ represents a negative feedback. We notice the same observations as for the logistic equation in section (2.2) where x reaches the equilibrium point x_1^*, as t increasing

for a constant $c, b > 0$, regardless of the initial value of $x(t = 0) = x_0$.

Benjamin Gompertz (1825) was the first to suggest and employ the Gompertz model, where he formulated his law of population mortality as in Eq. (3.1) which is a sigmoid

function [11, 33, 37, 96]. It is also explained mathematically as a model for time series, where there is a lack of growth after $t = 0$ before attaining the equilibrium point. Some more examples of using Gompertz curve in modelling different population as follows:

- fashion uptake; initially, costs were high, a period of fast growth was reached, followed by slower absorption where saturation was reached.
- Population in a limited area; at the beginning, the birth rates of population increase then slow as resource limits are reached.

3.3 The Gompertz equation with oscillation

Our focus in this section is the case where a periodic modulation appears in the model parameters. Specifically, when the parameters b and/or c in Eq. (3.2) are modified to include a periodic modulation as follows:

$$b = c = B + D_0 \sin(\omega t), \tag{3.3}$$

where D_0 and ω are the amplitude and frequency of the periodic modulation, respectively, B is a constant growth and more focus on the case $B = 0$, in which our model is only driven by a periodic modulation ($D_0 \sin(\omega t)$), we investigate the influence of changing ω and x_0 on the response of the Gompertz model.

Numerical and analytical calculations have been used to investigate the Gompertz equation (after adding a combined term of constant and purely oscillatory part) in different three cases which are illustrated by the following nonlinear ordinary differential equations:

Case-1: The same perturbation in the growth and death rates

$$\frac{dx}{dt} = (B + D_0 \sin(\omega t))\ x\ (1 - x \log x).$$

Case-2: Perturbation in the growth rate

$$\frac{dx}{dt} = (B + D_0 \sin(\omega t))\, x - bx \log x.$$

Case-3: Perturbation in the death rate

$$\frac{dx}{dt} = cx - (B + D_0 \sin(\omega t))\, x \log x.$$

Again as in the logistic model, the impact of the oscillatory control parameters vanish in the first two cases for sufficiently large ω while it shows different behaviour for the third case where the solution grows boundlessly for smaller ω when $B = D_0$. Each case will be consider separately in the following sections:

3.4 Case-1: The same fluctuation in the growth and death rates

A periodic modulation is included in the model parameters for both positive and negative feedback as follows:

$$\frac{dx}{dt} = (B + D_0 \sin(\omega t))\, x\, (1 - \log x). \tag{3.4}$$

By integrating Eq. (3.4), we obtain the analytical solution as shown in the following form:

$$x(t) = exp\Big(1 - \Big[(1 - \log(x_0))\, exp(-Bt - \alpha)\Big]\Big), \tag{3.5}$$

where

$$\alpha = \frac{D_0}{\omega}(1 - cos(\omega t)).$$

Here x_0 is the initial value of x at $t = 0$ and $log()$ refers to the natural logarithm

(a logarithm to the base e (= 2.71828)). It must be remarked that Eq. (3.4) has two equilibrium points, the first one is $x_1^* = e$ and the second one is $x_2^* = 0$. By checking the stability of these fixed points, we observe that the first point is stable whereas the second point is an unstable point.

From the analytical solution (Eq. 3.5), a cross-over behaviour of x between x_0 and $x_1^* = e$ in the limit of increasing t is observed. For example, when $\omega = 0$, $\cos(\omega t) = 1$ and $B = D_0 = constant$, the population tends to reach $x_1^* = e$ as $t \to \infty$ regardless initial conditions. While, when $B = 0$, the net growth rate takes its minimum value $x_{min} = x_0$ at times when $\cos(\omega t) = 1$.

3.4.1 Results for fixed ω and varying D_0 in the oscillatory term

We investigate the effects of changing the amplitude D_0 for $B = 0$ and fixed values of ω by choosing $\omega = 1, 2, 5$, and 10, respectively, where these values are chosen arbitrarily [63, 104].

From the following figure (Fig. 3.1), we present maximum values of x, $Max(x)$ against amplitude D_0. A similar behaviour is observed for all the values of ω. Specifically, for $\omega = 1$, the curve shows that the model has an initial transient then it starts to increase rapidly as D_0 increases until the solution approaches asymptotic value at $x_1^* = e$. For the other values of ω, $\omega = 2, 5$ and 10, the only difference is the value of D_0 where the solution approaches its asymptotic value (see Fig. 3.1).

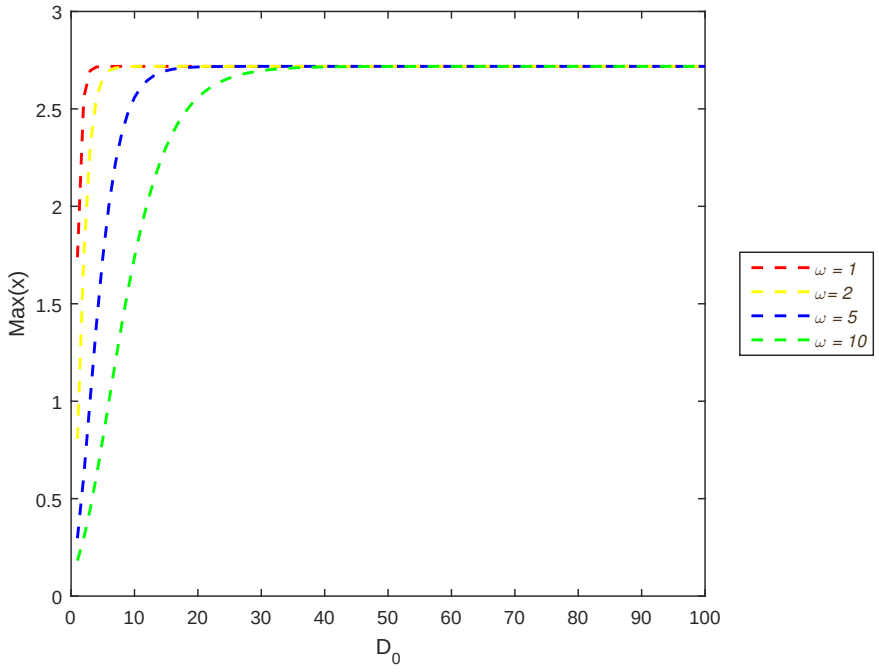

Figure 3.1: Maximum values of x for fixed $\omega = 1, 2, 5, 10$ and varying D_0 with $x_0 = 0.1$, and $B = 0$. The difference between the above curves is the time that the population spend before approaches its maximum values at e.

For sufficiently large D_0, the effects of the periodic perturbation disappear for different values of ω, similar to the observations concluded for the logistic model dynamics.

3.4.2 The cross-over behaviour between $x = x_0$ and $x = x_1^*$

In this section, we show the Gompertz model with a periodic modulation in both positive and negative feedback. The solution maintains its initial condition for sufficiently large values of ω. We fix the constant growth rate to be equal zero ($B = 0$), and is an interesting model where a growth is strongly inhibited as in the case of bacteria under the action of antibiotics, etc. Thus, Fig. 3.2 displays the typical time history of x for different values of ω and x_0.

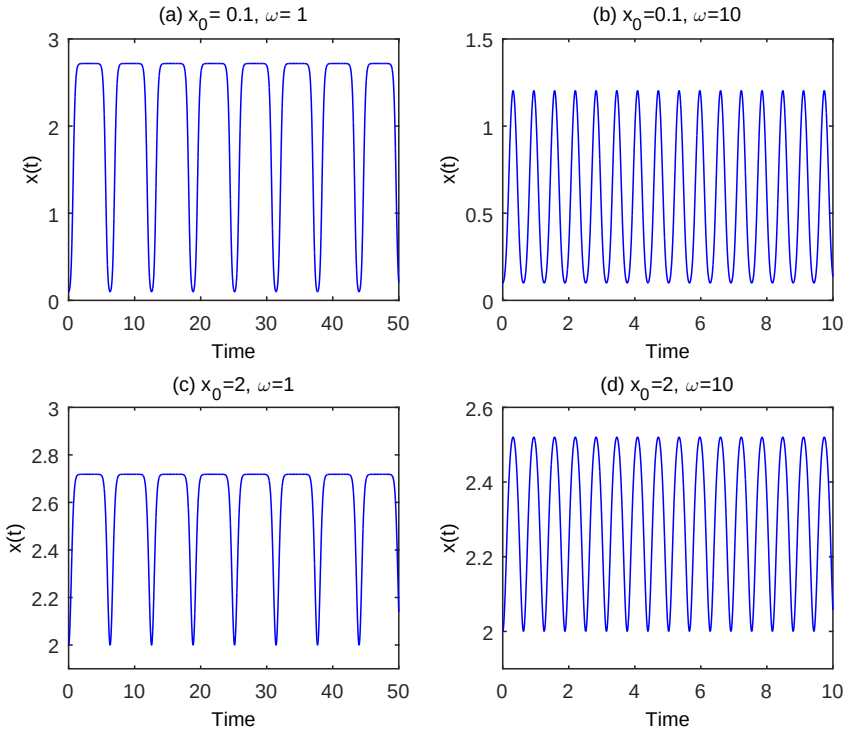

Figure 3.2: The time evolution of x for different values of $x_0 = 0.1, 2$ and $\omega = 1, 10$. For a small value of ω, $x(t)$ tends to reach the carrying capacity e while for large ω, $x(t)$ maintains its initial condition.

We observe that $x(t)$ tends to reach its maximum values at $x_1^* = e = 2.7183$ for a small value of ω regardless x_0, while for large ω, $x(t)$ maintains its initial condition and can never reach $x_1^* = e$ (see Fig. 3.2).

We display the time evolution for small ω and different x_0 in the left panels, where the time scale of perturbation becomes much larger than the growth rate, leading the system to reach x_1^*, in comparison with panels (b) and (d) where the time scale of perturbation is much shorter than the system's response time, therefore, the system does not approach x_1^* (similar observations can be seen in section 2.4.2).

In order to explain the behaviour in Fig. 3.2 in detail, we show another figure which contains maximum and minimum values of x in the $y-axis$ in blue solid line and red dashed line, respectively, and ω in the $x-axis$ for different values of initial conditions. We display the figures in panels (a)-(b) in log-log scale in panels (c)-(d), respectively.

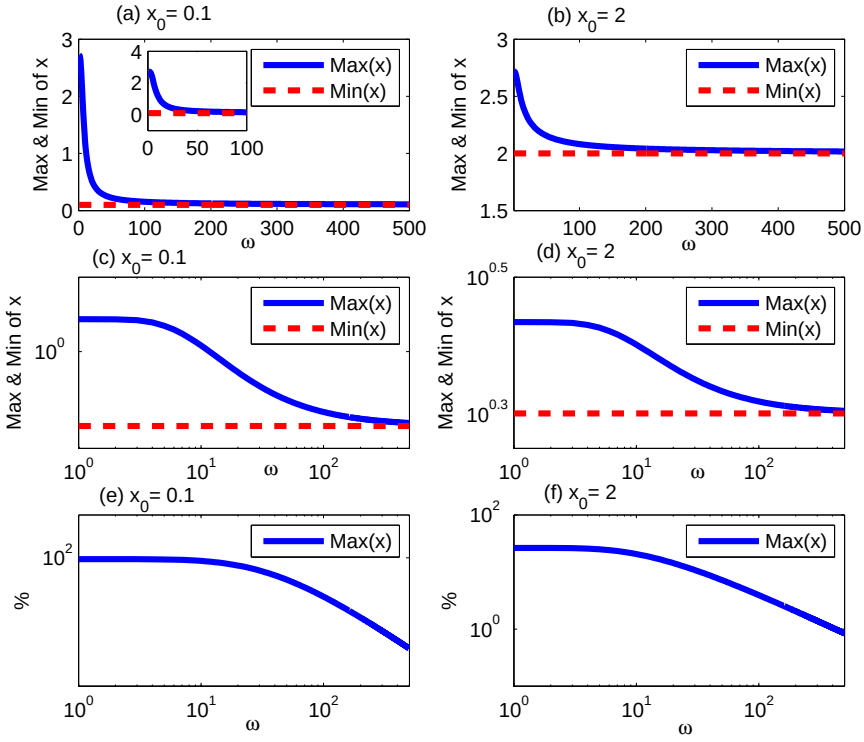

Figure 3.3: Maximum and minimum values of x against ω for $D_0 = 7$ and $x_0 = 0.1$ in panels (a), (c) and (e) and $x_0 = 2$ in panels (b), (d) and (f). (c), (d), (e) and (f) are explained in log-log scale.

A visual analysis of Fig. 3.3 shows a general tendency of $Max(x)$ monotonically decreasing as ω increases. Furthermore, we notice that $Min(x)$ approximately equals to x_0 in panels (a), (b), (c) and (d) as expected from the analytical solution.

We also observe a difference between the left and right panels which is due to the different initial conditions, for $x_0 = 0.1$, the maximum values of x show a much steeper decrease than for $x_0 = 2$, as $Max(x)$ is obtained by the approach to $x_1^* = e$. To support these findings, we employ the relative deviation measure of $Max(x)$ to determine the maintenance of initial values.

The ratio of change in $Max(x)$ is found according to Eq. (2.6) (Chapter Two), and the results are shown in Fig. 3.3 (e) and (f) by using log-log scale. In Fig. 3(e)-(f), we observe almost straight lines for $\omega \gg 1$, leads to a power-law relation in both cases as the percentage change decreases with ω.

3.4.3 Probability Density Function

From a statistical perspective, we compute the Probability Density Function (PDF) of x to examine the effects of ω and x_0 on PDF by relating the time spends by the system state at x to the probability of observing the system at a particular value of x (see [13, 25, 78]). Following the procedure developed for the logistic model in section (2.4.3), we comput PDF for the Gompertz model as follows:

$$p[x] = \frac{A}{(B + D_0 \sin(\omega t))\ x\ (1 - \log(x))}. \tag{3.6}$$

Since $p[x]$ is define according to the following expression:

$$p[x] = p[t] \left|\frac{dt}{dx}\right| = A \left|\frac{dt}{dx}\right| = \frac{A}{u},$$

where $u = \frac{dx}{dt}$ is simply given by Eq. (3.4). In order to replace Eq. (3.5) by a function which only depends on x, we solve Eq. (3.5) for $(\cos(\omega t))$ as in the following expression:

$$\cos(\omega t) = 1 + \left(\frac{\omega}{D_0} \log\Big(\frac{1 - \log(x)}{1 - \log(x_0)}\Big)\right), \tag{3.7}$$

by using the identity $\left(\sin(\omega t) = \sqrt{1 - \cos^2(\omega t)}\right)$, and substituting it in Eq. (3.6), the resulting equation is used to produce the figures in this section.

To illustrate how PDF depends on x_0 for fixed value of ω, we show that in Fig. 3.4 by using $\omega = 0.5$, a bimodal PDF with different distance between the two peaks for different parameter values is observed. The first peak appears at $x = x_0$ whereas the second peak can be seen at $x_1^* = e$. For $x_0 < x_1^*$, the right peak at $x_1^* = e$ is always higher than left peak at initial value while for $x_0 > x_1^*$, the left peak becomes higher than right peak as the initial condition is greater than $x_1^* = e$.

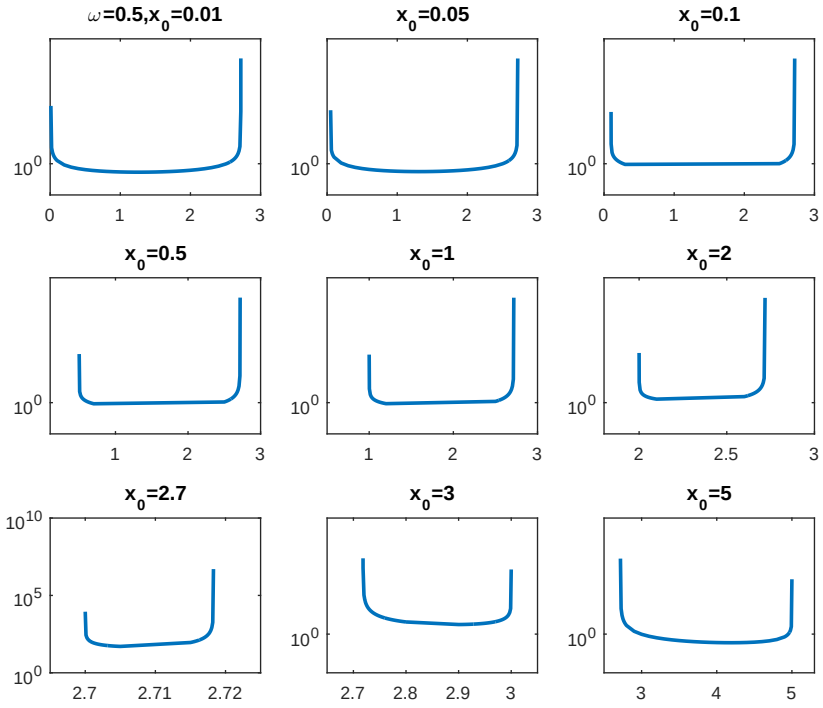

Figure 3.4: PDF of x for $D_0 = 7$ and $\omega = 0.5$ with different values of x_0. A bimodal PDF is observed for all x_0 with different distance between the two peaks.

For small values of x_0, the system shows a PDF with a broad distance between the two peaks while this broadness is getting smaller as x_0 increases, in other words, we can see that the PDF started to shrink and this behaviour can be related to the functionality of the system in Fig. 3.2, where the system can never reach $x_1^* = e$ but maintains its initial condition. In consideration of Fig. 3.4, we use another value of ω to be $\omega = 2$ to produce the following figure. Similar behaviour is observed.

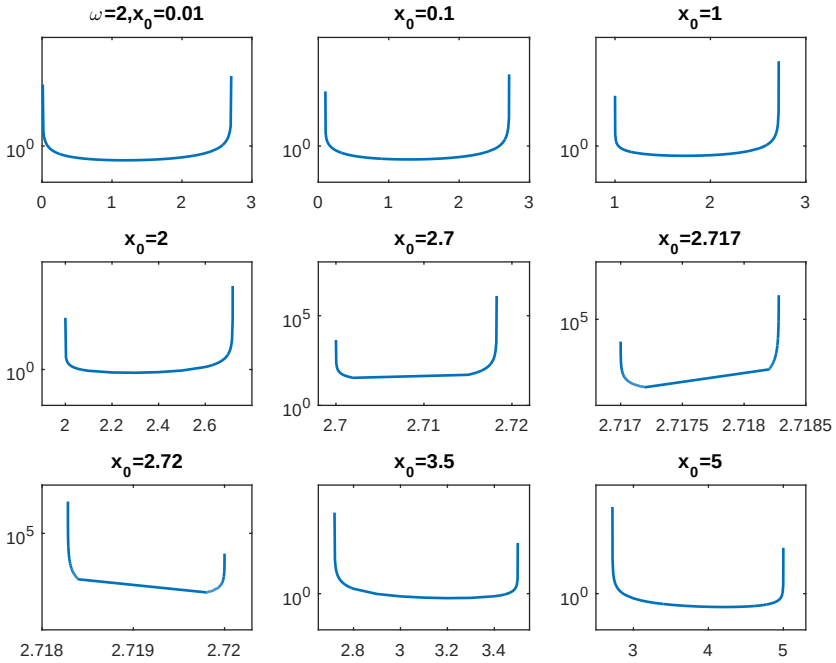

Figure 3.5: PDF of x for $D_0 = 7$ and $\omega = 2$ with different values of x_0. We notice a bimodal PDF for all x_0 with different distance between the two peaks.

The findings from Figs. 3.4 and 3.5 may have an interesting relation to Fisher information. Therefore we show Fisher information dependence on the initial conditions x_0 in the following section. We observe a large value of F_T at $x_0 \simeq x_1^*$, due to the shortest PDF at this initial value (see Fig. 3.5) with low variability, whereas for $x_0 > x_1^*$, the curve is monotonically decreasing as x_0 increases due to the higher variability as the system loses its functionality so we obtain lower F_T. In comparison with the logistic equation in Chapter 2, we observe similar behaviour in regards of the relation between Fisher information and PDF for fixed value of ω and different initial conditions.

3.4.4 Fisher information

Here we limit ourselves to monitoring Fisher information as the Gompertz equation shows a significant change due to the periodic modulation in the model parameters.

By using the results in Section (2.4.4) to find Fisher information, we calculate the time averaged Fisher information (F_T) for the Gompertz equation by using Eq. (2.14) with Eq. (3.4), as follows:

$$F_T = \frac{A}{T}\int_0^T \frac{1}{u^4}\left(\frac{du}{dt}\right)^2 dt \tag{3.8}$$

Since u is equal to the equation in (3.4), then we calculate F_T as follows:

$$F_T = \frac{A}{T}\int_0^T \frac{\Big[\alpha - \log(x)(B + D_0\sin(\omega t))\Big]^2}{\Big[(B + D_0\sin(\omega t))\ (x - x\log(x))\Big]^2}\, dt. \tag{3.9}$$

where

$$\alpha = \frac{D_0\omega\cos(\omega t)}{B + D_0\sin(\omega t)},$$

Here, F_T is the Fisher information averaged over the total time duration T; A is a normalization constant. In the following, we examine the variability/sustainability of the Gompertz equation with perturbation in positive and negative feedback by computing F_T for different cases using the formula in Eq. (3.9). We use the same values of $D_0 = 7$, $B = 0$ as before, and present F_T for different initial values and for the two values of ω, $\omega = 0.5$ and 2. To observe how F_T behaves with different x_0, the results for $\omega = 0.5$ plotted in Fig. 3.6. It shows that F_T increases as x_0 increases close to $(x_1^* = e)$.

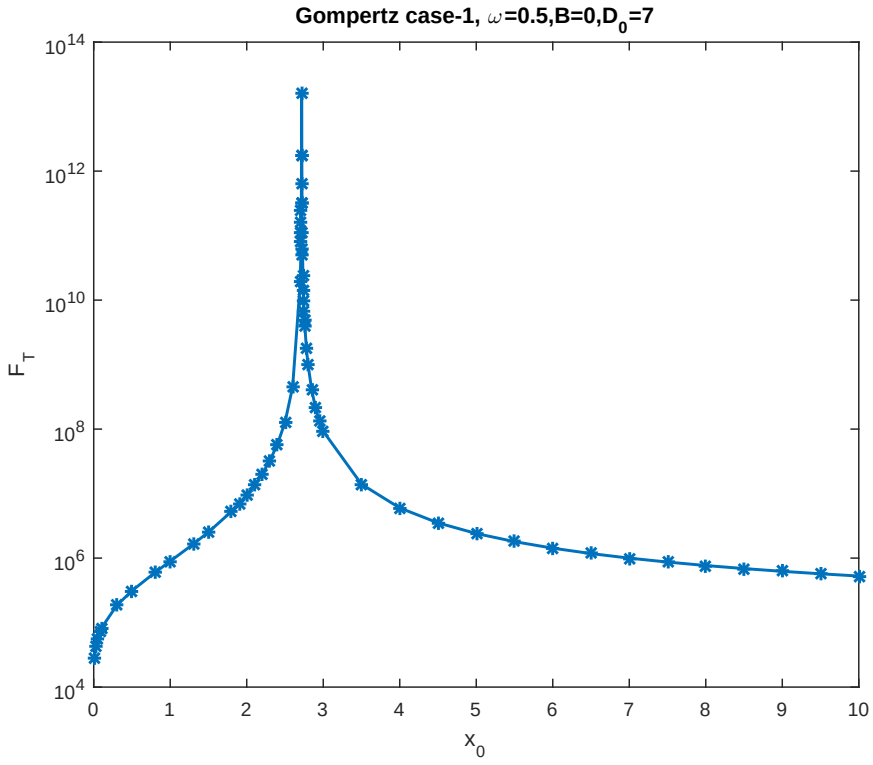

Figure 3.6: Asymptotic values of Fisher information averaged over time, F_T, against x_0 for $\omega = 0.5$, $D_0 = 7$ and $B = 0$.

In Fig. 3.6, the initial values on the left of $x_1^* = e$ yield values of F_T which are monotonically increasing to x_1^* as x_0 increases, then F_T values decreases as x_0 increases beyond x_1^*. Furthermore, this figure shows a local maximum at $x_0 \simeq x_1^*$. Similar results are found for $\omega = 2$ (figure not shown).

In this section, logistic and Gompertz equations have been compared and discussed by using PDF and Fisher information approach for different initial conditions. Both systems show larger value of F_T at initial condition closer to $x^* = K = 10$ for the logistic model and $x^* = e$ for the Gompertz model and we connect these results to the PDF for different initial values. larger F_T means less variability (unsustainable state with less dynamics to investigate) which relate to PDF with a short distance between the two peaks at the value of x_0 which is closer to x^*.

3.5 The Gompertz equation with different modulations

In previous sections, we investigated the Gompertz equation where the same modulation is applied to both positive and negative feedback. To pursue further analysis of the Gompertz equation, it is convenient to complete our investigation on the effects of the two different modulations; perturbation in the positive feedback or perturbation in the negative feedback.

3.5.1 Case-2: Perturbation in the positive feedback

We modify the birth rate c in Eq. (3.2) by including a periodic modulation, whereas we fix the death rate b as a constant as follows:

$$\frac{dx}{dt} = \Big((B + D_0 \sin(\omega t))\ x\Big) - bx \log(x). \tag{3.10}$$

The exact solution to Eq. (3.10) is found as:

$$x = \exp\left[\frac{(D_0\ b\ c) + (B\ a\ (1-d)) + (b\ D_0\ \omega\ d) + (a\ b\ d\ \log(x_0))}{a\ b}\right], \tag{3.11}$$

where

$$a = b^2 + \omega^2,$$

$$c = b \sin(\omega t) - \omega \cos(\omega t),$$

$$d = \exp(-bt).$$

From the analytical solution in Eq. 3.11, we show the typical time history of x for various values of ω, b and D_0 as in the following figure:

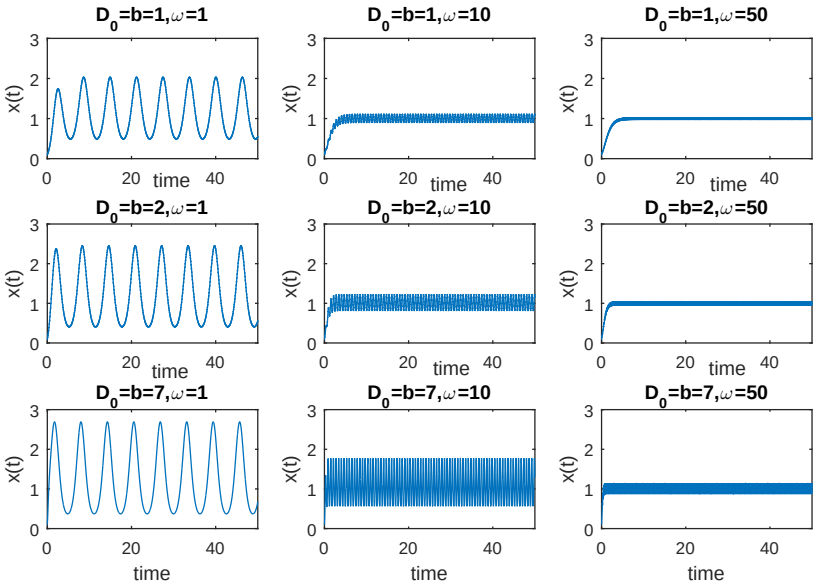

Figure 3.7: Time trace of x for different values of $D_0 = b = 1, 2, 7$ with $x_0 = 0.1$ and $\omega = 1, 10, 50$. For sufficiently small ω, the amplitude of the fluctuation is larger than the amplitude for larger values of ω.

In Fig. 3.7, we fix x_0, B and varying b $(= D_0)$ and ω. One interesting characteristic is the difference in the duration of the initial transient (the system's starting time), specifically, for small values of b, the system displays longer time before approaches the asymptotic state. If we remove the initial transient, the population settles and oscillates around a fixed point. On the other hand, for a sufficiently small ω, x fluctuates with a large amplitude in comparison for sufficiently large ω where x fluctuates with a very tight fluctuation around a fixed point. Also, for small values of ω, we observe that the time scale of perturbation becomes much larger than the growth rate in comparison with sufficiently large ω where the time scale of perturbation is much shorter than the system's response time. In this regards, we display another figure in relation to Fig. 3.7 for the same parameter values.

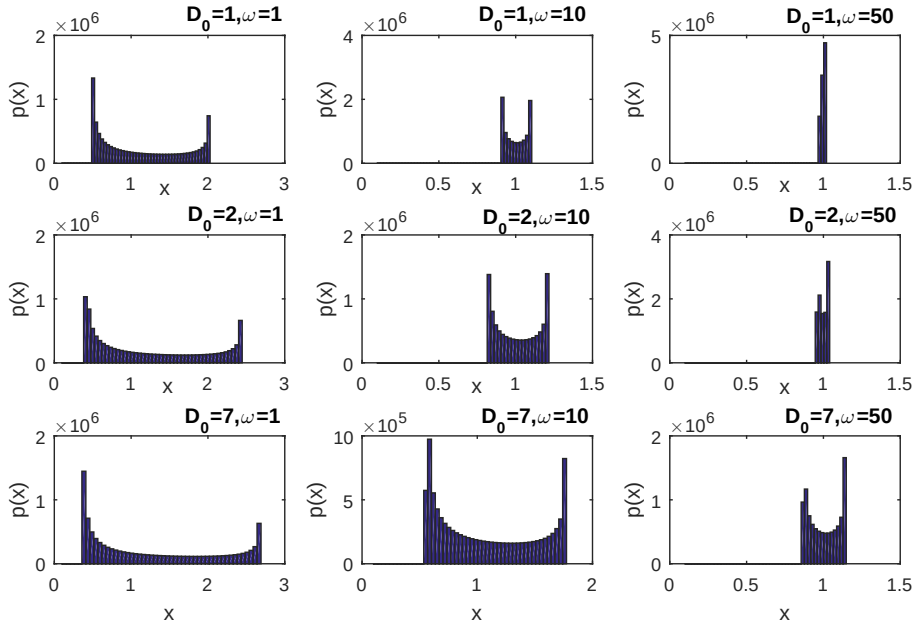

Figure 3.8: PDF of x for different D_0 and ω with $x_0 = 0.1$, $B = 0$ and $b = D_0$. The distance between the two peaks is getting smaller as ω increases.

In Figure 3.8, we illustrate the effects of different values of ω and b ($= D_0$) on PDF of x for $B = 0$, and $x_0 = 0.1$. We fix B to be $B = 0$, where the population's growth is strongly inhibited and is driven only by a periodic perturbation. Also, from our observations, we conclude that the model in Eq. (3.10) is independent of initial conditions, in other words, for different x_0 and large value of ω, the system shows a very tight PDF around $x = 1$. One more interesting feature of Fig. 3.8 is that a bimodal PDF is observed for all the parameter values with different distance between the two peaks. The distance between the two peaks of PDF becomes shorter for larger values of ω.

To make more sense, for $D_0 = b = 7$ and $x_0 = 0.1$, we compute maximum values of x for different values of ω in regards the results in Figs. 3.7 and 3.8 as follows:

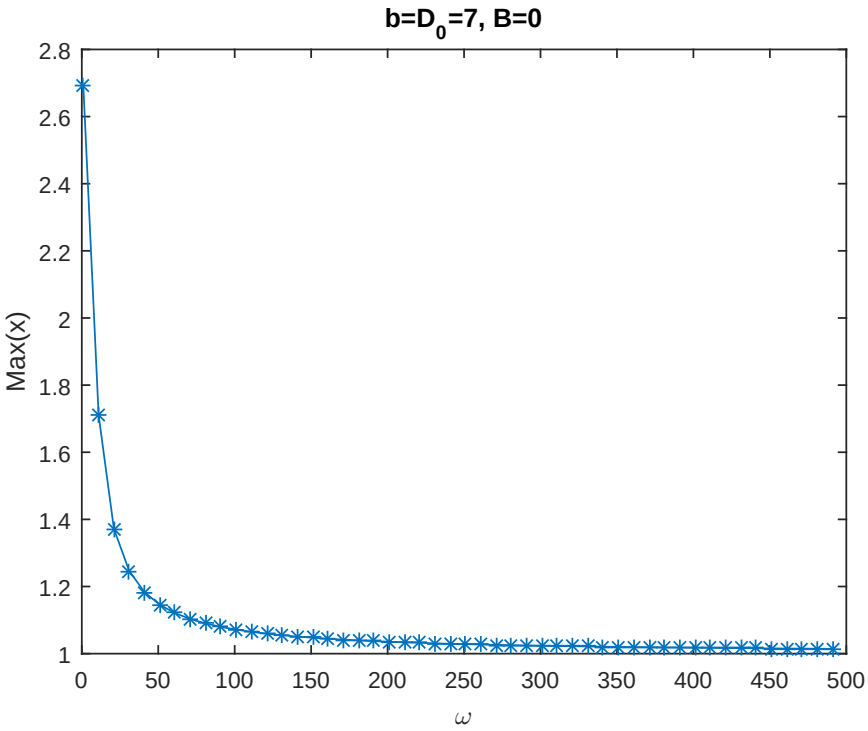

Figure 3.9: $Max(x)$ as a function of ω for $D_0 = b = 7, x_0 = 0.1$ and $B = 0$. $Max(x)$ values are monotonically decreasing as ω increases and finally show a static state at $x \simeq 1$.

An interesting behaviour of Fig. 3.9 is observed, for $D_0 = b = 7, x_0 = 0.1$ and $B = 0$, the maximum values of x are monotonically decreasing as ω increases and finally approach a static state at $x \simeq 1$.

The difference between the logistic case-2 (Fig. 2.20) and Gompertz case-2 (Fig. 3.9) is in the logistic case-2 analysis, $Max(x)$ is monotonically decreasing as ω increases and finally fluctuate around the initial conditions whereas in the Gompertz case-2, the same behaviour is observed for the $Max(x)$ but the difference is that the solution is ends at $x \simeq 1$.

In the following figure, we investigate the effects of varying the initial values on the behaviour of the Gompertz case-2. From the analytical solution in Eq. (3.11), we show the typical time history of x for different initial conditions in addition to PDFs of x in Fig. 3.10 as follows:

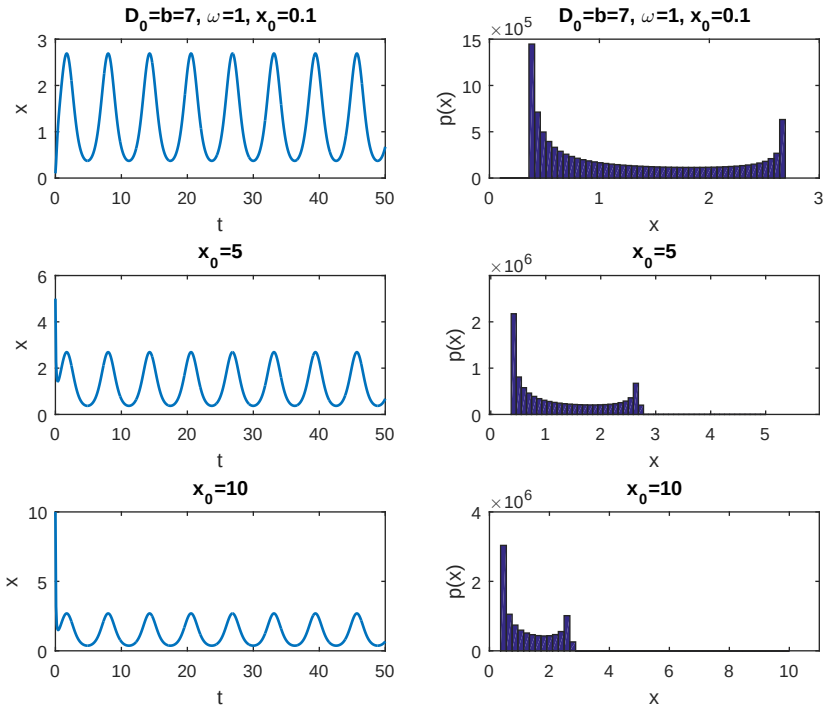

Figure 3.10: Time evolution of x in the left panels and PDFs of x in the right panels for different values of $x_0 = 0.1, 5, 10$, and fixed $D_0 = b = 7$ and $\omega = 1$.

Both, the time evolution in the left panels and PDFs in the right panels, demonstrate that the Gompertz case-2 model is independent of x_0, similarly to the logistic model. This leads to the Fisher information independence of the initial values, since Fisher information depends on the variability (gradient of PDF) of the system..

3.5.2 Case-3: Perturbation in the negative feedback

In this section and differently from case-2 just discussed, we investigate the Gompertz equation with a periodic modulation in the negative feedback whereas we have a constant in the positive feedback as follows:

$$\frac{dx}{dt} = cx - (B + D_0 \sin(\omega t))\ x\ \log(x). \tag{3.12}$$

A periodic modulation is added to the second term which includes log() where this perturbation reduces the effect of the death rate, pushing the system to grow exponentially.

Fig. 3.11 presents PDFs for $D_0 = 0.5$ in the upper panels and $D_0 = 1$ in the lower panels, respectively, for the same $x_0 = 0.1$, $B = 1$, and $c = 1$. We observe similar results as in Figure 2.20 for the logistic equation case-3 in Chapter 2.

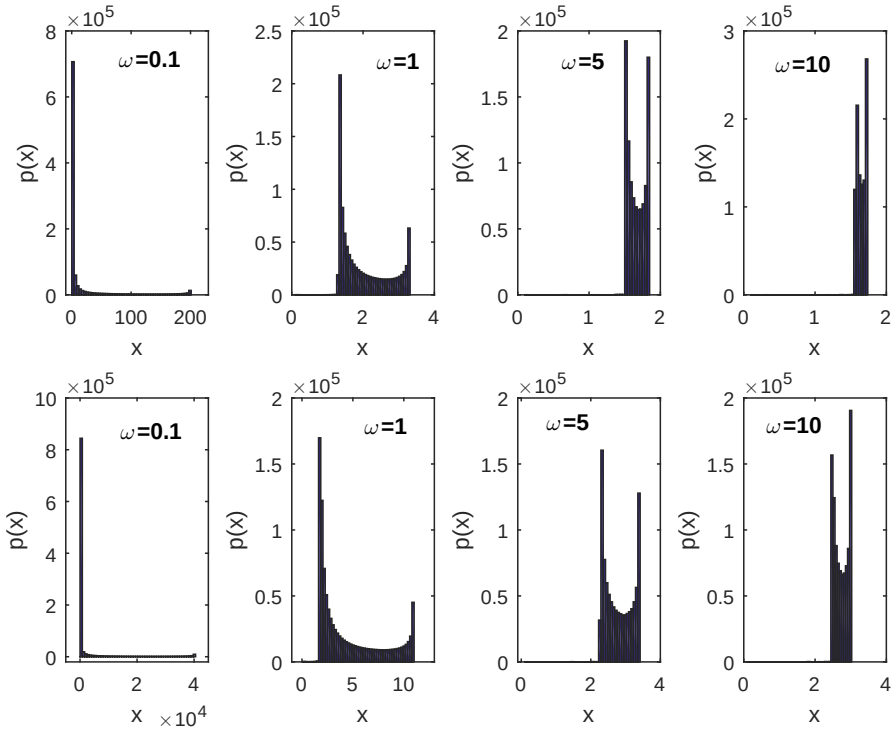

Figure 3.11: PDF of x for two different amplitude to be $D_0 = 0.5$ and 1 in the upper and lower panels, respectively. We fix the other parameter values to be $x_0 = 0.1$, $B = 1$, and $c = 1$.

In the above figure, the PDF of x becomes broadest as ω decreases and this is similar to our observation for the logistic equation case-3 whereas for larger values of ω, the system show narrowest PDF around a fixed point. For both values of D_0, the left peak at the initial condition is higher than the right peak for the small values of ω. We show these observations in detail in Fig. 3.12:

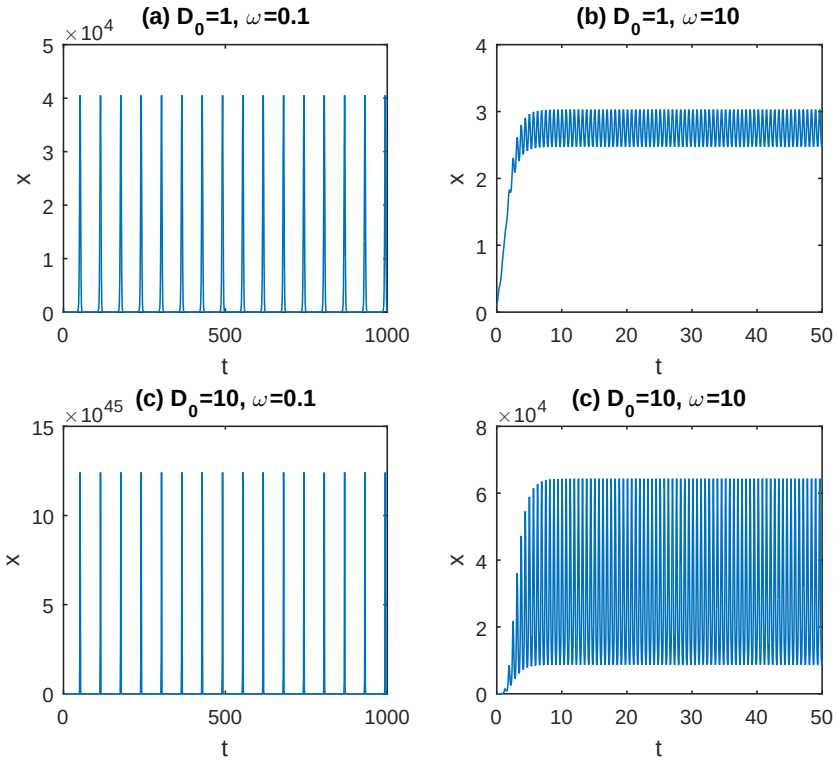

Figure 3.12: Time trace of x for two different D_0; $D_0 = 1$ and $D_0 = 10$ in the upper and lower panels, respectively and different ω. For all cases, we fix $x_0 = 0.1$, $B = 1$, and $c = 1$.

From Fig. 3.12 (b), for small D_0 and large value of ω, the solution approaches a static steady state at $x_1^* = e$. On the other hand, for sufficiently large values of D_0 and small ω such as in panel (c), the system shows an unbound grow.

3.6 Conclusions

This chapter presents the evolution of Fisher information approach and PDFs of x for the Gompertz equation for different parameter values to examine the variability/sustainability of this model. Considered jointly, the analytical and numerical analysis provide an interesting characteristics of the Gompertz equation, namely that the features of the Gompertz equation in three different cases are similar to those described

in Chapter 2 for the logistic equation.

In the case where the same periodic perturbation is added to the positive and negative feedback, the effect of different parameter values and initial conditions on the functionality of the Gompertz equation is examined. Simulation results for the Gompertz model show that the potential maintenance of a long-term memory of initial values when the characteristic time scale commitment to the disturbance is much shorter than the response time of the model, in addition to a bimodal PDF. From the point of view of variability/sustainability, maximum F_T exists at the initial condition that is closer to $x_0 \simeq x_1^*$ which is connected to the narrowest PDF (a short distance between the two peaks) with less variability (unsustainable state with less dynamics to investigate), followed by a decrease in F_T beyond $x_0 \simeq x_1^*$ which leads to an increase of the variability of the system while moving away from $x_0 \simeq x_1^*$ (beyond $x_0 \simeq x_1^*$).

That is, population of small size (corresponding to small x_0 in Gompertz model) maintains a broad bimodal PDF regardless of the value of ω whereas large values of x_0 and closer to $x_1^* = e$ show a narrowest PDF with larger F_T.

Chapter 4

A dynamical system with two-components

4.1 Introduction

Immunotherapy is an interesting therapeutic approach which is applied by modifying the tumour-immune system to achieve better results in terms of destroying the cancer population ([22]). Therefore, more attention has been paid to the characteristic interaction between the cancer cells and immune cells and, in this light, many researchers have used different mathematical models of cancer diffusion to investigate the tumour-immune behaviour (see [8] and the references there in). For example, the predator-prey model (coupled first-order differential equations) was described by [1, 13, 25] as a deterministic system in different contexts where the behaviour of the system shows a stable limit cycle solution (the solution can be seen in the same neighbourhood of the equilibrium point and they never cross each other), and the solution exhibits sensitive dependence on the initial values (Butterfly effect), in other words, a slight difference in the initial population produces a significant difference in the behaviour of the system over a long-term period. In this regard, we could observe a different trajectory for

each initial condition which leads to a family of nested closed loops or a limit cycle attractor where both variables will vary periodically with time, for example, at initial value x_0, the solution path moves in a simple limit circle over time and finally gets back to the initial value x_0 (see [12, 13, 64, 68]). For initial conditions close to the equilibrium point, x fluctuates around the equilibrium point in a tight limit close cycle where a narrow PDF is observed, while for initial points far from the equilibrium point, x fluctuates around the equilibrium but in a wider closed cycle and the PDF shows the broadest distance between the two peaks.

Our goal in this chapter is to investigate the system of two differential equations describing the interaction dynamics between cancer and immune cells from the point of view of variability/sustainability using Fisher information. In addition, we intend to explore how different sets of system parameter values could affect its dynamics; specifically, we examine in detail the system's evolution under different parameter values and its dynamics in the case of including perturbation. The main difference between our model and the classical deterministic model is the inclusion of a new term ($F\sin^2(\omega t)$) which represents the immunotherapy dose. A further consideration in our model is that the immune population has been promoted and cancer population has been forced to vanish by analysing a particular immunisation term.

The chapter is arranged as follows: Section 4.2 presents the predator-prey model in its deterministic conditions; we demonstrate the existence of equilibria, the stability and dynamics, variability, and estimate the system parameters' values; such as varying the prey mortality rate (cancer species) and finding its Fisher information. Section 4.3 presents details of the modifications made to the predator-prey model: replacement of the cancer growth rate with a logistic equation, addition of a periodic perturbation to the second equation, and then the investigation of variability/sustainability of the model using Fisher information measure. Finally, Section 4.4 presents conclusions to the chapter.

4.2 The predator-prey model

It is interesting to study the predator-prey model (coupled logistic equations for the growth of two species), due to its rich dynamics, in addition to further investigation and illustration for Fisher information as a measure of variability/sustainability. We employ the model of two differential equations given by:

$$\begin{aligned} \frac{dx}{dt} &= ax - bxy = f_1(x, y), \\ \frac{dy}{dt} &= -cy + exy = f_2(x, y). \end{aligned} \tag{4.1}$$

The two-species Lotka-Volterra equations given in Eqs. (4.1) without any fluctuation, describe a simple interaction between the population variables of two different species. Lotka (1925) and Volterra (1926) developed this model to characterize the evolution of the predator and prey fish populations where these species are referred to as the prey species $x(t)$, and its predator $y(t)$, using four parameters a, b, c, e as positive constants; (a) prey growth rate (intrinsic rate of prey population increase), (b) prey mortality rate due to predator feeding, (c) predator death rate (the mortality rate of the predator) and (e) predator growth rate. In our model, we assume the prey $x(t)$ to be cancer cells population which is attacked by the immune cells, whereas the predator $y(t)$ is the immune cells population which destroy the cancer cells. In the case of $y(t) = 0$, which means that there is no predator (immune cells), the prey population will grow exponentially according to the following equation:

$$\frac{dx}{dt} = ax. \tag{4.2}$$

The total predation is commensurate with lots of prey and lots of predators; there is no slowdown of predation in high prey abundance, and no interference between predators. The model state is defined through the densities of the population of the two species. The model has stable limit cycle behaviour, cycling with no trend either in towards the

equilibrium or out away from it, with $x(0) = x_0$ and $y(0) = y_0$ as initial conditions which initialize our analysis [25, 62, 78, 87].

The predator-prey model offers a simplistic mathematical performance of the observed dynamics of different species population in nature [87]. If the competition between the two species is not strong enough, then the two population can coexist stably but can never reach their carrying capacity in contrast to the case where one species is absent. In order to solve the differential equations, there are two different procedures: analytical and numerical approaches. As many dynamical systems have no analytical solutions under no conditions, therefore, the best choice is using numerical methods which is effortless and more common. The focus of the simulation is to examine the system's response to the different modulations.

4.2.1 Estimating parameters in predator-prey model

It is important to determine the appropriate values of the model parameters in order to better understanding the evolution of the behaviour of Eqs. (4.1). We employ the same parameter values that used in the predator-prey model presented by Cabezas et al. [13]. Furthermore, to meet our observations, we change a few parameter values and display the oscillation in the model. Details of these parameter variations and modifications applied to the model in Eqs. 4.1 are examined in the following sections.

By making the right hand side of the equations in (4.1) equal to zero ($\dot{x} = \dot{y} = 0$ [1]) as in the following set of equations, we obtain all the equilibrium points for the system.

$$\begin{aligned} 0 &= x(a - by), \\ 0 &= y(ex - c). \end{aligned} \tag{4.3}$$

From the analytical solution for Eqs. (4.3), there are two fixed points for the above system, the first one at the origin $[(x_1^*, y_1^*) = (0, 0)]$ and the second point which relies

[1] $\dot{x} = \frac{dx}{dt}$ and $\dot{y} = \frac{dy}{dt}$.

on the system parameters is $[(x_2^*, y_2^*) = (\frac{c}{d}, \frac{a}{b})]$, we analyse the stability of these points by examining the eigenvalues of the Jacobian matrix at each of these points. The Jacobian of the dynamics in Eqs. (4.1) is given by:

$$J(x, y) = \begin{pmatrix} a - by & -bx \\ ey & -c + ex \end{pmatrix}. \tag{4.4}$$

By analysing the eigenvalues of $J(x, y)$ in Eq. (4.4) using the above two equilibrium points, for the first point (x_1^*, y_1^*), we observe it is an unstable saddle point as we get one positive eigenvalue and one negative eigenvalue, whereas the second point (x_2^*, y_2^*) is found to be a centre as we can see from panel (c) in Fig. (4.1).

4.2.2 The dynamics and variability of predator-prey model

Although the mathematical models for predator-prey interaction are often deterministic, later, a periodic perturbation is added simply by modulating a deterministic model. The variability helps to investigate the sustainability of the predator-prey population where it depends on the kind of variability that could affect the dynamics of predator-prey model. For example, the reason of variability between the individuals of one species or variability between individuals from another species returns to the degree of bias for each individual or variation in the environment due to the random variation such as not all places offer good homes for animals in the same manner [19, 55, 98]. In the following figure, we present one of the effects of the variation that could affect the behaviour of the model in Eqs. (4.1) such as varying the initial conditions of the model. Here, the state of the system is now given by $(x(t), y(t))$.

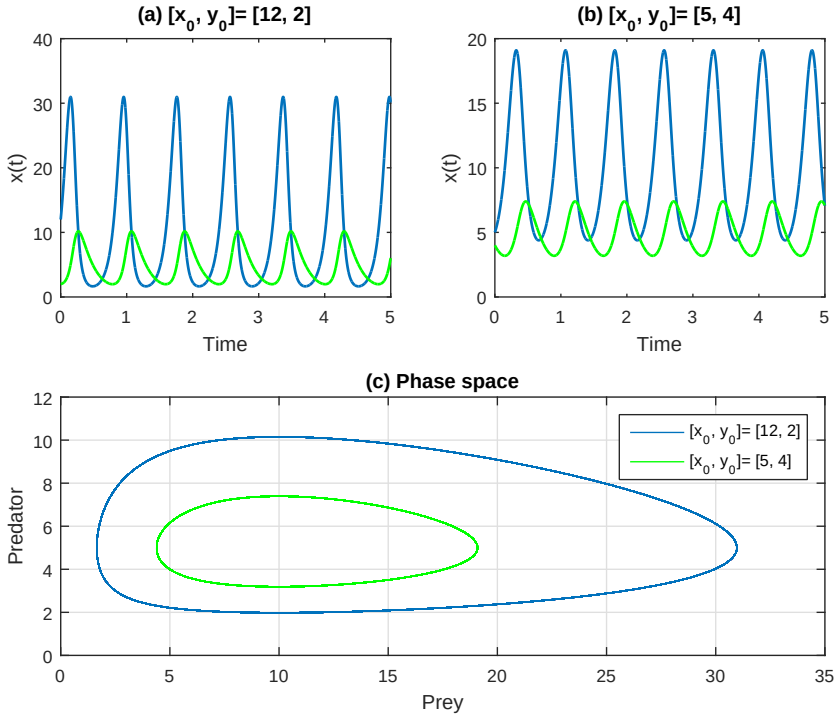

Figure 4.1: Time evolution in the upper panels and phase portrait in panel (c) for different initial conditions. A sensitivity to initial values (x_0, y_0) is observed for predator-prey model. Same parameter values are used for both curves but differ by the initial conditions.

In Fig. 4.1, the same parameter values ($a = 15$, $b = 3$, $c = 5$, $e = 0.5$) are used (similar to those used in [13]) with different initial densities for prey and predator. The graphical illustration given in Fig. 4.1 shows that this model has no asymptotic stability as it does not converge to an attractor (does not forget its initial conditions), for example, prey population may grow limitlessly without any resource limits and predators do not have saturation, their consuming average is indefinite.

In panel (c), where we construct a phase plot, i.e. a picture of the solution paths assigned by points $(x(t), y(t))$, a proportional change is observed in prey and predator densities for both initial conditions. Trajectories are closed lines. For the second initial value $[x_0, y_0] = [5, 4]$, the phase plot is very tightly distributed while for the other initial condition $[x_0, y_0] = [12, 2]$, we observe a wide elliptical phase diagram. This means that, one characteristic of the coupled logistic equations is sensitivity to the ini-

tial points. That is varying the initial values will affect the behaviour of the system which differs as time goes on (the intrinsic dynamic is controlled by the law that slight causes lead to significant effects). The amplitude and period of the cyclic population reveal its properties, (see Fig. 4.1), in which the amplitude is displayed on the $y-axis$ of panels (a) and (b) with a unit of population size. The period is the time duration of one population cycle and we can observe it on the $x-axis$ with time unit.
The predator-prey model has two equilibrium points, the first one is a saddle point at the origin of the phase portrait and the second one is a centre. This centre reflects the oscillating behaviour of the competition among both predator and prey (for food, nesting sites, etc.), which is distinguished by an oscillation frequency (number of cycles per unit time around the centre of the phase diagram).

4.2.3 Effects of changing the prey mortality rate

A convenient way to visualize the behaviour of the system is to plot the evolution of time of the population when varying the parameter values such as prey mortality rate and fixed the other parameter values to be $[x_0, y_0] = [12, 5]$ and $a = 15$, $c = 5$, $e = 0.5$. The selection of parameter values is the same as in [13].

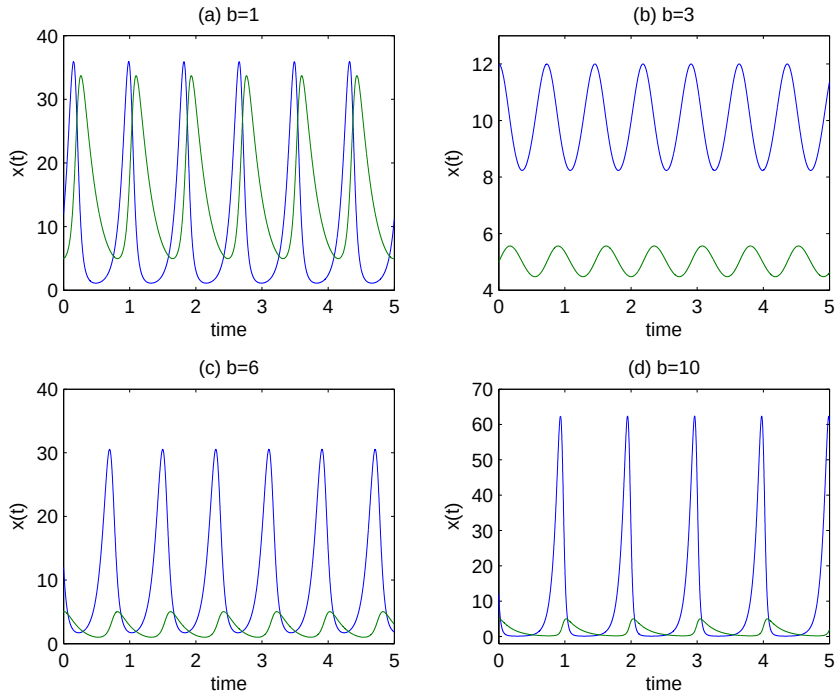

Figure 4.2: The evolution of predator-prey model for different prey mortality rate ($b = 1, 3, 6, 10$). This figure gives representation of different possible behaviour corresponding to various b. A blue line represents prey population and the green line stands for predator population.

In Fig. 4.2 we present the predator-prey model at different values of prey mortality rate. It is obvious that the dynamic of the model is different at different b. Specifically, from panel (b), we observe that there is no interaction between the cancer cells (blue line) and immune cells (green line) which leads to the state with less variability. On the other hand, for larger b, both species show a periodic behaviour spending much time near the equilibrium point as we observe from panels (c) and (d). Changing the prey mortality rate b leads to the monotonically decrease in the equilibrium points because the equilibrium points for the predator-prey model are $(x_1^*, y_1^*) = (0, 0)$ and $(x_2^*, y_2^*) = (c/d, a/b) = (10, 15/b)$, where the second equilibrium point completely depends on the model parameters a, b, c, e, since a, c, e have fixed values, then (x_2^*, y_2^*) relies only on the value of b, as we can see from the following figure:

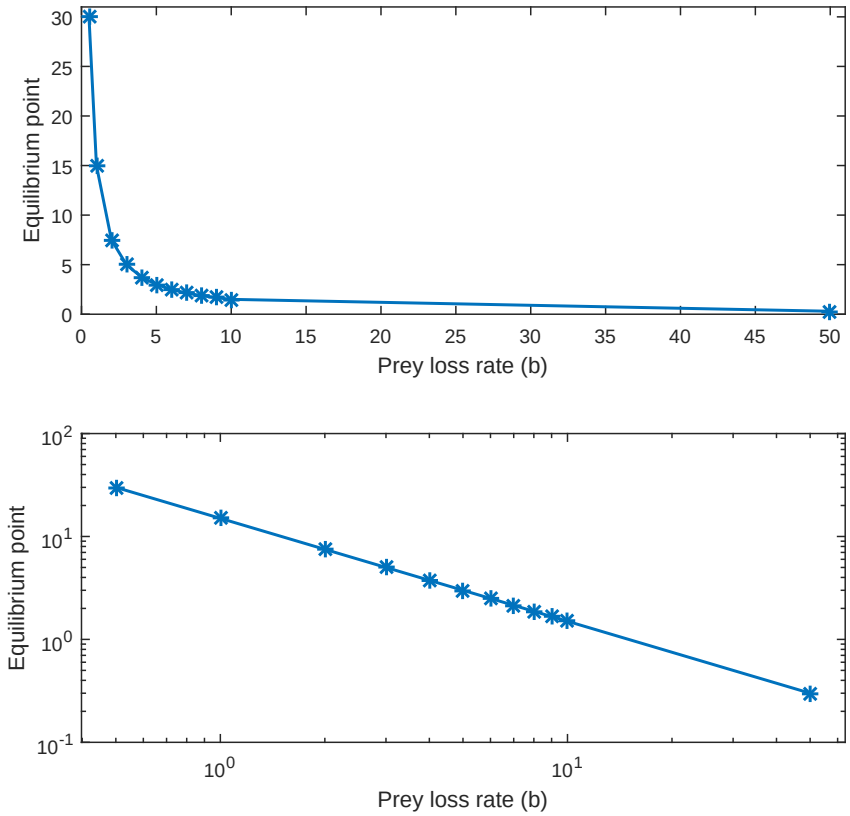

Figure 4.3: The evolution of predator equilibrium points for different prey mortality rate. Other parameters are $c = 5$, $d = 0.5$, $a = 15$ and $[x_0, y_0] = [12, 5]$. The equilibrium points are monotonically decreasing as b increases.

It is a power-law relation between the prey mortality rate and the equilibrium point as we observe from Fig. 4.3, if the prey mortality rate (cancer cells death rate) is increased, a flatten fluctuation for the predator population (immune cells) near the equilibrium point is noticed (see Fig. 4.2).

4.2.4 Fisher information for the predator-prey model

Based on the procedure of Fisher information theory presented in Appendix D, we calculate F_T, Fisher information averaged over the total time duration T from Eq. (4.1) for both species and each species, since Fisher information quantity as in Eq.

(2.14) is:

$$F_T = \frac{A}{T} \int_0^T \frac{\dot{s}^{\,2}}{s^{\,4}}\, dt\,, \tag{4.5}$$

where $s = \sqrt{\dot{x}^{\,2} + \dot{y}^{\,2}}$, A is a normalization constant and T is the total time duration, then

$$\frac{\partial s}{\partial t} = \frac{\partial s}{\partial x}\, \dot{x} + \frac{\partial s}{\partial y}\, \dot{y}\,, \tag{4.6}$$

by calculating $\frac{\partial s}{\partial x}$ and $\frac{\partial s}{\partial y}$ and substituting the results in 4.6, we obtain the following Fisher information quantity:

$$F_T = \frac{A}{T} \int_0^T \frac{\left(\dot{x}^2(a - by) + \dot{x}\dot{y}(ey - bx) + \dot{y}^2(-c + ex)\right)^2}{\left(\dot{x}^2 + \dot{y}^2\right)^3}\, dt\,, \tag{4.7}$$

In consideration to the results in section (4.2.3), for different values of prey mortality rate b and fixed $[x_0, y_0] = [12, 5]$, we compute F_T as a function of b as in Fig. 4.4, larger F_T is observed at $b = 3$, where the model shows a very tight cycle around the equilibrium point (less variability), (see Fig. 4.5), on the other hand, the model at this value is an undesirable state to investigate due to the lack of interaction between the two species and less dynamics. In comparison with the other values of b ($\neq 3$), where the state variables go through large oscillations and the system has lower F_T due to it is probably not functioning well (high variability). We consider b within a wide range to make significant observations.

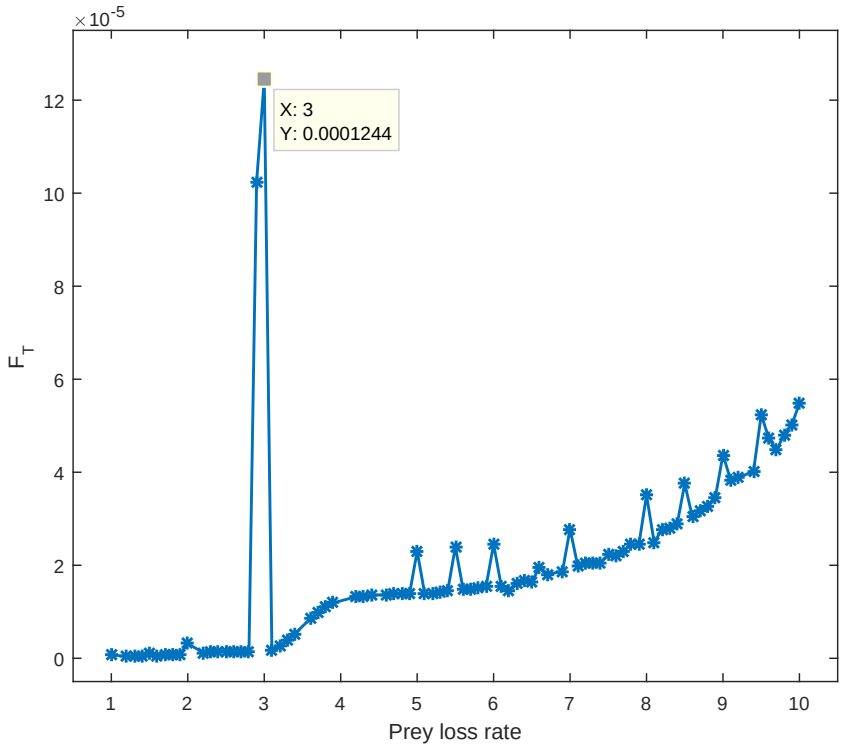

Figure 4.4: F_T against prey mortality rate b. We fix $[x_0, y_0] = [12, 5]$, $a = 15, c = 5, e = 0.5$ and varying b, A local maximum for F_T is noticed at $b = 3$.

In Fig. 4.4, we show F_T at different prey mortality rate which related to Figs. 4.2 and 4.3. The most interesting feature of the above figure is the local maximum of F_T at $b = 3$, then the curve begins to decrease beyond $b = 3$. In order to strength our conclusion, we display the PDF of x with a phase portrait in the following figure at different values of b.

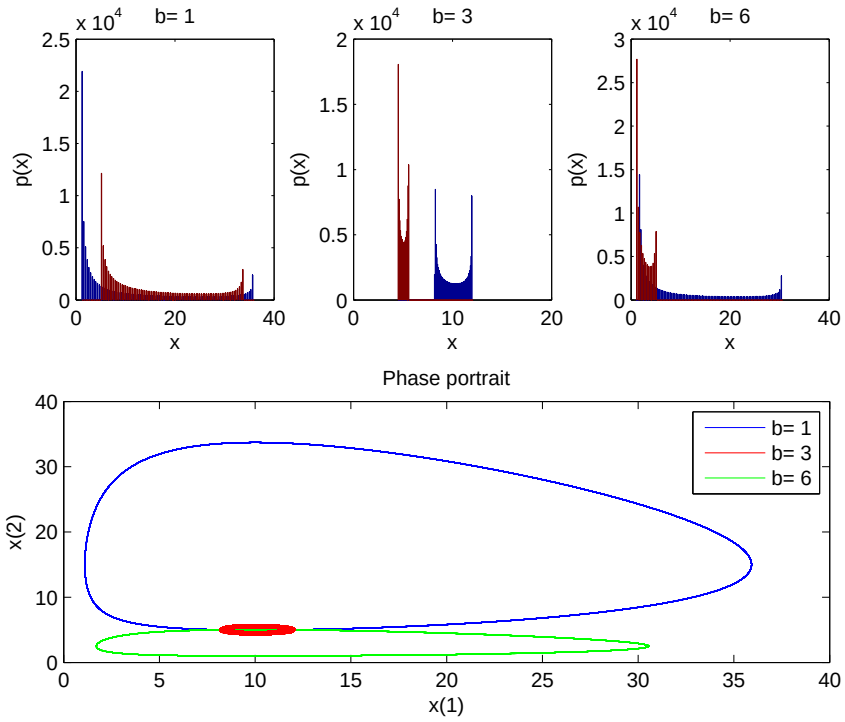

Figure 4.5: PDF of predator and prey population in the upper panels and phase portrait for different prey mortality rate ($b = 1, 3, 6$) in the lower panel. Other parameter values are taken as $[x_0, y_0] = [12, 5]$, $a = 15, c = 5, e = 0.5$. A very tight cycle is noticed for $b = 3$.

The dynamics of the model (pairs of first-order differential equations) is different at different b, such as when $b = 3$, we have a narrowest PDF around the equilibrium point $[10, 5]$, this is obvious from the phase portrait (red circle) for $b = 3$ which show a very tight cycle around the equilibrium point $[10, 5]$, in contrast to the other values of b where they show a wide elliptical. In addition to the lack of interaction between the two species. However, the global behaviour is a limit cycle but these $x - y$ cycles increase or decrease their amplitude depending on the value of b.

We perform another investigation for the model in Eqs. 4.1 by calculating F_T from both species in addition to F_T from each species for different initial conditions and fixed the other parameter values (figure not shown). Fisher information values obtained from one species (Predator or prey) are larger than Fisher information values which calculated from both species and there is one explanation for this trend which

is that the larger values of F_T from each species indicates to the less variability in the system as there is only one species survive but it is not necessarily to be a more desirable state.

The above results indicate the importance of Fisher information as a function of variability/sustainability, where we conclude from the above figures that we have a peak at b value where there is no interaction between the two species. This leads to the less sustainable case (boring case) in which there is no real interaction.

Here, we present the observations of the deterministic model which means that the cancer and immune population are behaving under natural conditions whereas modifications in the model (4.1) are considered in the following sections.

4.3 Modifications to the predator-prey model

4.3.1 Prey density dependence

As discussed earlier, the predator-prey model behaviour has been studied by many researchers in its deterministic form and a random or periodic form. Here, replacing the exponential growth of the prey population (cancer cells) by a logistic growth with a carrying capacity $N = \frac{1}{K}$ yields the model:

$$\begin{aligned} \frac{dx}{dt} &= ax\,(1 - Nx) - bxy, \\ \frac{dy}{dt} &= -cy + exy. \end{aligned} \tag{4.8}$$

In this model, the prey growth (cancer cells) is given by the logistic equation with a deterministic growth rate a. N is the reciprocal of the carrying capacity of the cancer cells population ($\frac{1}{N}$ is the maximum population size of cancer cells). By investigating the stability of the above model, we found three equilibrium points, the first equilibrium point is at the origin $(x_1^*, y_1^*) = (0, 0)$, the second one which depends on the value

of N is $(x_2^*, y_2^*) = (\frac{1}{N}, 0)$, and the third one is $(x_3^*, y_3^*) = \left(\frac{c}{e}, \frac{a}{b}(1 - \frac{c\,N}{e})\right)$. The Jacobian matrix of the dynamics in Eqs. (4.8) is given by

$$J(x, y) = \begin{pmatrix} a - 2aNx - by & -bx \\ ey & -c + ex \end{pmatrix}. \tag{4.9}$$

The first equilibria (x_1^*, y_1^*) is a saddle point everywhere. The stability of the system depends on the parameter values, for example, if $a = b = c = e = 1$, then the system has a stable spiral at $\left(\frac{c}{e}, \frac{a}{b}(1 - \frac{cN}{e})\right) = (1, 0.9)$ whereas if $a = 15, b = 3, c = 5, e = 0.5$, then the system stabilize at a stable node $(\frac{1}{N}, 0) = (10, 0)$ with fixed $N = 0.1$, as we can see from Fig. 4.6.

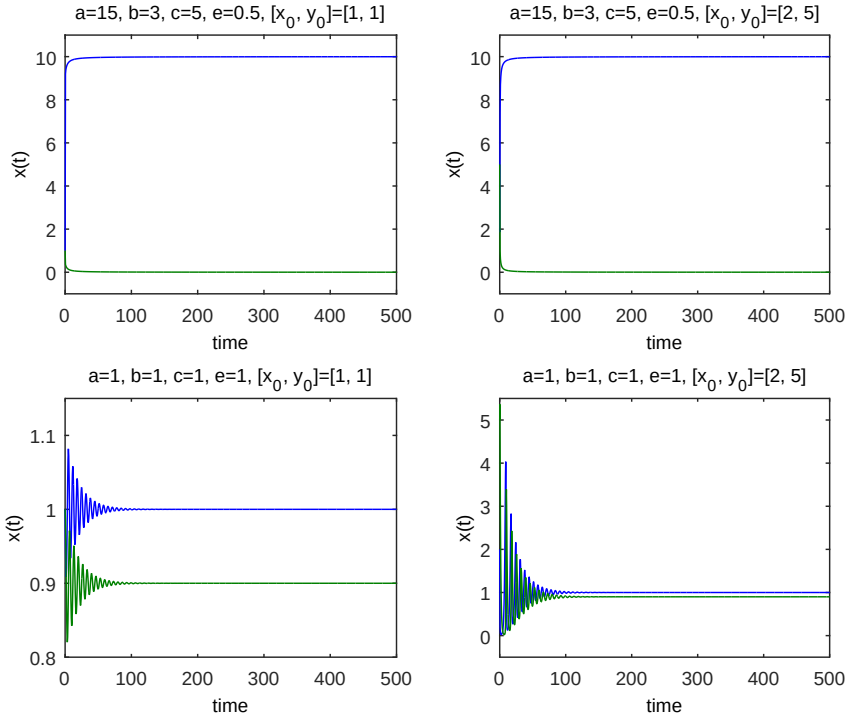

Figure 4.6: Time evolution for different parameter values with a logistic equation in the prey density. Same parameter values are used in the upper panels, but with different $[x_0, y_0]$, similar case for the lower panels. A blue line for cancer cells and green for immune cells.

We use two different initial conditions in Fig. 4.6 for the sake of completeness where

the system shows its independence on the initial values. For the different initial values and different parameters, the solutions tend to positive equilibrium points. In the lower panels, we observe that the amplitude of the solution becomes smaller and smaller over time, this means that the stability of the equilibrium point becomes more robust as t increases. The only difference between the two initial conditions is the initial transient for the model.

The predator-prey model is given as follows after applying a dimensionless procedure (the details are presented in Appendix A)

$$\begin{aligned} \frac{du}{d\mathcal{T}} &= u(1-u) - \alpha uv\,, \\ \frac{dv}{d\mathcal{T}} &= -\beta v + \gamma uv\,. \end{aligned} \tag{4.10}$$

where the quantities in Eqs. (4.8) are rescaled according to

$$u = \frac{b}{a}\,x, \quad v = \frac{e}{c}\,y \quad \textit{and} \quad \mathcal{T} = a\,t,$$

As a result, we obtain the model (4.10) with less parameters. The parameter $\mathcal{T}$ is an arbitrary time constant. Solving a dimensionless version in (4.10) yields three equilibrium points, $(u_1^*, v_1^*) = (0,0)$, $(u_2^*, v_2^*) = (1,0)$ and $(u_3^*, v_3^*) = \left(\frac{\beta}{\gamma}, \frac{1}{\alpha}(1-\frac{\beta}{\gamma})\right)$. The Jacobian matrix of the dynamics in Eqs. (4.10) is given by

$$J(x,y) = \begin{pmatrix} 1-2u-\alpha v & -\alpha u \\ \gamma v & -\beta+\gamma u \end{pmatrix}. \tag{4.11}$$

By analysing the stability of these equilibrium points which depends on the nature of the solutions to the linear system of ODEs, we can classified the equilibrium points as either stable or unstable points. An equilibrium point $(u_1^*, v_1^*) = (0,0)$ is found to be a saddle point (eigenvalues with different signs), whereas the second equilibrium point $(u_2^*, v_2^*) = (1,0)$ is found to be a stable point regardless initial conditions as we can see in Fig. 4.7.

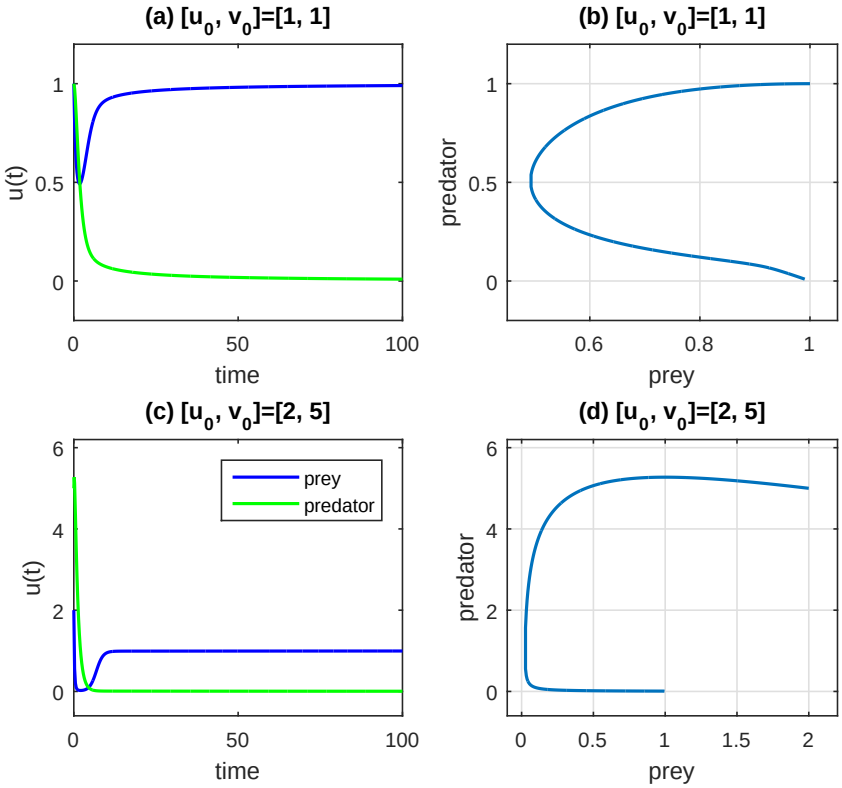

Figure 4.7: Time trace and phase portrait for different initial values and fixed parameter values $\alpha = \beta = \gamma = 1$. The left panels represent the time trace and right panels stand for the phase portrait.

In Fig. 4.7, we show the predator-prey model presented in Eqs. 4.10 with a logistic growth for the cancer population, fixed values of α, β and γ are used to be $= 1$ and different values of initial conditions in the upper and lower panels, respectively. One interesting characteristic of the model in Eqs. (4.10), where the cancer and immune cells grow without any control this means in the absence of therapy, is that the system shows a stable solution at the equilibria $(u_2^*, v_2^*) = (1, 0)$ with no interaction between the two species after passing the initial transient.

4.3.2 The predator-prey model with a periodic function in the immune population

The predator-prey model (4.8) is exposed to an external periodic stimulus such as adding a periodically function to the second equation in order to control the periodical dose of the treatment (immunotherapy), which is expected to affect the behaviour of the non-infected (immune cells), and infected cells (cancer cells) by promoting and inhibiting their growth and/or death, (immune cells win, whereas the cancer population is driven to extinction) [8]. Therefore, Eqs. (4.8) can be rewritten as

$$\frac{dx}{dt} = ax(1 - Nx) - bxy\,, \tag{4.12a}$$

$$\frac{dy}{dt} = -cy + exy \; + F\sin^2(\omega t). \tag{4.12b}$$

Here, $x(t)$ represents cancer cells population at time t with a growth rate a and carrying capacity N, $y(t)$ denotes to the population of immune cells and the term $F\sin^2(\omega t)$ represents the external source of immune cells (immunotherapy), where F is the periodic signal amplitude with ω as a periodic signal frequency. The effects of these parameters (the amplitude F and frequency ω) are analysed numerically, in order to find out under any circumstances the cancer cells can suffer extinction (the cancer cells show zero average at specific values of parameters). The model shows a periodic form after applying a periodic modulation to the model parameters such as a sinusoidal form [39]. Also, we observe that the population has enough time to reach the equilibrium point (equilibrium point for the mean value of the perturbation) for small values of ω [5, 39]. All of the following analysis seeks to observe the changes in both species as changing the amplitude, frequency and initial values. It is also important to show if the cancer population can reach an extinction state because of the external periodic stimulus. The equations in (4.12), can be present in a dimensionless form as follows:

$$\begin{aligned} \frac{du}{d\mathcal{T}} &= u(1-u) - \alpha uv, \\ \frac{dv}{d\mathcal{T}} &= -\beta v + \gamma uv + \delta F sin^2(\Omega\mathcal{T}), \end{aligned} \tag{4.13}$$

we rescaled the quantities in Eqs. (4.12) according to

$$\mathcal{T} = at, \;\; u = \frac{b}{a}x, \;\; v = \frac{e}{c}y, \;\; N = \frac{b}{a}, \;\; \alpha = \frac{cb}{ae},$$
$$\beta = \frac{c}{a}, \;\; \gamma = \frac{e}{b}, \;\; \delta = \frac{e}{ac} \;\; and \;\; \Omega = \frac{\omega}{a}.$$

The first equation in (4.13) indicates the rate of change of the cancer cells population and the second equation represents the immune cells dynamics. In order to find the equilibrium points for the model (4.13) (equilibrium points for the mean value of the perturbation), we make the right-hand sides of the equations equal to zero and fixed the values of $\alpha = 1$, $\beta = 1.291$, $\gamma = 1$, $\delta = 1$ and $\Omega = 1$, three fixed points are found. The first one is $(u_1^*, v_1^*) = (0, \frac{F}{2.582})$, the second one is $(u_2^*, v_2^*) = (1.1455 - \sqrt{\frac{0.0847+2F}{2}}, -0.1455 + \sqrt{\frac{0.0847+2F}{2}})$, and the third equilibrium point is $(u_3^*, v_3^*) = (1.1455 + \sqrt{\frac{0.0847+2F}{2}}, -0.1455 - \sqrt{\frac{0.0847+2F}{2}})$. By utilizing the Jacobian matrix for the model (4.13), we investigate the stability of these equilibrium points (equilibrium points for the mean value of the perturbation) depending on the value of amplitude F such as, when $F = 0.1$, $(u_1^*, v_1^*) = (0, 0.0387)$ and $(u_3^*, v_3^*) = (1.4123, -0.4123)$ are unstable saddle points, whereas $(u_2^*, v_2^*) = (0.8787, 0.1213)$ is a stable spiral as we can see from Fig. 4.8:

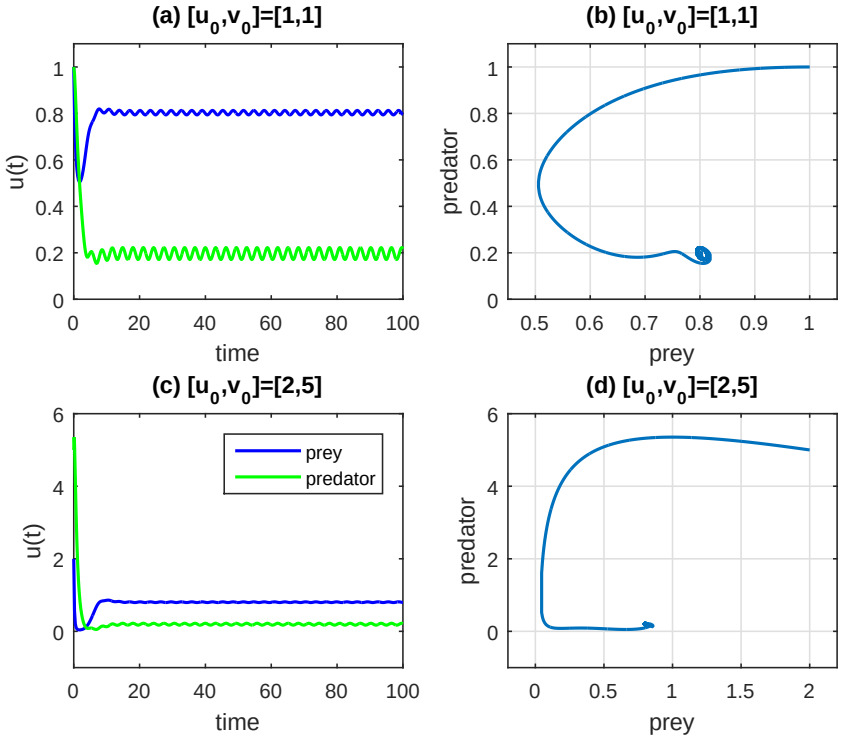

Figure 4.8: Time evolution in the left panels and phase portrait in the right panels for $\alpha = 1$, $\beta = 1.291$, $\gamma = 1$, $\delta = 1$, $\Omega = 1$ and $F = 0.1$ with different initial conditions. We observe a fixed point $(u_2^*, v_2^*) = (0.8032, 0.1968)$ which is stable and attracts all the solutions.

In Fig. 4.8, we fix the initial value of the system to be $[u_0, v_0] = [1, 1]$ in the upper panels and $[u_0, v_0] = [2, 5]$ in the lower panels, where the left panels represent the time evolution of the model (4.13), while the right panels represent the phase portrait.

On the other hand, for larger values of amplitude F such as $F = 3$, the model (4.13) have three equilibrium points (equilibrium points for the mean value of the perturbation) but with different stability behaviour. When $F = 3$, the three fixed points are $(u_1^*, v_1^*) = (0, 1.1619)$, $(u_2^*, v_2^*) = (-0.0879, 1.0879)$ and $(u_3^*, v_3^*) = (2.3789, -1.3789)$. The first equilibrium point is a stable node while the other points are unstable saddle points as in the following figure.

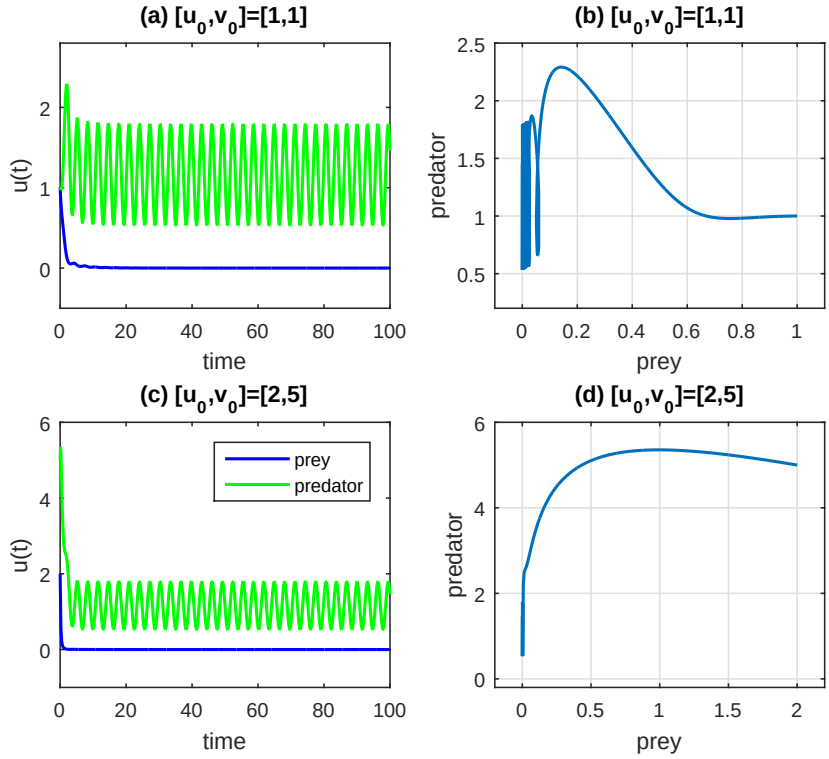

Figure 4.9: Time evolution in the left panels and phase portrait in the right panels for $\alpha = 1$, $\beta = 1.291$, $\gamma = 1$, $\delta = 1$, $\Omega = 1$ and $F = 3$ with different initial conditions. We observe a stable node $(u_1^*, v_1^*) = (0, 1.1619)$ for all initial conditions.

The observations obtained can be explained in terms of a biological model of cancer growth. For simplicity, we fix $\alpha = 1$, $\beta = 1.291$, $\gamma = 1$, $\delta = 1$ and $\Omega = 1$ in our computation. For larger values of the amplitude F in the periodic function (a periodic therapy which enhance the growth of immune cells and destroy the cancer population), the solution is still stable everywhere but we observe how the prey (cancer cells) vanish as it is obvious from Fig. 4.9 (left panels), regardless the initial values.

From the perspective of variability/sustainability, for $F = 3$, the variability/sustainability of the model (4.13) is less than that in model (4.10) (without immunotherapy term), because one of the species is vanishing at specific value of F.

Changing parameter values such as F and x_0 in the model (4.13) may change our observations which is quite normal because the whole treatment plan relies on the con-

ditions of the patient, their defence mechanism, gender and more various factors. The following figures will illustrate the advantages of adding an effective immunisation against the evolution of cancer growth. Also, for sufficiently small values of Ω, it is observed that this convergence occurs for any initial value in the limits of initial values and the equilibrium points (equilibrium points for the mean value of the perturbation). The prey which represents cancer cells population in Fig. 4.8 where $F = 0.1$ and Fig. 4.9 with $F = 3$, is switch from the steady stable state for sufficiently small values of the amplitude F to the extinct state for sufficiently large F. The amount of the therapy dose (the amplitude of a periodic modulation in the second equation in model (4.13) is added to control the growth of the cancer density and keep them in their lower level in the host body. Thus, in consideration of the above observations and to make more sense, we display $Max(x)$ for cancer and immune cells as a function of Ω for fixed amplitude value in the following figure.

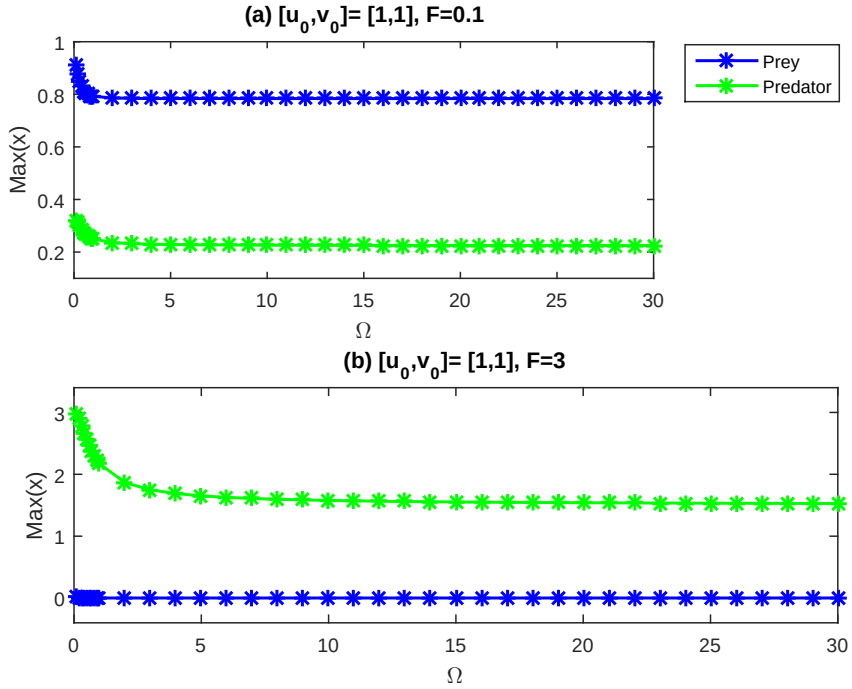

Figure 4.10: Maximum values of population against Ω for different amplitude with $\alpha = 1$, $\beta = 1.291$, $\gamma = 1$ and $\delta = 1$. $Max(x)$ values are monotonically decreasing as Ω increases for both amplitude values. The difference between panels (a) and (b) is that for larger values of amplitude, we observe the eradication of the cancer cells.

In Fig. 4.10, we display maximum values of cancer and immune population (blue and green lines, respectively), with two different amplitude values against Ω ($F = 0.1$ in panel (a) and $F = 3$ in panel (b)). We notice that for $F = 3$, the immune cells are in a higher level than the cancer cells for all the values of Ω in comparison with the results in panel (a). Also, the cancer cells eradicated at $F = 3$.

In the following figure, since our goal is to reduce or at least control the number of cancer cells, we only consider maximum values of cancer population (prey species) due to its harmful effects on the host body. In order to complete our investigation regarding the optimal values of F and Ω in the periodic modulation in Eqs. (4.13), we provide Fig. 4.11 which presents $3D$ figure for Ω, F and $Max(x)$.

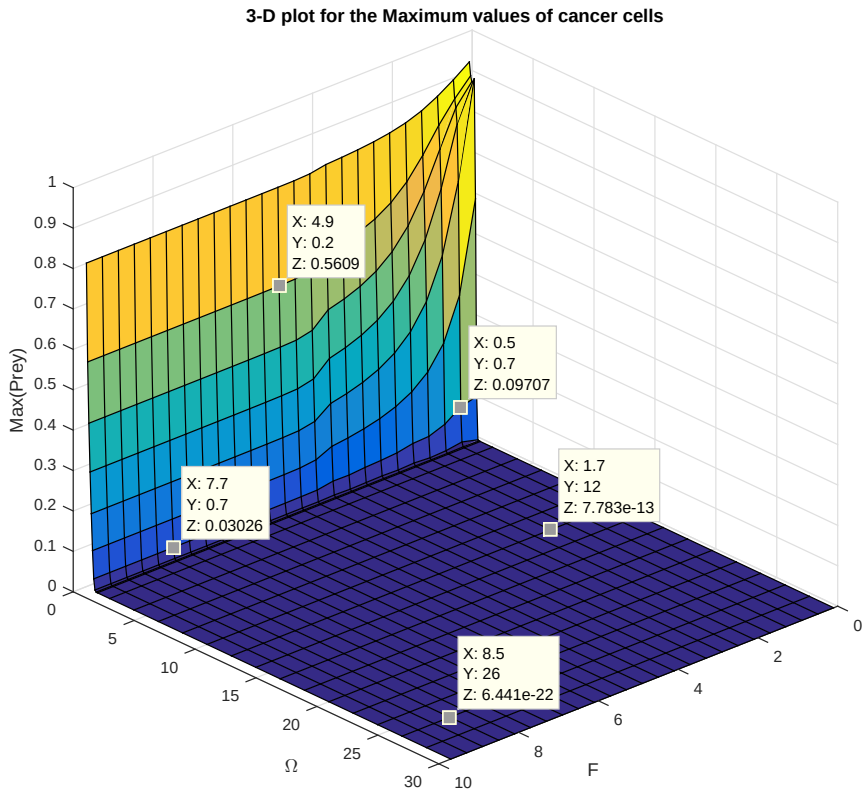

Figure 4.11: Maximum values of cancer population (prey) on the $z-axis$, F on the $x-axis$ and Ω in the $y-axis$ in a $3D$ plot. A monotonic decrease is noticed in the prey population for a sufficiently large Ω. We fixed $[u_0, v_0] = [1, 1]$, $\alpha = 1$, $\beta = 1.291$, $\gamma = 1$ and $\delta = 1$.

Maximum values of prey in the above figure show a monotonic decrease as Ω increases. In this light, we select all the values of F and Ω where $Max(prey)$ is observed around zero. The results are displayed in the following figure (Fig. 4.12), in order to determine the optimal value of the amplitude which eliminate the cancer cells population.

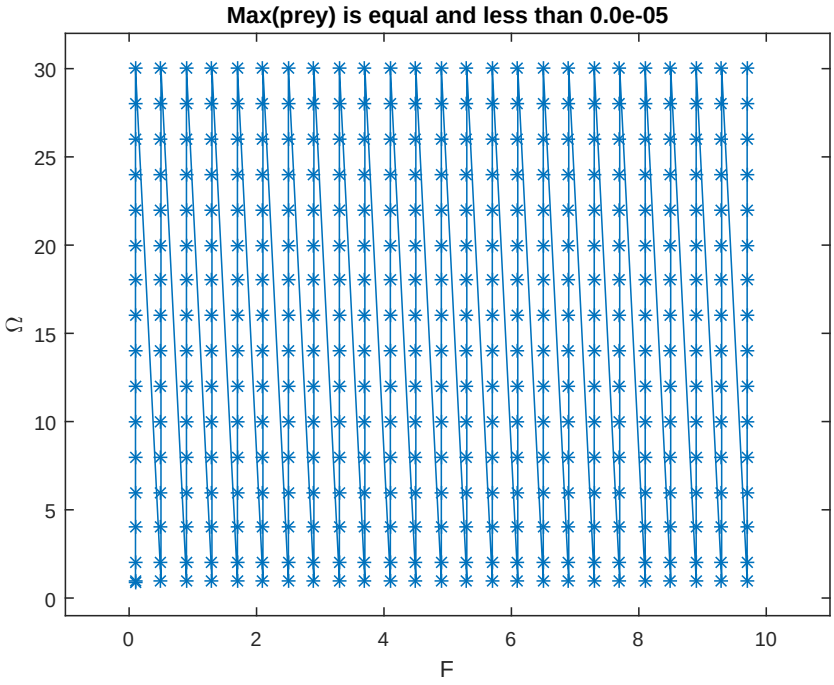

Figure 4.12: Maximum values of cancer population (prey species) when it is equal and less than 0.0e-05 for $[u_0, v_0] = [1, 1]$, $\alpha = 1$, $\beta = 1.291$, $\gamma = 1$ and $\delta = 1$.

In Fig. 4.12, the existence of fluctuation in the values of $Max(prey)$ is due to the frequency Ω of the periodic modulation in model (4.13). Based on this, instead of including the periodic modulation ($sin^2(\Omega T)$) (periodic therapy dose), we only consider the anti-cancer therapy in the second equation of model (4.13) as a constant such as ($\frac{F}{2}$) (mean value of the perturbation), this means without any fluctuation, and the results are presented in the following figure, in order to compare between the two cases (with fluctuation and with a constant).

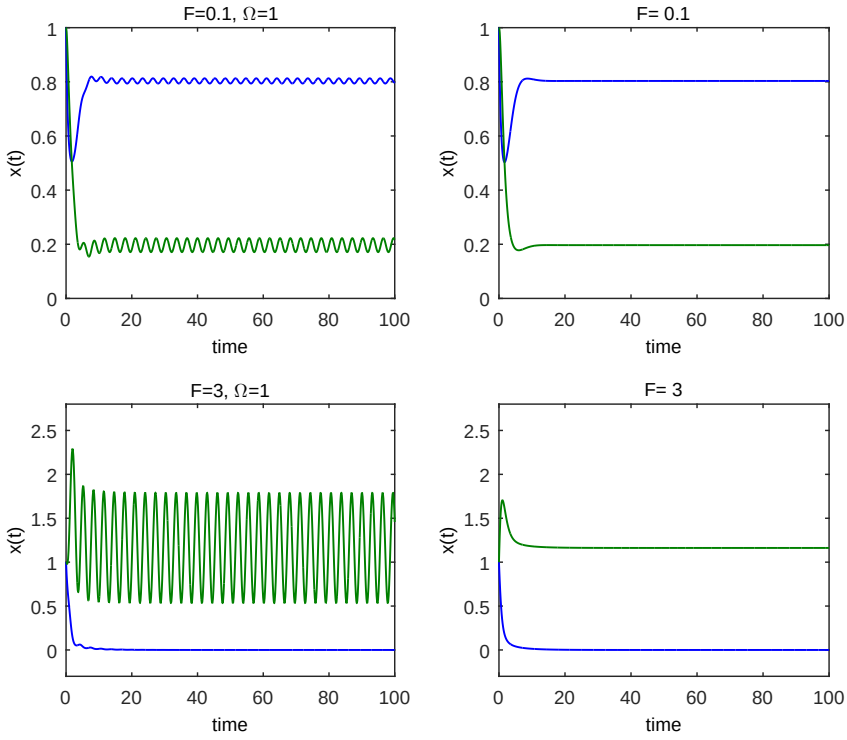

Figure 4.13: Time trace of population for different values of F with and without fluctuation for $[u_0, v_0] = [1, 1]$, $\alpha = 1$, $\beta = 1.291$, $\gamma = 1$, $\delta = 1$ and $\Omega = 1$. Blue line represents prey while the green line stands for predator.

The difference between the left panels which include fluctuation ($sin^2(\Omega T)$) and the right panels which only include a constant ($\frac{F}{2}$) is obvious. It is also important to clarify that the output ω in left panels from Fig. 4.13, is twice as the frequency in Eqs. (4.13), $\omega_{Output} = 2\Omega$. For example, when $F = 0.1$ and $\Omega = 1$, we observe that the distance T between two peaks is 3.15 on the $x - axis$, then we calculate ω_{Output} according to the following form:

$$\omega_{OutPut} = \frac{2\pi}{T},$$

here, we obtain $\omega_{Output} \approx 2$ which is twice as the frequency Ω (Ω_{Input}) in Eqs. (4.13), that is equal to 1. Similar observations have been obtained for different values of Ω.

4.3.3 Fisher information in the modified predator-prey model

We investigate the model in (4.13) from the perspective of information theory. By following the procedure of Fisher information theory presented in Appendix D for the deterministic predator-prey model, we calculate F_T for the model in (4.13) as follows:

$$F_T = \frac{A}{T} \int_0^T \frac{\dot{s}^{\,2}}{s^{\,4}}\, dt\,, \tag{4.14}$$

where $s = \sqrt{\dot{u}^{\,2} + \dot{v}^{\,2}}$, A is a normalization constant and T is the total time duration, then

$$\frac{\partial s}{\partial t} = \frac{\partial s}{\partial u}\,\dot{u} + \frac{\partial s}{\partial v}\,\dot{v}, \tag{4.15}$$

by calculating $\frac{\partial s}{\partial u}$ and $\frac{\partial s}{\partial v}$ and substituting the results in 4.15, we obtain:

$$F_T = \frac{A}{T} \int_0^T \frac{\Big([\dot{u}^2\,(1 - 2u - \alpha v)] + [\dot{v}^2\,(\gamma u - \beta)] + [\dot{u}\dot{v}(\gamma v - \alpha u)]\Big)^2}{\Big(\dot{u}^2 + \dot{v}^2\Big)^3}\, dt, \tag{4.16}$$

Using Eq. 4.16, for different control values of F which represents immunotherapy treatment and fix $[u_0, v_0] = [1, 1]$, $\alpha = 1$, $\beta = 1.291$, $\gamma = 1$, $\delta = 1$ and $\Omega = 1$ to find Fisher information as an index of variability/sustainability.

For $F = 0$, which means that there is no external effects (no doses of immunotherapy) included in the system, a periodic behaviour is noticed for the two population and from the point of view of sustainability, the system is less sustainable in this case due to the absence of the interaction between the two species (boring case study) with large value of Fisher information [8, 78]. Based on the background theory displayed in thousands of references on cancer. it is worth to investigate the interaction between the two species.

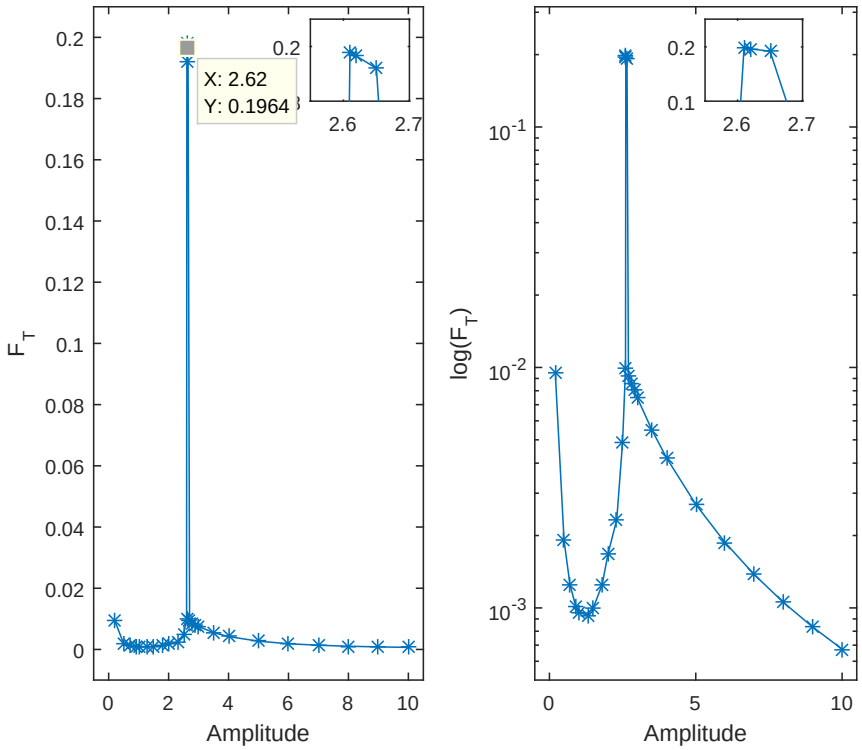

Figure 4.14: Fisher information against F for $[u_0, v_0] = [1, 1]$, $\alpha = 1$, $\beta = 1.291$, $\gamma = 1$, $\delta = 1$ and $\Omega = 1$. A peak for F_T is observed at $F = 2.62$ which leads to state with less variability.

In Fig. 4.14, we focus on the second panel in log-scale for the $y - axis$. We observe that F_T is monotonically increasing as F increases until we get to the optimal value of the amplitude $F = 2.62$, where one of the population which is the cancer cells starts to vanish, then F_T is monotonically decreasing beyond $F = 2.62$, because the cancer cells population is vanishing (unsustainable state due to lack of dynamics). Finally, we performed simulations for the model at three specific values of the amplitude as we can see in Fig. 4.15 in relation to Fig. 4.14.

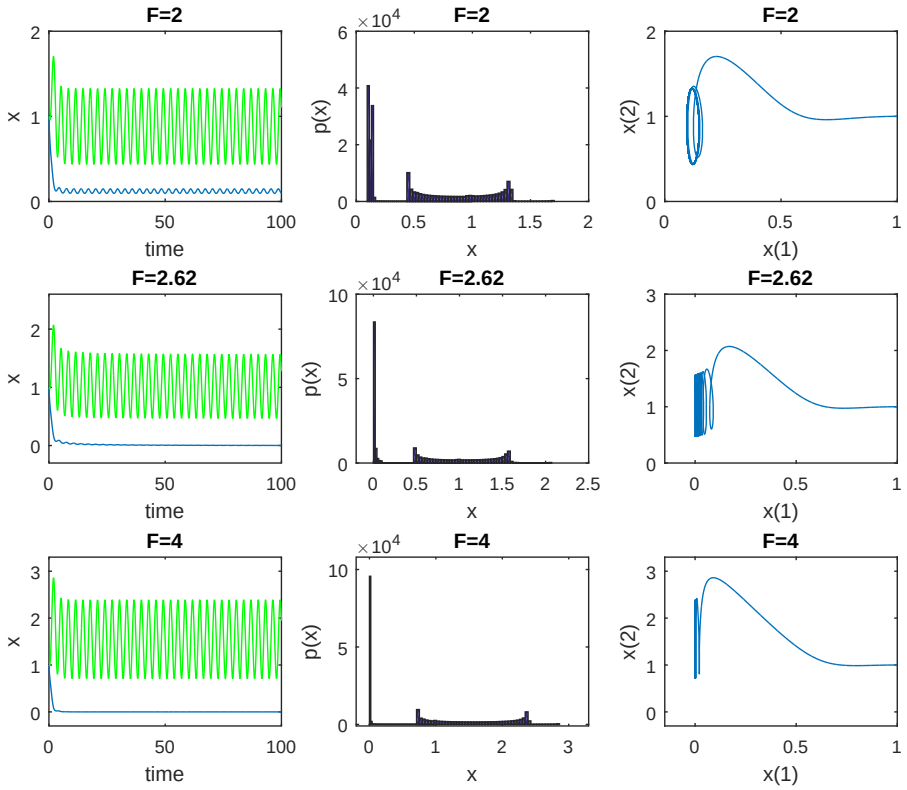

Figure 4.15: Time evolution of x, PDFs and phase portrait for different values of F and fix other parameter values as $[u_0, v_0] = [1, 1]$, $\alpha = 1.291$, $\beta = 1$ and $\Omega = 1$.

In the upper panels, when $F = 2$, the cancer cells population is surviving with a small fluctuation near zero in contrast to $F = 2.62$, this population is eradicated, while the immune cells population show a stable behaviour. For larger F such as in the lower panels, the amplitude for the immune cells fluctuation is growing while the cancer cells appeared at zero.

Furthermore, we investigate the predator-prey model with and without perturbation for different initial conditions. For example, for initial values close to the equilibrium point (equilibrium point for the mean value of the perturbation), we obtain larger Fisher information because their PDF are very tightly distributed, while for starting points far from equilibrium (equilibrium point for the mean value of the perturbation), the system

is more spread and have lower Fisher information with a broad elliptical phase charts. The probability of finding the system in a particular state is low because each variable transports among a wide range of states, and this leads to the lower values of Fisher information.

4.4 Conclusions

In this chapter, the influence of the immunisation term on the dynamical properties of a tumour-immune growth model described by coupled logistic equations is investigated. We improve a deterministic predator-prey model by including a periodic perturbation in the model parameters and then we study the effects of changing the model parameters on the behaviour of the system.

Using the predator-prey model which describes the cancer cells population as prey and immune cells population as predator, worthwhile observations are made through investigating the dynamical characteristics and interaction of the predator-prey model in its original condition (deterministic model) as well as its behaviour after modifications in the model parameters.

The common features of the predator-prey model in its original condition are a periodic behaviour with a limit cycle in addition to sensitive dependence on the initial conditions where the system behaviour is varied by varying the initial points. Also, changing the prey mortality rate b (cancer death rate), in the first equation leads to monotonic decrease in the equilibrium point, based on our observation that the equilibrium point depends on the parameter values. From the point of view of information theory, we observe a peak for F_T at $b = 3$ where the PDF of (x, y) at this value shows a shorter distance between the two peaks, leads to conclude that the model at this value is an undesirable state to investigate due to the lack of interaction between the two species (less variability). In comparison with the other values of b $(\neq 3)$, where the state variables go through large oscillations and the system has lower F_T due to is probably not

functioning well (high variability).

The conclusions of our investigation for the case of the predator-prey model with modifications in the model parameters are presented simply as follows: the population of cancer cells is consumingly affected by a periodic modulation (immunisation term) where the optimal value of the amplitude in the periodic dose which is $F = 2.62$ could induce the number of cancer cells in the host body to decrease and at the same time can motivate the growth of the immune cells. In other words, prey density will break down at sufficiently specific doses of immunotherapy. Furthermore, switching from the stable steady state to the extinct state for the prey population is accelerated by specific value of F. This leads us to conclude that for a specific value of the periodic perturbation, a decline in the cancer cells' density occurs to a very low value at $F = 2.62$. In addition, we notice a maximum F_T at this value which means that our system has less variability and shows a static steady state but from the viewpoint of sustainability, this state is the most unsustainable state since the survival of only one species renders the dynamics insufficient to conduct an investigation.

Chapter 5

A dynamical system with three-components

5.1 Introduction

Researchers have employed many different mathematical models for tumour-immune dynamics and applied modifications in different mechanisms to investigate the effects of immunotherapy (external stimulus of the immune cells). They observed that while this treatment may reduce the number of tumour cells they may regrow and begin to increase (see [43,54]). As a result, it is observed that the elimination of cancer cells relies on the average values of the therapy term for realistic values of the T period [22, 47]. In our work, we show that a mathematical model with a periodic perturbation is able to eradicate the cancer cells population. On the other hand, whereas those results relate to the effectiveness of immunotherapy treatment in destroying the cancer cells, at the same time we believe that large doses of such treatment can have negative side effects. The population of cancer cells is consumingly affected by a periodic therapy. In other words, prey density will break down at sufficiently specific doses of immunotherapy (biological treatment).

A third species is considered in the predator-prey model which represents healthy cells population along with cancer and immune cells populations. We examine the effects of the periodic perturbation on the evolution of the system to show how the oscillatory behaviour persists for a long time and is sustained at certain parameter values in the immunotherapy treatment.

This chapter is arranged as follows: Section 5.2 deals with the introduction of a three species model, the investigation of the three species stability and dynamics, and demonstrates the existence of equilibrium points (equilibrium point for the mean value of the perturbation). Section 5.3 describes in detail the modification of the three species model to track its behaviour, the variation of the parameter values, and presents figures to show the variability/sustainability of the model. Section 5.4 contains the conclusions. Our goal in this chapter is to show the changes in the functionality of the three species model through inclusion of immunotherapy and to describe the influence of the periodic therapy on the behaviour of the species from the point of view of information theory.

5.2 Mathematical definition of the three species model

We expand the model in (4.12) to include a third species which represents the healthy cells, and we construct our dynamical equations as follows:

$$\frac{dx}{dt} = ax\,(1 - N_1 x) - bxy - dxz, \tag{5.1a}$$

$$\frac{dy}{dt} = -cy + \frac{eyx}{g_2 + x} - fyx + F\sin^2(\omega t), \tag{5.1b}$$

$$\frac{dz}{dt} = gz(1 - N_2 z) - hzx. \tag{5.1c}$$

Here, $x(t)$ represents cancer cells population, $y(t)$ stands for immune cells population, and $z(t)$ represents the healthy cells population. We consider the growth of the cancer

and healthy population to be logistic with including two different carrying capacities $N_1(> 0)$ and $N_2(> 0)$, respectively. $a(> 0)$ is the growth of cancer cells, $e(> 0)$ is the growth of the immune cells, $g(> 0)$ is the growth of the healthy cells, $c(> 0)$ is the natural death rate of the immune cells, $b(> 0)$ is the rate of predation of cancer cells by the immune cells, $f(> 0)$ is the rate of predation of immune cells by the cancer cells, $d(> 0)$ is the rate of predation of cancer cells by the healthy cells, $h(> 0)$ is the rate of predation of healthy cells by the cancer cells, F and ω are the amplitude and angular frequency of the periodic therapy, respectively. The second term in the second equation is of Michaelis-Menten form to reference the saturated effects of the immune reaction (the finite interaction between the immune and cancer cells) (see [43, 78]).
The model in (5.1) has to be reformulated by minimizing the number of parameters, the result is presented in the following dimensionless form (see Appendix B for the detailed proof of the following equations):

$$\begin{aligned} \frac{du}{d\mathcal{T}} &= u(1-u) - uv - a_{13}ur, \\ \frac{dv}{d\mathcal{T}} &= a_{21}[\frac{uv}{g_2 + \alpha u} - v] - a_{22}uv + a_{23}\sin^2(\Omega\mathcal{T}), \\ \frac{dr}{d\mathcal{T}} &= a_{31}r(1-r) - a_{32}ru. \end{aligned} \tag{5.2}$$

Here, u stands for the density of cancer cells, v represents the density of immune cells and r represents the density of healthy cells. $u_0 = u(t = 0)$ is the cancer initial density, $v_0 = v(t = 0)$ is the initial density of immune population and $r_0 = r(t = 0)$ is the starting point of the healthy cells population. The competition mode divided into two, the first competition is between the healthy cells population r and cancer cells population u on the available resources, whereas the cancer cells population u and immune cells population v are competing in the predator-prey style. We perform a set of numerical simulations for the parameter values in Eqs. (5.2) where we consider a set of parameters given in the following table and the choice of parameters are similar to the one used in [54]:

Table 5.1: Parameter values for numerical simulation

Deterministic parameters	**Values**
a_{13}	1.2
a_{21}	1.291
g_2	0.3
α	1
a_{22}	1.1
a_{31}	1.2
a_{32}	4.8
u_0	1
v_0	1
r_0	1
Stochastic parameters	**Values**
a_{23}	
Ω	1

5.2.1 Local stability analysis and equilibria

By taking the right hand sides of the Equations in (5.2) equal to zero, we find all the equilibrium points (equilibrium point for the mean value of the perturbation) recognized by the system 5.2 and examine the dynamics of the system. The equilibrium points (equilibrium point for the mean value of the perturbation) for the system are $(0, \frac{a_{23}}{2a_{21}}, 0)$, $(0, \frac{a_{23}}{2a_{21}}, 1)$, $(u^* = 1 - v^*, v^*, 0)$, where v^* is the solution for the following equation:

$$a_{21}\left[\frac{v(1-v)}{g_2 + \alpha(1-v)} - v\right] - a_{22}v(1-v) + \frac{a_{23}}{2} = 0$$

and the other point is $(u^{**} = \frac{a_{31}v^{**} + a_{31}(a_{13}-1)}{a_{32}a_{13}-a_{31}}, v^{**}, r^{**} = \frac{a_{32}-a_{31}-a_{32}v^{**}}{a_{32}a_{13}-a_{31}})$ where v^{**} is the solution to the following equation:

$$a_{21}\left[\frac{v\left(\frac{a_{31}v+a_{31}(a_{13}-1)}{a_{32}a_{13}-a_{31}}\right)}{g_2 + \alpha\left(\frac{a_{31}v+a_{31}(a_{13}-1)}{a_{32}a_{13}-a_{31}}\right)} - v\right] - a_{22}v\left(\frac{a_{31}v + a_{31}(a_{13}-1)}{a_{32}a_{13} - a_{31}}\right) + \frac{a_{23}}{2} = 0$$

The Jacobian of the dynamics in Eqs. 5.2 is given by:

$$J(u,v,r) = \begin{pmatrix} 1-2u-v-a_{13}r & -u & -a_{13}u \\ \frac{a_{21}\ g_2 v}{(g_2+\alpha u)^2} - a_{22}v & \frac{a_{21}u}{(g_2+\alpha u)} - a_{21} - a_{22}u & 0 \\ -a_{32}r & 0 & a_{31} - 2a_{31}r - a_{32}u \end{pmatrix} \tag{5.3}$$

We analyse the stability of the above equilibrium points (equilibrium point for the mean value of the perturbation) through the study of the eigenvalues of the Jacobian in (5.3) at each fixed point. For example, when $a_{23} = 1$, the first point $(0, 0.3873, 0)$ is a saddle point with one negative eigenvalue and two positive eigenvalues, whereas the point $(0, 0.3873, 1)$ has three negative eigenvalues (smaller than zero) lead to a stable solution where only immune and healthy cells exist whereas the cancer cells are zero.
In consideration of the above, in the following figures we attempt to understand the dynamics of the model in (5.2). For example, in Fig. 5.1, we fix almost parameter values as in table (5.1), and we use different values of the amplitude a_{23}. When $a_{23} = 5$, we observe that the orbit is derived from the initial values (in the right panels, we display the phase portrait after removing the initial transient), is characterized by low values of cancer cells. From the point of view of biology, this means that the therapy is helpful in eliminating the cancer population in comparison with the case when the amplitude is small such as the results in the upper panels in Fig. 5.1.
Changing the initial values for the above system will not make any changes to the system's behaviour as all the equilibrium points (equilibrium point for the mean value of the perturbation) depend on the value of the amplitude in the immune equation (second equation). On the other hand, varying the value of the amplitude leads to the change in the dynamics of the system as in the following figure:

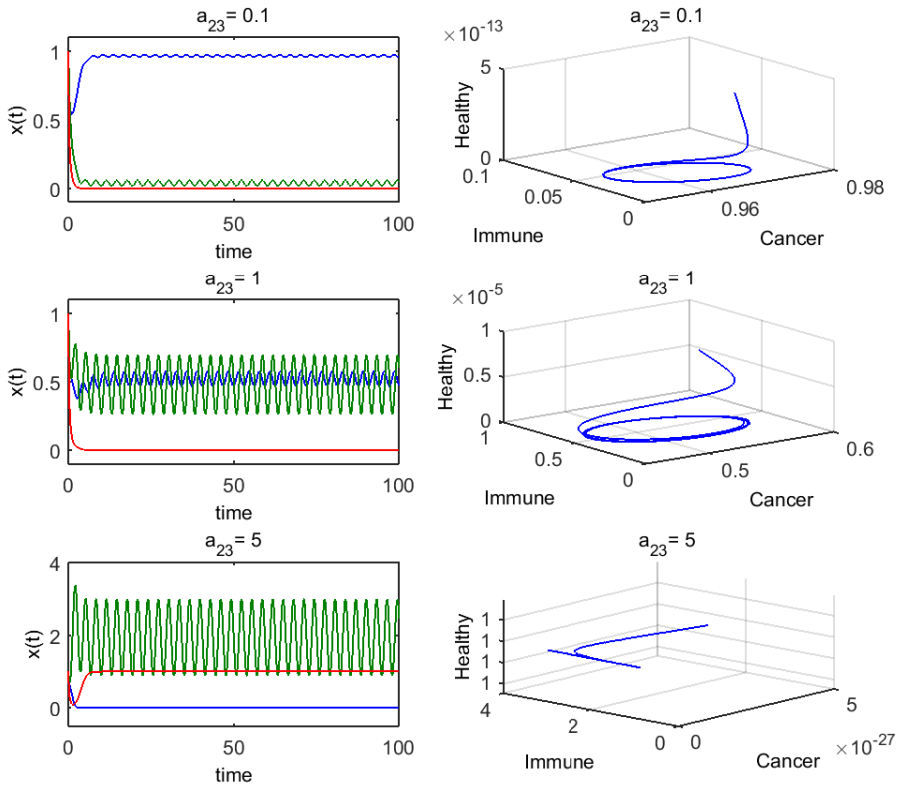

Figure 5.1: Time evolution and phase portrait of Eqs. (5.2) for different a_{23}, the other parameters are shown in Table (5.1) and $[u_0, v_0, r_0] = [1, 1, 1]$. A blue line represents cancer, green for immune and red for healthy cells. The right panels are a phase portrait for each a_{23} after removing the initial transient.

The right panels show a representation of possible behaviours at different parameter values with plots of the $xyz - plane$ which is usually called "phase portrait", whereas the left panels display the corresponding solutions for the model in (5.2). Investigating the behaviour of the system in (5.2) by varying the parameter values, enable us to build an idea about its dynamics. From Fig. 5.1, it is obvious that our model has an optimal value of the amplitude a_{23} where the cancer cells start vanishing and induce the immune population to grow, so we perform another figure to display the average of each species at different values of a_{23}, also, to determine the optimal value of a_{23} in which the cancer cells population eradicate, the results are display in the following figure:

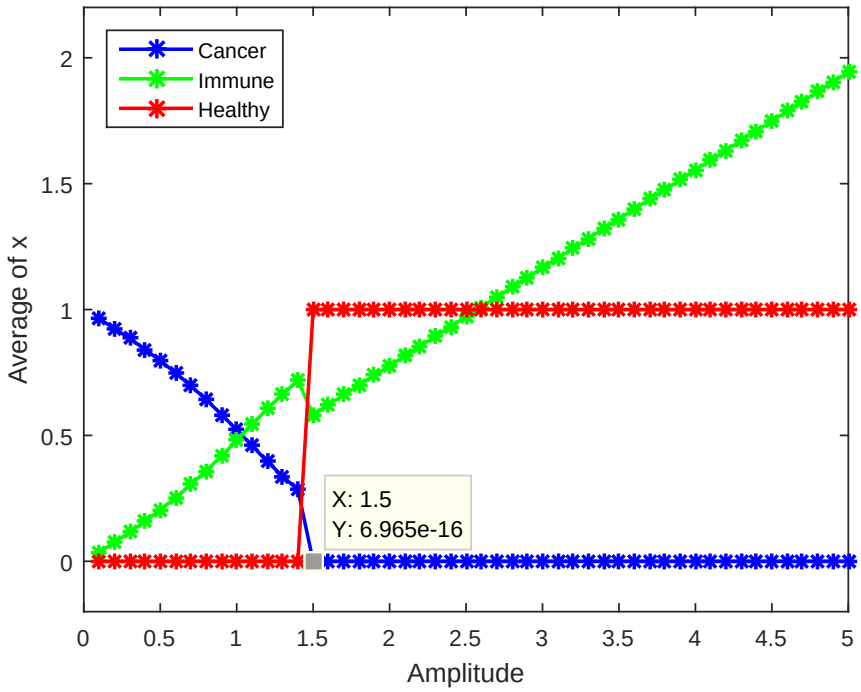

Figure 5.2: The average of x as a function of the periodic amplitude, fixing all the parameter values as shown in Table (5.1), $[u_0, v_0, r_0] = [1, 1, 1]$ and changing the value of a_{23}.

In comparison between the results from Chapter 4 (two species model) and Chapter 5 (three species model) where healthy cells are presented in model (5.1) as a third species, in Fig. 4.15, we observe that the cancer population is eradicated at $F = 2.62$, whereas in the above figure (Fig. 5.2), we observe similar observations for cancer population but with a difference in the value of amplitude which is $a_{23} = 1.5$ (the amplitude F in the two species model (4.13) is equal to a_{23} in the three species model (5.2)). On the other hand, from Fig. 5.2, we notice that the healthy population shows a static state at 1, whereas the immune population increases as a_{23} increases because we have a stable equilibrium point (equilibrium point for the mean value of the perturbation) at $(0, \frac{a_{23}}{2a_{21}}, 1)$.

For more details, we examine the time evolution of the model (5.2) for fixed parameter values and different values of a_{23} as in the following figure:

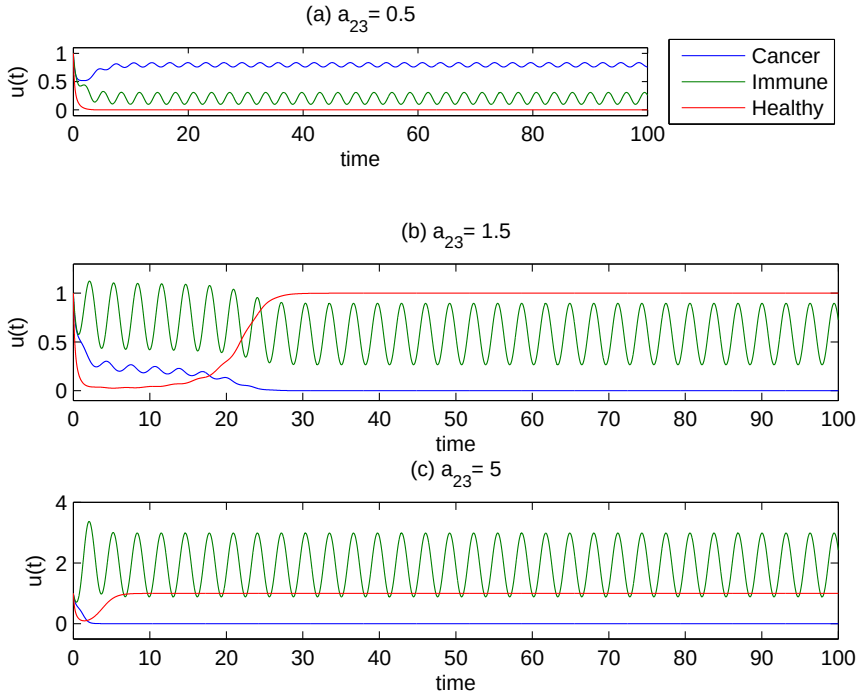

Figure 5.3: Time evolution of x for different values of a_{23}, $[u_0, v_0, r_0] = [1, 1, 1]$ and the other parameters are shown in Table (5.1).

From the above figure, we observe that the cancer cells population started to eradicate at $a_{23} = 1.5$, as a result, we conclude that at this amplitude value, the solution show a steady state equilibrium which leads to the less variability in the model's behaviour. The difference between the three panels in Fig. 5.3, is the optimal value of a_{23} where the immunotherapy induced immune cells to grow and eliminate the cancer cells.

Our concern is to observe the variability/sustainability of the tumour-immune system. Thus we are, looking for the unsustainable state where one of the species (cancer cells) eradicated, so we obtain Fisher information at different values of amplitude a_{23}, and the results are presented in the following figure:

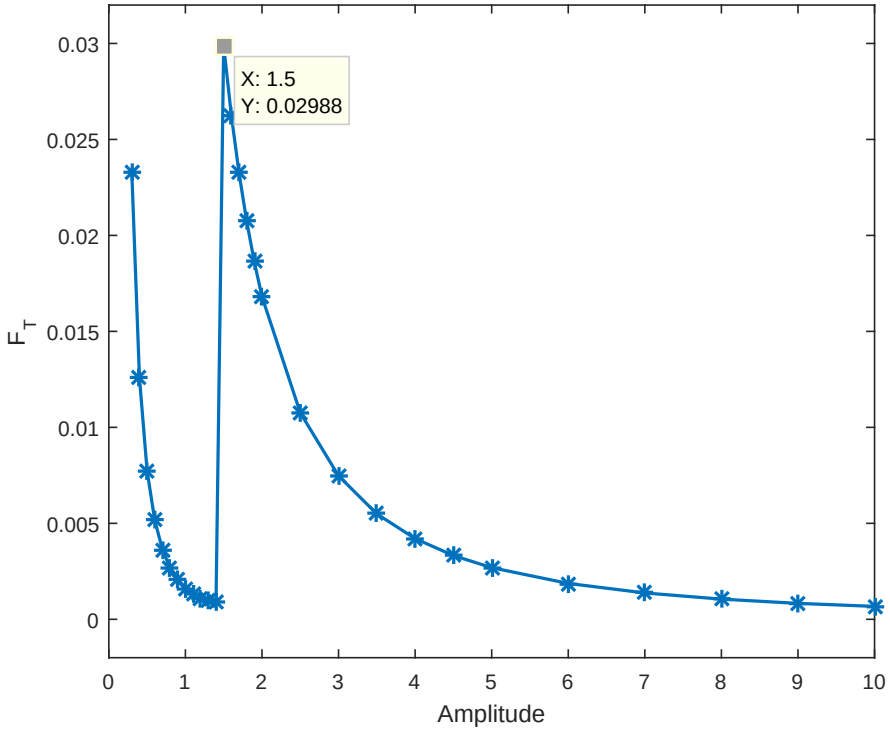

Figure 5.4: F_T as a function of amplitude for $[u_0, v_0, r_0] = [1, 1, 1]$ and fixed other parameter values. A peak is noticed at $a_{23} = 1.5$ which is the same value where the cancer cells begin to vanish in Figs. 5.2. and 5.3.

F_T peak in the above figure is observed at $a_{23} = 1.5$ which is the value of the amplitude where the cancer population is eradicated and the immune cells increase (see Fig. 5.3), this leads to the unsustainable state (less variability) where the model loses one of its species which means not enough dynamics available in the model to build an investigation. The large value of F_T means again that the system show low disorder which is obvious from Fig. 5.4, and the system is expected to display a narrow PDF at this amplitude value due to the less variability. F_T curve decreases as the amplitude increases and this is because the immune population is kept increases and one of the species is vanishing.

5.3 Modifications to the three species model

We further enhance the model in (5.2) by including perturbation in the cancer growth rate, then we investigate the functionality of the model (5.4) by following similar analysis as we performed for the model (5.2). The only difference between the two models is that we reduce the growth of cancer cells by including perturbation of a constant in addition to a periodic modulation with amplitude ϵ and frequency Ω, as follows:

$$\begin{aligned} \frac{du}{d\mathcal{T}} &= (1 + \epsilon sin(\Omega\mathcal{T}))\, u\,(1-u) - uv - a_{13}ur, \\ \frac{dv}{d\mathcal{T}} &= a_{21}[\frac{uv}{g_2 + \alpha u} - v] - a_{22}uv \; + a_{23}\sin^2(\Omega_1\mathcal{T}), \\ \frac{dr}{d\mathcal{T}} &= a_{31}r\,(1-r) - a_{32}ur. \end{aligned} \tag{5.4}$$

The first equation stands for the rate of change in the number of cancer cells u, the second equation describes the dynamics of immune cells population v, and the last equation describes the rate of change in the number of healthy cells r. The stability analysis of the model (5.4) recognizes the positions of the critical points along with their stability conditions where we notice similar equilibrium points (equilibrium point for the mean value of the perturbation) to those in model (5.2), with a small difference due to the enhancement of the cancer growth in the first equation.

5.3.1 Dynamic properties of the model

By varying the parameters in the cancer cells perturbation, we conclude our observations for the behaviour of the system. Using $\Omega = 0$, ($sin(\Omega t) = 0$), leads to similar behaviour as for the model (5.2). On the other hand, for different values of ϵ such as $\epsilon = 0.1, 1.5, 5$ and fixed $\Omega = \Omega_1 = 1$, and $[u_0, v_0, r_0] = [1, 1, 1]$, we vary the amplitude a_{23} in the immune equation, in order to compare the results with those for the model (5.2), (see Fig. 5.2).

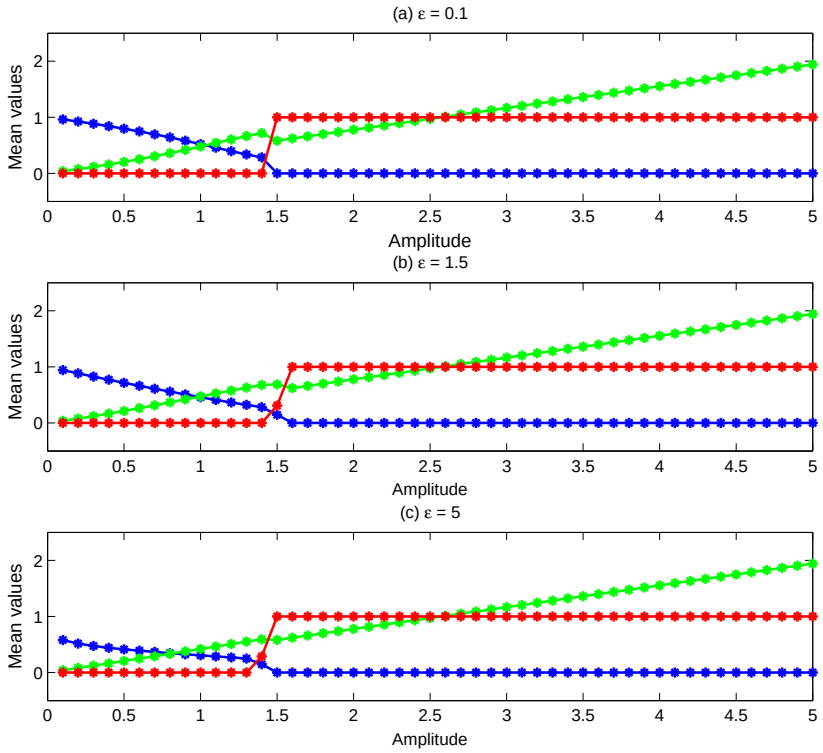

Figure 5.5: Average values of each population against the amplitude a_{23} for $[u_0, v_0, r_0] = [1, 1, 1]$, different ϵ and fixed the other parameter values. A blue line for cancer cells, green for immune cells and red for healthy cells.

In Fig. 5.5, we fix all parameter values according to table (5.1), in addition to $\Omega = \Omega_1 = 1$ and varying the amplitude a_{23} in the periodic perturbation for different ϵ. We obtain similar observations as in Fig. 5.2, which means that adding little perturbations ϵ to cancer growth population with different values of ϵ and $\Omega = 1$ does not induce a significant change. On the other hand, cancer population started to vanish at $a_{23} = 1.5$, and to investigate its variability at this value, we plot Fisher information in Fig. 5.6 using $\epsilon = 0.1$.

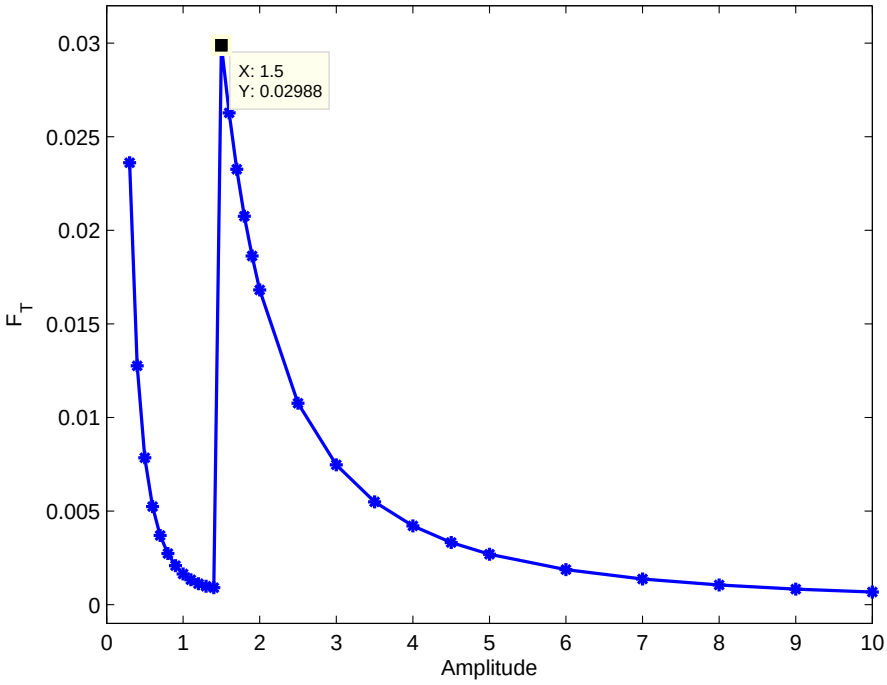

Figure 5.6: F_T against the amplitude a_{23} for $\Omega = \Omega_1 = 1$, $\epsilon = 0.1$ and $[u_0, v_0, r_0] = [1, 1, 1]$. A peak is observed at $a_{23} = 1.5$ which is the same value where the cancer cells start vanishing in Fig. 5.5.

We notice that the results in Fig. 5.6 above have a distinct shape with a distinct F_T peak at $a_{23} = 1.5$ and are very close to those in Fig. 5.4. In this case, we conclude that the perturbation ϵ does not induce a significant change. Similar findings are reported for different values of ϵ such as 1.5 and 5 in the next section.

5.3.2 Effects of varying the amplitude ϵ

To introduce these effects into our model, we fix a_{23}, Ω, Ω_1 and varying ϵ to investigate the effects of changing this parameter on the growth of cancer population. We show the time-history of each species against ϵ in Fig. 5.7:

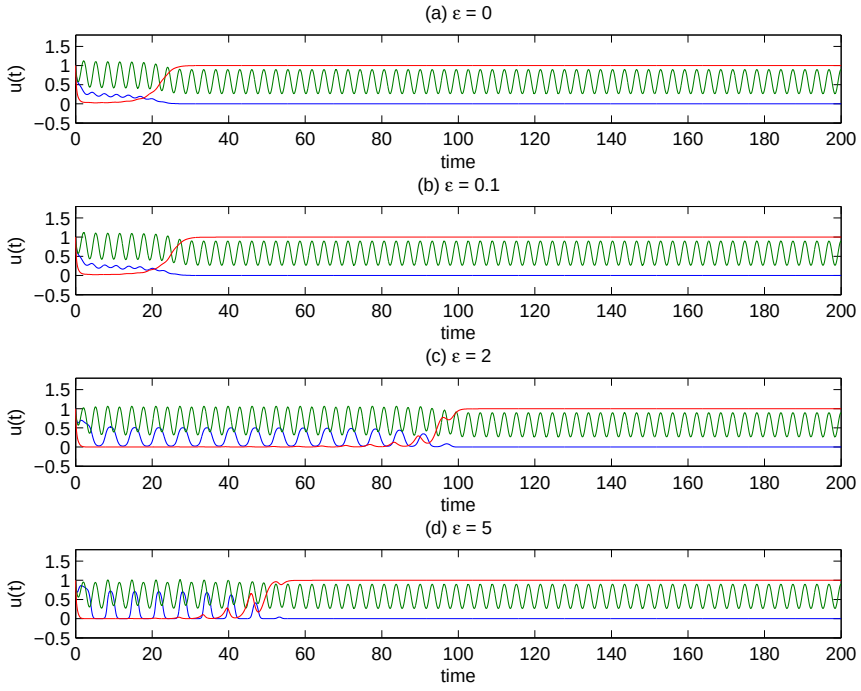

Figure 5.7: We use different values of ϵ to plot the dynamics of the model for fixed parameter values such as $a_{23} = 1.5$, $\Omega = \Omega_1 = 1$ and $[u_0, v_0, r_0] = [1, 1, 1]$. Blue line for cancer cells, green for immune cells and red for healthy cells.

Figure 5.7 shows the effects of changing ϵ on the time evolution of the model. We fix $a_{23} = 1.5$, $\Omega = \Omega_1 = 1$ and the other parameter values, and different values of ϵ. In all cases, all species approach the same final state. However, the larger ϵ, the shorten transient time before approaching such final state. In this light, we show the average evolution of the populations in model (5.4) for various rates of growth as in the following figure:

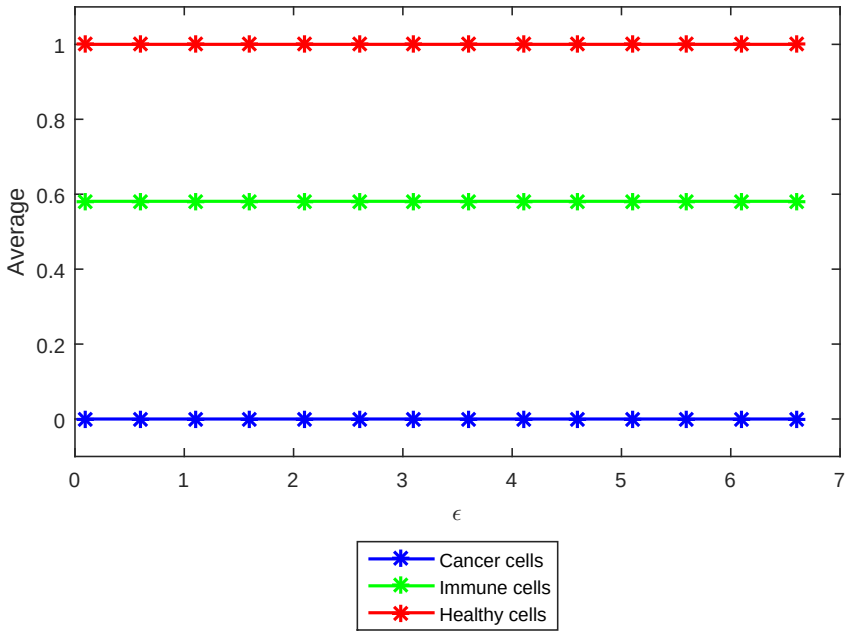

Figure 5.8: We display the average of each species in different colours as a function of ϵ with fixed values for the other parameters. No changes are noticed in the average values which means that our model is independent of ϵ.

To track the behaviour of the model (5.4) presented in Figs. 5.7 and 5.8 from the point of view of Fisher information, we calculate F_T at different values of ϵ and fixed Ω to be $\Omega = 1$, and amplitude to be $a_{23} = 1.5$ (figure not shown). We observe that F_T values don't change over time, which means again that the system at a steady state solution does not loss or gain Fisher information. We attempt another value of $a_{23} = 4$ in which we realize the same behaviour for Fisher information.

5.3.3 Effects of varying Ω

In order to examine the behaviour of the model in (5.4), and the effects of changing parameter values within the perturbation included in the cancer growth, such as Ω, we display the results in the following figure:

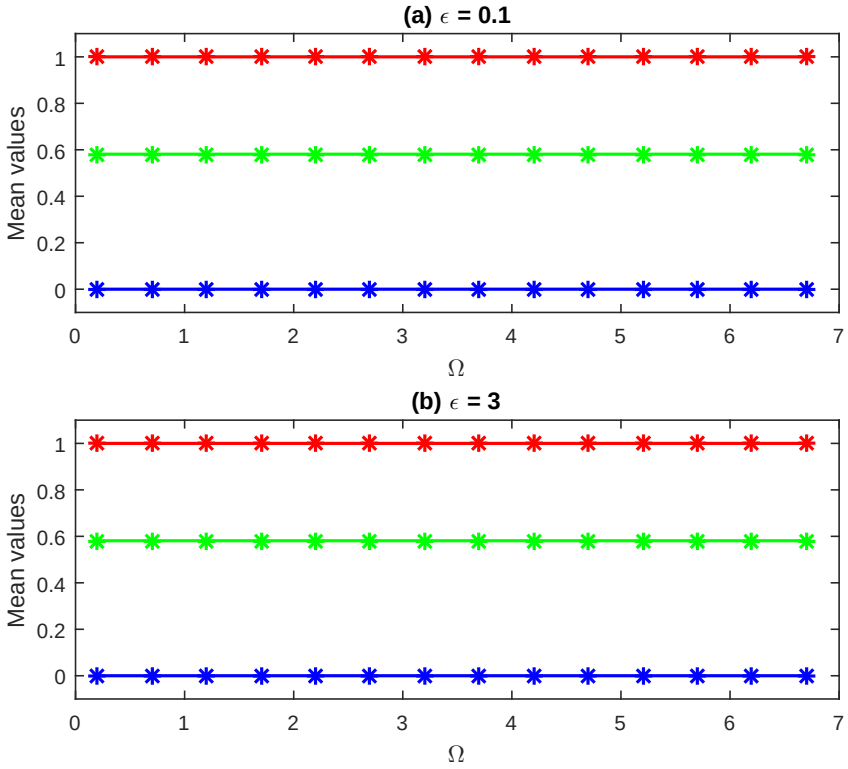

Figure 5.9: The average values of each species against Ω for two different values of ϵ with fixed $\Omega_1 = 1$, $[u_0, v_0, r_0] = [1, 1, 1]$ and $a_{23} = 1.5$. No changes are observed in the average values as Ω increases.

In Fig. 5.9, we use initial condition to be $u(0) = v(0) = r(0) = 1$, and other parameter values are similar to those in table (5.1), and we display the results of increasing Ω. It is obvious that there is no change in the average values for the three species as Ω increases. From the perspective of information theory, we employ Fisher information index as a function of Ω at two different values of ϵ, and we observe a fixed value for F_T for all the values of Ω, which means that at a steady state solution, Fisher information do not change over time.

5.4 Conclusions

We improve the predator-prey model by including a third equation to represent healthy cells population and by including perturbation in the model parameters. We investigate the behaviour of this model by varying the model parameters. On the other hand, the concept of Fisher information is used as a measure of variability and to determine the optimal value of immunotherapy which enhances the growth of immune and healthy cells while helping to eradicate the cancer cells, or at least to control the growth of cancer population.

We study two different mechanisms of the three species model, with and without modifications. For the model in (5.2) without any additional adjustment, we note that the value of the amplitude ($a_{23} = 1.5$) leads the cancer cells to vanish and the model reaches an equilibrium relationship between the three species. Similar results are observed in the second case of the model (5.4) which includes modifications in the model parameters, $(1 + \epsilon sin(\Omega T))$ in the first equation. As confirmed earlier, in the presence of immunotherapy at different values of the amplitude, the results show a periodic solution. One interesting feature of this chapter is the optimal value of amplitude ($a_{23} = 1.5$) at which the cancer cells start vanishing and we confirm our results by exploring Fisher information dynamics with different values of amplitude, with a peak observed at $a_{23} = 1.5$. In this light, we conclude that our inclusion of $(1 + \epsilon sin(\Omega T))$ in the growth of the cancer cells in the first equation does not change the long-time behaviour where the only difference in the behaviour of the system was the initial transient for different values of Ω and ϵ.

Finally, the main difference between the two species model and three species model is the value of the amplitude in the periodic perturbation (in the second equation) which reduced the number of cancer cells ($F = 2.62$ in the two species model and $a_{23} = 1.5$ in the three species model). Our work could help to identify the right doses of treatment of cancer, one of the leading causes of mortality worldwide.

Chapter 6

Conclusions and future work

6.1 Summary of the results

The dynamical features and the complications of dynamical systems can largely be controlled by varying some parameter values. Mathematical models have been proposed for modelling the population growth dynamics and to study the interaction between several species. The models we suggest in this thesis are quite simple and of a general type. Specifically, we investigate and discuss different nonlinear dynamical models with perturbations in the model parameters which can affect the behaviour of the system depending on the parameter values, in addition, we use Fisher information index as a measure of variability/sustainability. Also, we offer numerical and/or analytical results in which our models can represent some significant biological cases.
In the second chapter, we employ the simple logistic equation to study its behaviour after including perturbation in the model parameters and study the effects of the perturbation on the dynamics of the logistic equation from the point of view of Fisher information. One interesting characteristic of the logistic equation with a periodic modulation in both positive and negative feedback is a bimodal PDF with different distance between the two peaks for different parameter values, which is a result of its

cross-over behaviour between its initial values and the carrying capacity of the population. Particularly, for small initial conditions (far from carrying capacity which we fixed to be $K = 10$) and different values of periodic frequency ω such as $\omega = 1$, the logistic equation shows a bimodal PDF with two peaks, at x_0 and K, respectively. From the point of view of information theory, we observe a distinct maximum for Fisher information at a specific parameter value which means that the modal at this parameter value has less variability, whereas this characteristic does not exist for different initial values such as $x_0 = 5$ where Fisher information monotonically increases as ω increases. Then we perform another investigation regarding varying x_0 with fixed value of ω, we notice a local maximum for Fisher information at initial condition which is closer to K, ($x_0 \simeq K$) and we linked this to the narrowest PDF at this initial value with less variability (unsustainable state with less dynamics to investigate). The investigation of the logistic equation with perturbation from the perspective of sustainability leads to significant information to understand the population with small density such as bacteria or tumours which continue to survive regardless of the use of antibiotics (e.g. [83]), as observed from a PDF peak around small population x_0.

In chapter 3, we discuss the significant features of the analytical and numerical calculations of the Gompertz equation. We observe similar findings to those obtained for the logistic equation in three different cases with only one difference for case-2. Specifically, we include a periodic modulation in the model parameters for positive and negative feedback in order to investigate the behaviour of the model from the point of view of variability/sustainability using Fisher information index, and we obtain a distinct maximum for Fisher information at initial condition which is closer to the equilibrium point ($x_0 \simeq x_1^*$) and which is related to the narrowest PDF (a short distance between the two peaks) with less variability that leads to unsustainable state due to the lack of functionality, followed by Fisher information decreasing beyond ($x_0 \simeq x_1^*$), which leads to the increase of variability in the system while moving away from the equilibrium point.

In the fourth chapter, we present the predator-prey mode. We induce the growth of

immune cells that can potentially stop the growth of cancer cells which offers an interesting topic for research because cancer being one of the most deadly diseases in the modern world and one that can affect all people regardless of their age, gender, or ethic background, controlling its growth is an urgent task; therefore we investigate the functionality of a two species model (tumour-immune system) over all possible parameter values. The main characteristic of the predator-prey model (in its deterministic conditions) is the sensitivity dependence on initial points in addition to a periodic behaviour with a limit cycle. The presence of a periodic modulation term (periodic dose of treatment) tends to destroy the cancer population and to promote the growth of immune cells. This leads us to conclude that for a specific value of amplitude in an immunotherapy term such as $F = 2.62$, a decrease occurs in the cancer cells' density to a very low value; also, we notice larger Fisher information at this value which means that our model has less variability and shows a static steady state, although from the perspective of sustainability, it is necessary to say that this is the most unsustainable state where the existence of only one surviving species renders the dynamics insufficient to conduct an investigation. Also, we study the effects of varying the prey mortality rate on the behaviour of both species from the point of view of information theory, and we observe a peak for Fisher information at $b = 3$ with narrowest PDF at this value (shorter distance between the two peaks) in comparison with other values of b.

In chapter 5, we discuss the inclusion of another species in the predator-prey model in the form of healthy cells in order to provide a complicated task that could be summarised. We vary the parameter values in an attempt to detect and determine accurately the value of the immunotherapy dose where eradication of the cancer cells population starts. One interesting feature of this chapter's findings is the optimal value of a_{23} ($a_{23} = 1.5$) at which the cancer cells start vanishing, a result which we confirm by exploring Fisher information dynamics with different values of the amplitude, with a peak observed at $a_{23} = 1.5$. Furthermore, we include perturbation $(1 + \epsilon sin(\Omega T))$ in the growth of the cancer cells which does not improve our observations. Finally, The main difference between the two species model and three species model is the value of

the amplitude in the periodic perturbation which reduces the number of cancer cells.
The study of nonlinear differential equations has a long history. Although many publications have offered sufficient outlines of dynamical systems, our efforts move in the direction of adding new and detailed knowledge by investigating the functionality of the above mentioned models from the point of view of variability/sustainability, which leads us to conclude that Fisher information can be used as a measure of disorder in the case where it has a distinct maximum as a result of the existence of a narrowest bimodal PDF with two distinct peaks.

6.2 Future work

The main difference between this work and that of other researchers is that we include a periodic modulation in the model parameters, investigating the dynamics of these models in addition to their variability/sustainability from the point of view of information theory. An alternative approach in this direction is to include a stochastic noise rather than a periodic modulation in components in the above models.
The above observations may be useful to all people concerned with controlling the growth of this terrifying disease *cancer* and that it would be useful to study the above systems with inclusion of a time delay in one or more species as, according to observations by Marchuk (see [6,59]), involving a time delay in the immune system modelling is a significant factor in terms of its influence on the cancer model, with and without immunotherapy.
The models investigated in this thesis present only a few of the possible modifications of models for eradication of cancer cells, and suggestions for future work could include constructing the growth of the cancer or the interaction for the cancer and immune cells by using a non-exponential function or conducting a similar investigation on models containing medicine resistance and more kinds of specific immune cells.
It is hoped that new approaches and new theories will be develop to support the results

from our suggested models and strengthen our findings to enable their future inclusion in the treatment of cancer sufferers.

Appendix A

A dimensionless form for the predator-prey model

As discussed earlier, the predator-prey model behaviour has been studied by many researchers in its deterministic conditions as well as stochastic variations. Here, replacing the predator-prey model's exponential growing of the prey population by a logistic growth equation with a carrying capacity $N = \frac{1}{K}$ yields the model:

$$\frac{dx}{dt} = ax(1 - Nx) - bxy, \tag{A.1a}$$

$$\frac{dy}{dt} = -cy + exy. \tag{A.1b}$$

Our purpose is to simplify the above model and work with a dimensionless version. It has two species in addition to five parameters, which means that there are lots of choices for the dimensionless parameters. By dividing the first equation (A.1a) by a and the second equation (A.1b) by c as follows:

$$\begin{aligned} \frac{dx}{dat} &= x(1 - Nx) - \frac{b}{a}\, xy, \\ \frac{dy}{dct} &= -y + \frac{e}{c}\, yx. \end{aligned} \tag{A.2}$$

We rescale the parameters in Eqs. (A.2) according to:

$$u = \frac{b}{a}\, x, \quad v = \frac{e}{c}\, y \quad \textit{and} \quad \mathcal{T} = a\, t,$$

where $\mathcal{T}$ is a time constant. As a result, the following model has been emerged from the evolution of Eqs. (A.2) with the latter quantities

$$\frac{d}{d\mathcal{T}}\frac{a}{b}\, u = \frac{a}{b}\, u(1 - N\,\frac{a}{b}\, u) - \frac{c}{e}uv, \tag{A.3a}$$

$$\frac{1}{c}\frac{ad}{d\mathcal{T}}\frac{c}{e}v = -\frac{c}{e}v + \frac{a}{b}uv. \tag{A.3b}$$

For simplicity, we multiply Eq. (A.3a) by $\frac{b}{a}$ and Eq. (A.3b) by $\frac{e}{a}$ to derive the following equations:

$$\begin{aligned} \frac{du}{d\mathcal{T}} &= u(1 - \frac{a}{b}Nu) - \frac{bc}{ae}uv, \\ \frac{dv}{d\mathcal{T}} &= \frac{-c}{a}v + \frac{e}{b}uv. \end{aligned} \tag{A.4}$$

Furthermore, lets consider the following quantities in Eqs. (A.4) in order to get a dimensionless form.

$$N = \frac{b}{a}, \quad \alpha = \frac{bc}{ae}, \quad \beta = \frac{c}{a} \quad \textit{and} \quad \gamma = \frac{e}{b}.$$

Then, the predator-prey model can be displayed as follows after a dimensionless procedure (fewer parameters) is applied:

$$\begin{aligned} \frac{du}{d\mathcal{T}} &= u(1 - u) - \alpha uv, \\ \frac{dv}{d\mathcal{T}} &= -\beta v + \gamma uv. \end{aligned} \tag{A.5}$$

As a result, we obtain a model with less parameters which is easier to investigate and examine its dynamical properties such as the equilibrium point (u_*, v_*) that can be

obtain at which $\dot{u}$ and $\dot{v}$ vanish. This means

$$u_*(1 - u_*) - \alpha u_* v_* \;=\; 0 \;=\; -\beta v_* + \gamma u_* v_*.$$

Appendix B

A dimensionless form for the three species model

We expand the predator-prey model by including a third species which represents the healthy cells population as we can see from the following equations:

$$\frac{dx}{dt} = ax(1 - N_1 x) - bxy - dxz, \tag{B.1a}$$

$$\frac{dy}{dt} = -cy + \frac{eyx}{g_2 + x} - fyx + F\sin^2(\omega t), \tag{B.1b}$$

$$\frac{dz}{dt} = gz(1 - N_2 z) - hzx. \tag{B.1c}$$

By dividing the first equation (B.1a) by a, the second equation (B.1b) by c and the third equation (B.1c) by g, we obtain the following equations:

$$\begin{aligned} \frac{dx}{dat} &= x(1 - N_1 x) - \frac{b}{a}xy - \frac{d}{a}xz, \\ \frac{dy}{dct} &= -y + \frac{eyx}{c(g_2 + x)} - \frac{f}{c}yx + \frac{F}{c}\sin^2(\omega t), \\ \frac{dz}{dgt} &= z(1 - N_2 z) - \frac{h}{g}zx. \end{aligned} \tag{B.2}$$

In order to simplify the latter model in (B.2), we introduce cancer x, immune y and healthy z populations in addition to the time t in terms of dimensionless quantities as follows:

$$\mathcal{T} = at, \quad u = \frac{e}{c}x, \qquad v = \frac{b}{a}y \quad and \quad r = \frac{h}{g}z.$$

As a result, we obtain the following model after including all the above dimensionless quantities and more simplification:

$$\begin{aligned}
\frac{c}{e}\frac{du}{d\mathcal{T}} &= \frac{c}{e}u(1 - N_1\frac{c}{e}u) - \frac{c}{e}uv - \frac{cdg}{aeh}ur, \\
\frac{a^2}{cb}\frac{dv}{d\mathcal{T}} &= -\frac{a}{b}v + \frac{a}{b}\frac{vu}{g_2 + \frac{c}{e}u} - \frac{af}{be}vu + \frac{F}{c}\sin^2(\frac{\omega}{a}\mathcal{T}), \\
\frac{a}{h}\frac{dr}{d\mathcal{T}} &= \frac{g}{h}r(1 - N_2\frac{g}{h}r) - \frac{c}{e}ru.
\end{aligned} \tag{B.3}$$

Furthermore, lets consider the following quantities in Eqs. (B.3) in order to get a form with less parameters.

$$N_1 = \frac{e}{c}, \quad N_2 = \frac{h}{g}, \quad \Omega = \frac{\omega}{a} \quad and \quad \alpha = \frac{c}{e}.$$

The three species model in its final form can be display as follows, as a result of applying a dimensionless and simplification procedure.

$$\begin{aligned}
\frac{du}{d\mathcal{T}} &= u(1 - u) - uv - a_{13}ur, \\
\frac{dv}{d\mathcal{T}} &= a_{21}\left[\frac{vu}{g_2 + \alpha u} - v\right] - a_{22}vu + a_{23}\sin^2(\Omega\mathcal{T}), \\
\frac{dr}{d\mathcal{T}} &= a_{31}r(1 - r) - a_{32}ru.
\end{aligned} \tag{B.4}$$

Appendix C

Fisher information construction for the logistic model

By following the procedure presented by several researchers, we calculate Fisher information index for the logistic model. We display the logistic model expressed in Eq. (2.3) as follows:

$$\frac{dx}{dt} = [B + N_0 \sin(\omega t)]\, x\, (1 - \frac{x}{K}). \tag{C.1}$$

We fix the constant growth B to be $B = 0$. Since Fisher information quantity as in Eq. (2.14) is:

$$F_T = \frac{A}{T} \int_0^T \frac{\dot{u}^{\,2}}{u^{\,4}}\, dt, \tag{C.2}$$

where $\dot{u} = \frac{du}{dt}$ and $u = \frac{dx}{dt}$, A is a normalization constant and T is the total time duration. We may now differentiate the function u with respect to x as follows:

$$\dot{u} = \frac{\partial u}{\partial x}\, \frac{dx}{dt}, \tag{C.3}$$

substituting the results of Eq. C.3 and Eq. (C.1) together in Eq. C.2, we obtain the following Fisher information quantity:

$$F_T = \frac{A}{T}\int_0^T \frac{(N_0\ sin(\omega t)\ (\dot{x} - \frac{2x\dot{x}}{K})) + (N_0\ \omega\ cos(\omega t)\ (x - \frac{x^2}{K}))}{u^2}\ dt, \tag{C.4}$$

We employ the formula in (C.4) to produce the figures in subsection (2.4.4) for different parameter values. Similar form for Fisher information is calculated for the Gompertz equation.

Appendix D

Fisher information construction for the predator-prey model

Fisher information can be calculate based on the background theory explained by several researchers. In the following, we present the procedure of obtaining Fisher information for the predator-prey model. We display the predator-prey model expressed in Eqs.(4.1) by the following set of equations:

$$\begin{aligned} \frac{dx}{dt} &= ax - bxy = f_1(x,y), \\ \frac{dy}{dt} &= -cy + exy = f_2(x,y). \end{aligned} \tag{D.1}$$

We expand Fisher information quantity in Eq. (2.14) as follows:

$$F_T = \frac{A}{T}\int_0^T \frac{\dot{s}^{\,2}}{s^{\,4}}\, dt\,, \tag{D.2}$$

where $s = \sqrt{\dot{x}^{\,2} + \dot{y}^{\,2}}$, A is a normalization constant and T is the total time duration. In consideration of the above, we obtain $\dot{s} = \frac{ds}{dt}$ as follows:

$$\dot{s} = \frac{\partial s}{\partial x}\,\frac{dx}{dt} + \frac{\partial s}{\partial y}\,\frac{dy}{dt}, \tag{D.3}$$

or the equation in (D.3) could be written as:

$$\dot{s} = \frac{\partial s}{\partial x}\,\dot{x} + \frac{\partial s}{\partial y}\,\dot{y},$$

we may now differentiate the function s with respect to cancer population x as follows:

$$\frac{\partial s}{\partial x} = \frac{\dot{x}(a - by) + ey\dot{y}}{s}, \tag{D.4}$$

and the next derivative is for s with respect to y as follows:

$$\frac{\partial s}{\partial v} = \frac{-bx\dot{x} + \dot{y}(-c + ex)}{s}, \tag{D.5}$$

substituting the results of Eqs. (D.4) and (D.5) together in Eq. (D.3) and finally includes the outcome results in Eq. (D.2), we obtain the following Fisher information quantity:

$$F_T = \frac{A}{T}\int_0^T \frac{\left(\dot{x}^2(a - by) + \dot{x}\dot{y}(ey - bx) + \dot{y}^2(-c + ex)\right)^2}{\left(\dot{x}^2 + \dot{y}^2\right)^3}\,dt, \tag{D.6}$$

The latter formula (D.6) is used to produce the figures in subsection (4.2.4), and similar calculations can be follow in order to construct Fisher information equation in the other sections in Chapter 4 with small differences.

Appendix E

Fisher information construction for the three species model

We calculate Fisher information by an integral equation, and its computation is subject to a group of ordinary differential equations (ODEs). Here, we show how to calculate Fisher information for the three species model.

We display the dimensionless form for the three species model which is expressed in (5.2) by the following set of equations:

$$\begin{aligned} \frac{du}{d\mathcal{T}} &= u\,(1-u) - uv - a_{13}ur, \\ \frac{dv}{d\mathcal{T}} &= a_{21}[\frac{uv}{g_2+\alpha u} - v] - a_{22}uv \; + a_{23}\sin^2(\Omega_1\mathcal{T}), \\ \frac{dr}{d\mathcal{T}} &= a_{31}r\,(1-r) - a_{32}ur. \end{aligned} \tag{E.1}$$

Since Fisher information quantity is:

$$F_T = \frac{A}{T}\int_0^T \frac{\dot{s}^{\,2}}{s^{\,4}}\,dt, \tag{E.2}$$

where $s = \sqrt{\dot{u}^{\,2} + \dot{v}^{\,2} + \dot{r}^{\,2}}$, A is a normalization constant and T is the total time duration. In consideration of the above Fisher information (Eq. E.2), we obtain $\dot{s} = \frac{ds}{dt}$

as follows:

$$\frac{\partial s}{\partial t} = \frac{\partial s}{\partial u}\frac{du}{dt} + \frac{\partial s}{\partial v}\frac{dv}{dt} + \frac{\partial s}{\partial r}\frac{dr}{dt}, \tag{E.3}$$

or the derivative of s in equations (E.3) could be written as:

$$\dot{s} = \frac{\partial s}{\partial u}\dot{u} + \frac{\partial s}{\partial v}\dot{v} + \frac{\partial s}{\partial r}\dot{r},$$

we may now apply the calculus of a simple differentiation for the function s with respect to cancer population u as follows:

$$\frac{\partial s}{\partial u} = \frac{\dot{u}(1-2u-v-a_{13}r) + \dot{v}(\frac{a_{21}v(g_2+\alpha u)-a_{21}\alpha uv}{(g_2+\alpha u)^2} - a_{22}v) - a_{32}r\dot{r}}{s}, \tag{E.4}$$

the next derivative is for s with respect to v as follows:

$$\frac{\partial s}{\partial v} = \frac{\frac{a_{21}u\dot{v}}{g_2+\alpha u} - u\dot{u} - a_{21}\dot{v} - a_{22}u\dot{v}}{s}, \tag{E.5}$$

and the evolution equation of the derivative of s with respect to r can be as follows:

$$\frac{\partial s}{\partial r} = \frac{a_{31}\dot{r} - a_{13}u\dot{u} - 2a_{31}r\dot{r} - a_{32}u\dot{r}}{s}, \tag{E.6}$$

by substituting the results of Eqs. (E.4), (E.5) and (E.6) together in the Eq. (E.3) and finally includes the outcome results in Eq. (E.2), we obtain the following Fisher information quantity:

$$F_T = \frac{A}{T}\int_0^T \frac{\left(\dot{u}^2 a + \dot{v}^2 b + \dot{r}^2 c + \dot{u}\dot{v}d - \dot{u}\dot{r}e\right)^2}{\left(\dot{u}^2 + \dot{v}^2 + \dot{r}^2\right)^3}\, dt, \tag{E.7}$$

where:

$$a = 1 - 2u - v - a_{13}r,$$

$$b = \frac{a_{21}u}{g_2 + \alpha u} - a_{21} - a_{22}u,$$

$$c = a_{31} - 2a_{31}r - a_{32}u,$$

$$d = \frac{a_{21}v(g_2 + \alpha u) - a_{21}\alpha uv}{(g_2 + \alpha u)^2} - a_{22}v - u,$$

$$e = a_{32}r + a_{13}u.$$

As a result, we obtain Fisher information index which it has been used to produce Fisher information figures in Section (5.2), similar quantity can be compute for different dynamical systems by following the same procedure in Appendixes C, D, & E.

Bibliography

[1] Abrams, P. A. "Why don't predators have positive effects on prey populations?" Evolutionary Ecology 6, no. 6 (1992): 449-457.

[2] Abrams, P. A. and Ginzburg, L. R. "The nature of predation: prey dependent, ratio dependent or neither?" Trends in Ecology & Evolution 15, no. 8 (2000): 337-341.

[3] Ai, B-Q., Wang, X-J., Liu, G-T. and Liu, L-G. "Correlated noise in a logistic growth model." Physical Review E 67, no. 2 (2003): 022903.

[4] Akakaya, H. R., Ginzburg, L. R., Slice, D. and Slobodkin, L. B. "The theory of population dynamics-II. Physiological delays." Bulletin of Mathematical Biology 50, no. 5 (1988): 503-515.

[5] Al-Saffar, A. and Kim, E. "Sustainable theory of a logistic model-Fisher Information approach." Mathematical biosciences 285 (2017): 81-91.

[6] Asachenkov, A. L., Marchuk, G. I., Mohler, R. R. and Zuev, S. M. "Immunology and disease control: a systems approach." IEEE Transactions on Biomedical Engineering 41, no. 10 (1994): 943-953.

[7] Aziz-Alaoui, M. A., and Okiye, M. D. "Boundedness and global stability for a predator-prey model with modified Leslie-Gower and Holling-type II schemes." Applied Mathematics Letters 16, no. 7 (2003): 1069-1075.

[8] Banerjee, S. and Sarkar, R. R. "Delay-induced model for tumor-immune interaction and control of malignant tumor growth." Biosystems 91, no. 1 (2008): 268-288.

[9] Barbolosi, D. and Iliadis, A. "Optimizing drug regimens in cancer chemotherapy: a simulation study using a PKPD model." Computers in Biology and Medicine 31, no. 3 (2001): 157-172.

[10] Bose, T. and Trimper, S. "Stochastic model for tumor growth with immunization." Physical Review E 79, no. 5 (2009): 051903.

[11] Boxenbaum, H. "Gompertz mortality analysis: aging, longevity hormesis and toxicity." Archives of gerontology and geriatrics 13, no. 2 (1991): 125-137.

[12] Braun, M. "Differential equations and their applications." (1993).

[13] Cabezas, H. and Fath, B. D. "Towards a theory of sustainable systems." Fluid phase equilibria 194 (2002): 3-14.

[14] Cabezas, H., Pawlowski, C. W., Mayer, A. L. and Hoagland, N. T. "Sustainable systems theory: ecological and other aspects." Journal of Cleaner Production 13, no. 5 (2005): 455-467.

[15] Can-Jun, W., Di, L. and Dong-Cheng, M. "Pure multiplicative noises induced population extinction in an anti-tumor model under immune surveillance." Communications in Theoretical Physics 52, no. 3 (2009): 463.

[16] Cayuela, J. S. "Dynamics, evolution and information in nonlinear dynamical systems of replicators." Universitat Pompeu Fabra, 2009.

[17] Chatterjee, T., Chatterjee, B. K., Majumdar, D. and Chakrabarti, P. "Antibacterial effect of silver nanoparticles and the modeling of bacterial

growth kinetics using a modified Gompertz model." Biochimica et Biophysica Acta (BBA)-General Subjects 1850, no. 2 (2015): 299-306.

[18] Chattopadhyay, J., and O. Arino. "A predator-prey model with disease in the prey." Nonlinear Analysis: Theory, Methods & Applications 36, no. 6 (1999): 747-766.

[19] Chesson, P. "Predator-prey theory and variability." Annual Review of Ecology and Systematics 9, no. 1 (1978): 323-347.

[20] De Pillis, L. G. and Radunskaya, A. "A mathematical tumor model with immune resistance and drug therapy: an optimal control approach." Computational and Mathematical Methods in Medicine 3, no. 2 (2001): 79-100.

[21] De Pillis, L. G. and Radunskaya, A. "The dynamics of an optimally controlled tumor model: A case study." Mathematical and Computer Modelling 37, no. 11 (2003): 1221-1244.

[22] d'Onofrio, A. "A general framework for modeling tumor-immune system competition and immunotherapy: Mathematical analysis and biomedical inferences." Physica D: Nonlinear Phenomena 208, no. 3 (2005): 220-235.

[23] Eason, T. and Cabezas, H. "Evaluating the sustainability of a regional system using Fisher information in the San Luis Basin, Colorado." Journal of environmental management 94, no. 1 (2012): 41-49.

[24] Fan, Meng, and Ke Wang. "Optimal harvesting policy for single population with periodic coefficients." Mathematical Biosciences 152, no. 2 (1998): 165-178.

[25] Fath, B. D., Cabezas, H. and Pawlowski, C. W. "Regime changes in ecological systems: an information theory approach." Journal of theoretical biology 222, no. 4 (2003): 517-530.

[26] Fisher, R. A. "Theory of statistical estimation." In Mathematical Proceedings of the Cambridge Philosophical Society, vol. 22, no. 5, pp. 700-725. Cambridge University Press, 1925.

[27] Fisher, R. A. "The logic of inductive inference." Journal of the Royal Statistical Society 98, no. 1 (1935): 39-82.

[28] Frieden, B. R. and Soffer, B. H. "Lagrangians of physics and the game of Fisher-information transfer." Physical Review E 52, no. 3 (1995): 2274.

[29] Frieden, B. R., Plastino, A. and Soffer, B. H. "Population genetics from an information perspective." Journal of theoretical biology 208, no. 1 (2001): 49-64.

[30] Frieden, B. Roy. "Science from Fisher information: a unification." Cambridge University Press, 2004.

[31] Gao, X., Qiuhui Pan, Mingfeng He, and Yibin Kang. "A predator-prey model with diseases in both prey and predator." Physica A: Statistical Mechanics and its Applications 392, no. 23 (2013): 5898-5906.

[32] Gil, Maria M., Teresa RS Brandao, and Cristina LM Silva. "A modified Gompertz model to predict microbial inactivation under time-varying temperature conditions." Journal of Food Engineering 76, no. 1 (2006): 89-94.

[33] Gompertz, B. "On the nature of the function expressive of the law of human mortality, and on a new mode of determining the value of life

contingencies." Philosophical transactions of the Royal Society of London 115 (1825): 513-583.

[34] Gonzalez-Mejia, A. M., Eason, T., Cabezas, H. and Suidan, M. T. "Computing and interpreting Fisher information as a metric of sustainability: regime changes in the United States air quality." Clean Technologies and Environmental Policy 14, no. 5 (2012): 775-788.

[35] Gonze, D. "The logistic equation." (2015): 1-22.

[36] Goodall, L., van, H., et al. "Innocent killers." No. 599.74427 L3. 1970.

[37] Greenwood, Major. " 'Laws' of Mortality from the Biological Point of View." The Journal of hygiene 28, no. 3 (1928): 267-294.

[38] Gra, P. F. "The logistic equation and a linear stochastic resonance." arXiv preprint cond-mat/0401213 (2004).

[39] Jian-Chun, C., Can-Jun, W. and Dong-Cheng, M. "Stochastic resonance in the tumour cell growth model." Chinese Physics Letters 24, no. 5 (2007): 1162.

[40] Jiang, D. and Shi, N. "A note on nonautonomous logistic equation with random perturbation." Journal of Mathematical Analysis and Applications 303, no. 1 (2005): 164-172.

[41] Juki, D., Kralik, G. and Scitovski, R. "Least-squares fitting Gompertz curve." Journal of Computational and Applied Mathematics 169, no. 2 (2004): 359-375.

[42] Kimura, M. "Diffusion models in population genetics." Journal of Applied Probability 1, no. 2 (1964): 177-232.

[43] Kirschner, D. and Panetta, J. C. "Modeling immunotherapy of the tumor-immune interaction." Journal of mathematical biology 37, no. 3 (1998): 235-252.

[44] Klosek, M. M. "Multiscale analysis of effects of additive and multiplicative noise on delay differential equations near a bifurcation point." Acta Physica Polonica B 35 (2004): 1387.

[45] Kullback, S. "Information theory and statistics." (1968).

[46] Kuznetsov, V. A., Makalkin, L. A., Taylor, M. A. and Perelson, A. S. "Nonlinear dynamics of immunogenic tumors: parameter estimation and global bifurcation analysis." Bulletin of mathematical biology 56, no. 2 (1994): 295-321.

[47] Kuznetsov, V. A. and Knott, G. D. "Modeling tumor regrowth and immunotherapy." Mathematical and Computer Modelling 33, no. 12-13 (2001): 1275-1287.

[48] Laird, A. K. "Dynamics of tumour growth." British journal of cancer 18, no. 3 (1964): 490.

[49] Laird, A. K. "Dynamics of tumour growth: comparison of growth rates and extrapolation of growth curve to one cell." British Journal of Cancer 19, no. 2 (1965): 278.

[50] Lee, U., Skinner, J. J., Reinitz, J., Rosner, M. R. and Kim, E. "Noise-driven phenotypic heterogeneity with finite correlation time in clonal populations." PloS one 10, no. 7 (2015): e0132397.

[51] Linaro, D. (2011). PhD Thesis in Electrical Engineering (Doctoral dissertation, University of Genoa).

[52] Liu, M. and Wang, K. "Persistence and extinction of a non-autonomous logistic model with random perturbations." Communications in Mathematical Sciences 10, no. 3 (2012): 977-987.

[53] Lznarov, E. and Pekr, S. "Dangerous prey is associated with a type 4 functional response in spiders." Animal behaviour 85, no. 6 (2013): 1183-1190.

[54] Lpez, . G., Sabuco, J., Seoane, J. M., Duarte, J., Janurio, C. and Sanjun, M. AF. "Avoiding healthy cells extinction in a cancer model." Journal of theoretical biology 349 (2014): 74-81.

[55] Lotka, A. J. "Elements of physical biology." Science Progress in the Twentieth Century (1919-1933) 21, no. 82 (1926): 341-343.

[56] Loyd, J., Minnich A. and Mondragon O. "Project 1: Logistic map and chaotic dynamics." CS 423 (2013): 523.

[57] Lu, C. and Ding, X. "Survival analysis of a nonautonomous logistic model with stochastic perturbation." Journal of Applied Mathematics 2012 (2012).

[58] Luo, S. "Maximum Shannon entropy, minimum Fisher information, and an elementary game." Foundations of Physics 32, no. 11 (2002): 1757-1772.

[59] Marchuk, G. I. "Mathematical modelling of immune response in infectious diseases." Vol. 395. Springer Science & Business Media, 2013.

[60] May, R. M. "Stability and complexity in model ecosystems." Monographs in population biology 6 (1973): 1-235.

[61] May, R. M. "Simple mathematical models with very complicated dynamics." Nature 261, no. 5560 (1976): 459-467.

[62] Mayer, A. L., Pawlowski, C. W. and Cabezas, H. "Fisher information and dynamic regime changes in ecological systems." ecological modelling 195, no. 1 (2006): 72-82.

[63] Mohamed, M., and Kim, E. "Oscillatory control parameters in nonlinear chaotic systems." Physica Scripta 89, no. 1 (2013): 015202.

[64] Murray, J. D. "Mathematical biology: I. An introduction." (2002).

[65] Nagy, A. "Fisher information in density functional theory." The Journal of chemical physics 119, no. 18 (2003): 9401-9405.

[66] Nguimkeu, P. "A simple selection test between the Gompertz and Logistic growth models." Technological Forecasting and Social Change 88 (2014): 98-105.

[67] Nobile, A. G., Ricciardi, L. M. and Sacerdote, L. "On Gompertz growth model and related difference equations." Biological Cybernetics 42, no. 3 (1982): 221-229.

[68] OTT, E. "Chaos in dynamical systems." (1993).

[69] Pal, D., G. S. Mahaptra, and G. P. Samanta. "Optimal harvesting of prey-predator system with interval biological parameters: a bioeconomic model." Mathematical biosciences 241, no. 2 (2013): 181-187.

[70] Pang, P. YH, and Mingxin Wang. "Strategy and stationary pattern in a three-species predator-prey model." Journal of Differential Equations 200, no. 2 (2004): 245-273.

[71] Papana, A. D. "Nonlinear statistical analysis of biological time series." PhD diss., Aristole University of Thessaloniki, 2009.

[72] Pawlowski, C. W., Fath, B. D., Mayer, A. L. and Cabezas, H. "Towards a sustainability index using information theory." Energy 30, no. 8 (2005): 1221-1231.

[73] Pearl, R. "The growth of populations." Quarterly Rev. of Biol. 2 (1927): 532-48.

[74] Plastino, A., Plastino, A. R. and Soffer, B. H. "Fisher info and thermodynamics first law." Physica A: Statistical Mechanics and its Applications 369, no. 2 (2006): 432-438.

[75] Priede, J., Avalos-Zuiga, R. and Plunian, F. "Homopolar oscillating-disc dynamo driven by parametric resonance." Physics Letters A 374, no. 4 (2010): 584-587.

[76] Prigogine, I., Stengers, I. and Prigogine, I. "Order out of chaos: Man's new dialogue with nature." Vol. 13. New York: Bantam books, 1984.

[77] Ranjan, R. and Bagchi, S. "Functional response and body size in consumer-resource interactions: Unimodality favors facilitation." Theoretical population biology 110 (2016): 25-35.

[78] Rico-Ramirez, V., Reyes-Mendoza, M. A., Quintana-Hernandez, P. A., Ortiz-Cruz, J. A., Hernandez-Castro, S. and Diwekar, U. M. "Fisher information on the performance of dynamic systems." Industrial & Engineering Chemistry Research 49, no. 4 (2010): 1812-1821.

[79] Robert R. "Dynamical system theory in biology." No. Sirsi) i9780471735502. 1970.

[80] Rodriguez-Perez, D., Sotolongo-Grau, O., Riquelme, R. E., Sotolongo-Costa, O., Miranda, J.A. S. and Antoranz, J. C. "Assessment of cancer

immunotherapy outcome in terms of the immune response time features." Mathematical medicine and biology: a journal of the IMA 24, no. 3 (2007): 287-300.

[81] Snchez-Moreno, P., Plastino, A. R. and Dehesa, J. S. "A quantum uncertainty relation based on Fisher's information." Journal of Physics A: Mathematical and Theoretical 44, no. 6 (2011): 065301.

[82] Sarkar, R. R. and Banerjee, S. "Cancer self remission and tumor stability stochastic approach." Mathematical Biosciences 196, no. 1 (2005): 65-81.

[83] Shalek, A. K., Satija, R., Adiconis, X., Gertner, R. S., Gaublomme, J. T., Raychowdhury, R., Schwartz S., et al. "Single-cell transcriptomics reveals bimodality in expression and splicing in immune cells." Nature 498, no. 7453 (2013): 236-240.

[84] Shannon, C. E. "A mathematical theory of communication, Part I, Part II." Bell Syst. Tech. J. 27 (1948): 623-656.

[85] Shannon, C. E. and Weaver, W. "The mathematical theory of communication." University of Illinois press, 1998.

[86] Shastri, Y. and Diwekar, U. "Sustainable ecosystem management using optimal control theory: Part 1 (deterministic systems)." Journal of theoretical biology 241, no. 3 (2006): 506-521.

[87] Shastri, Y. and Diwekar, U. "Sustainable ecosystem management using optimal control theory: Part 2 (stochastic systems)." Journal of theoretical biology 241, no. 3 (2006): 522-532.

[88] Sinha, S., and Parthasarathy, S. "Behaviour of simple population models under ecological processes." Journal of Biosciences 19, no. 2 (1994): 247-254.

[89] Sood, A. and Kim, E. "Dynamic model of dynamo (magnetic activity) and rotation." Astronomy & Astrophysics 555 (2013): A22.

[90] Sotolongo-Costa, O., Molina, L. M., Prez, D. R., Antoranz, J. C. and Reyes, M. C. "Behavior of tumors under nonstationary therapy." Physica D: Nonlinear Phenomena 178, no. 3 (2003): 242-253.

[91] Strogatz, S., Friedman, M., Mallinckrodt, A. J. and McKay, S. "Nonlinear dynamics and chaos: With applications to physics, biology, chemistry, and engineering." Computers in Physics 8, no. 5 (1994): 532-532.

[92] Strogatz, Steven H. "Nonlinear dynamics and chaos: With applications to physics, biology, chemistry, and engineering." Hachette UK, 2014.

[93] Swierniak, A. and Smieja, J. "Cancer chemotherapy optimization under evolving drug resistance." Nonlinear Analysis: Theory, Methods & Applications 47, no. 1 (2001): 375-386.

[94] Tenks, L-M., Hollerbach, R. and Kim, E. "Time-dependent probability density functions and information geometry in stochastic logistic and Gompertz models." Journal of Statistical Mechanics: Theory and Experiment 2017, no. 12 (2017): 123201.

[95] Thattai, M. and Oudenaarden, A. "Stochastic gene expression in fluctuating environments." Genetics 167, no. 1 (2004): 523-530.

[96] Tjrve, Kathleen MC, and Even Tjrve. "The use of Gompertz models in growth analyses, and new Gompertz-model approach: An addition to the Unified-Richards family." PloS one 12, no. 6 (2017): e0178691.

[97] Vieira, S. and Hoffmann, R. "Comparison of the logistic and the Gompertz growth functions considering additive and multiplicative error terms." Applied Statistics (1977): 143-148.

[98] Volterra, V. "Fluctuations in the abundance of a species considered mathematically." (1926): 558.

[99] Waliszewski, P. and Konarski, J. "The Gompertzian curve reveals fractal properties of tumor growth." Chaos, Solitons & Fractals 16, no. 5 (2003): 665-674.

[100] Waliszewski, P. "A principle of fractal-stochastic dualism and Gompertzian dynamics of growth and self-organization." Biosystems 82, no. 1 (2005): 61-73.

[101] Wang, C-Y., Gao, Y., Wang, X-W., Song, Y., Zhou, P. and Yang, H. "Dynamical properties of a logistic growth model with cross-correlated noises." Physica A: Statistical Mechanics and its Applications 390, no. 1 (2011): 1-7.

[102] Wang, C-J. "Effects of non-Gaussian noise on the dynamical properties of a logistic system." Chinese Physics B 22, no. 6 (2013): 060502.

[103] Winsor, Charles P. "The Gompertz curve as a growth curve." Proceedings of the national academy of sciences 18, no. 1 (1932): 1-8.

[104] Wright, T., Twaddle, J., Humphries, C., Hayes, H. and Kim, E. "Variability and degradation of homeostasis in self-sustained oscillators." Mathematical Biosciences 273 (2016): 57-69.

[105] Xiao, Y. and Chen, L. "Modeling and analysis of a predator-prey model with disease in the prey." Mathematical Biosciences 171, no. 1 (2001): 59-82.

[106] Zhang, X.-a., Chen, L. and Neumann, A. U. "The stage-structured predator-prey model and optimal harvesting policy." Mathematical Biosciences 168, no. 2 (2000): 201-210.

[107] Zhang, X-M., and B-Q. Ai. “Genotype selection model with two time-correlated white noises.” The European Physical Journal B-Condensed Matter and Complex Systems 73, no. 3 (2010): 433-437.

[108] Zhong, W., Shao, Y., and He, Z. “Stochastic resonance in the growth of a tumor induced by correlated noises.” Chinese Science Bulletin 50, no. 20 (2005): 2273-2275.

[109] Zwietering, M. H., Jongenburger, I., Rombouts, F. M. and Van’t Riet, K. “Modeling of the bacterial growth curve.” Applied and environmental microbiology 56, no. 6 (1990): 1875-1881.